Multifunctional Virus Scaffolds for Energy Applications: Nanomaterials Synthesis and Two Dimensional Assembly

by

Ki Tae Nam
B.S. & M.S, Seoul National University

SUBMITTED TO THE DEPARTMENT OF
MATERIALS SCIENCE AND ENGINEERING
IN PARTIAL FULFILLMENT OF THE REQUIREMENT FOR THE DEGREE OF

DOCTOR OF PHILOSOPHY

AT THE
MASSACHUSETTS INSTITUTE OF TECHNOLOGY

JUNE 2007

Signature of Author: _____
Department of Materials Science and Engineering
March 14th, 2007

Certified by: _____
Angela M. Belcher
Professor Materials Science and Engineering and Biological Engineering
Thesis Supervisor

Accepted by: _____
Samuel M. Allen
POSCO Professor of Physical Metallurgy
Chair, Departmental Committee on Graduate Students

Multifunctional Virus Scaffolds for Energy Applications: Nanomaterials Synthesis and Two Dimensional Assembly

By
Ki Tae Nam

Submitted to the Department of Materials Science and Engineering
On March 22nd, 2007 in Partial Fulfillment of the Requirements for
The Degree of Doctor of Philosophy

Abstract

Biological systems inherently posses the ability to synthesize and assemble nanomaterials with remarkable precision, as evident in biomineralization. These unique abilities of nature continue to inspire us to develop new approaches of nanobiotechnology to integrate advanced materials into medicine and electronics. Particularly, peptides are believed to play an important role in biotemplating and biological self-assembly. In order to understand the interface between inorganic materials and peptides and realize biological self-assembly, this work adopted M13 virus as a model system. The genetic engineering of M13 viruses enables us to grow various nanomaterials and achieve virus monolayer assembly on charged polyelectrolyte multilayers.

The fundamental understanding and new discoveries obtained by this work can mature into an engineering discipline demonstrating that biological approaches may represent a new paradigm to provide novel technological advantages. The use of a biological template for a nanostructured battery electrode ramps up the device's performance and scales down its overall size. This work presents a new way of exploiting biological entities for the bottom-up assembly of battery devices by utilizing biological self-assembly and biotemplating. Viruses are genetically engineered such that they function as a toolkit for constructing the battery.

Thesis Supervisor: Angela M. Belcher
Title: Professor of Materials Science and Engineering, and Biological Engineering

Thesis Committee: Professor Paula T. Hammond and Professor Yet-Ming Chiang

ACKNOWLEDGEMENTS

First of all, I sincerely thank my advisor, professor Angela Belcher for encouraging, supporting, and inspiring me as well as for teaching me throughout my Ph.D program at MIT. I also thank my committee members, professor Yet-Ming Chiang for his scientific and insightful guidance and professor Paula T. Hammond for her kind openness and critical advice. I gratefully acknowledge Dr. Pil J. Yoo for the successful collaboration and his kind advice on both research and life. I appreciate Dr. Dong-Wan Kim for the fruitful discussion, Nonglang Meethong with help of the electrochemical measurement, Dr. Soo-Kwan Lee for his kind help in genetic engineering. I appreciate and remember the joyful and enthusiastic discussion with our Belcher's Group colleagues, especially with Asher, Chiang, Eric, Mo, Sreekar, Saeeda and Dr. Yun. I really thank Beau and Dr. Seung-Wuk Lee for their friendship and scientific discussion. I also appreciate Yunjung and Forrest who contributed to this work and will continue to extend our projects. My friends at MIT and in my church helped me balance my graduate life. I also appreciate pastor Dae-Sung Choi and deacon Mooje Sung for their prayers. More importantly, I sincerely and eternally appreciate my father in heaven and my mother in Korea for supporting me throughout my entire life and for making me who I am. I also thank my sister, Soo Yeon, brother in law, Won Jae and my lovely niece Kun Myung.

BIOGRAPHICAL NOTE

EDUCATION

Massachusetts Institute of Technology, Cambridge, MA
Ph.D. Candidate in Material Sci. & Eng. **Present**
Research focus: Bio-inspired materials science and bio-nanoelectronics

Seoul National University
M.S. in Material Sci. & Eng. **2002**
Research focus: Interfacial reaction in the nanostructured film

Seoul National University
B.S. in Material Sci. & Eng. **2000**
Cum laude

RESEARCH & WORK EXPERIENCE

Institute of Soldier Nanotechnology, MIT **2002-Present**
Dissertation: Multifunctional M13 virus scaffold for nanoelectronics
- Established collaborative project
- Filed three US patents

Teaching Assistant, Seoul National University **2001**
- Taught 50 students weekly recitation sessions to supplement class material and emphasize problem solving skills

Researcher, Seoul National University **2000-2002**
Dissertation: Improved diffusion barrier for Cu metallization
- Got two best paper awards
- Filed one patent and published four paper in peer-reviewed journal

AWARDS AND SCHOLARSHIPS

Finalist of 2006 Collegiate Inventors Competition **2006**
- National competition, one of eleven finalists

Outstanding PhD thesis research award **2006**

Martin Family Society of Fellows for Sustainability **2005**
- Honored society of MIT graduate students engaged in environmental and sustainability studies

Samsung Lee Kun Hee Scholarship **2006**

Applied Materials Korea, Seoul
Best paper award **2001**
- Awarded to student who wrought the significant paper

Brain Korea 21 material symposium, Korea
Best paper award **2001**
- Nominated and selected by student committee and professors

Seoul National University

Best honored student award **1999**

- Awarded from the president of Seoul National University
- Awarded to one student leader in department.

PUBLICATION

1. **K. T. Nam**, A. Datta, S.-H. Kim and K.-B. Kim, "Improved diffusion barrier by stuffing the grain boundaries of TiN with a thin Al interlayer for Cu metallization", ***Appl. Phys. Lett.*** 79(16), 2549 (2001).

2. A. Datta, **K. T. Nam**, S.-H. Kim and K.-B. Kim, "Optimization of Al interlayer thickness for a novel multilayer diffusion barrier scheme in Cu metallization", ***J. Appl. Phys***. 92(2), 1099 (2002).

3. S.-H. Kim, **K. T. Nam**, A. Datta and K.-B. Kim, "Failure mechanism of TiN/Al/TiN multiplayer diffusion barrier for Cu metallization", ***J. Appl. Phys***. 92(9), 5512 (2002).

4. S.-H. Kim, **K. T. Nam**, A. Datta, H.-M. Kim, D.-H. Hwan and K.-B. Kim, ""Multilayer diffusion barrier using a thin interlayer metal (M = Ru, Cr, Zr) between two TiN films for copper metallization", **J. Vac. Sci. Tech, B** 21 (2), 804 (2003).

5. **K. T. Nam**, B. R. Peelle, S.-W. Lee and A. M. Belcher, "Genetically driven assembly of nanorings based on the M13 virus", **Nano Lett**. 4(1), 23 (2004). (one of the most accessed articles in Nano Lett.)

6. S. Jaffar, **K. T. Nam**, A. Khademhosseini, J. Xing, R. Langer and A. M. Belcher, "Layer-by-layer surface modification and patterned electrostatic deposition of quantum dots", **Nano Lett**. 4(8), 1421 (2004).

7. P. J. Yoo*, **K. T. Nam***, J. Qi, S.-K. Lee, J. Park, A. M. Belcher and P. T. Hammond, "Spontaneous assembly of viruses on multilayered polymer surfaces", ***Nat. Mater***. 5, 234 (2006). **** equal contribution***.

8. **K. T. Nam**, D.-W. Kim, P. J. Yoo, C.-Y. Chiang, N. Meethong, P. T. Hammond, Y.-M. Chiang and A. M. Belcher, "Virus enabled synthesis and assembly of nanowires for lithium ion battery electrodes", ***Science*** 312, 885 (2006).

9. S. Jaffar, **K. T. Nam**, G. T. Zugates, R. Langer and A. M. Belcher, "Assembly of hybrid nanostructures for enhanced gene delivery and optical tracking", (submitted).

10. **K. T. Nam**, Y. J. Lee, E. M. Krauland, S. T. Kottmann and A. M. Belcher, "Peptide-mediated reduction of silver ions on the engineered biological

scaffolds". (submitted).

PATENTS

1. A. M. Belcher, B. R. Peelle, **K. T. Nam**, "Multifunctional biomaterials as scaffolds for electronic, optical, magnetic, semiconducting, and biotechnological applications", US patent 20050170336.

2. **K. T. Nam**, C. Y. Chiang, A. M. Belcher, "Virus scaffold for flexible Li ion battery electrode", US patent filed.

3. P. J. Yoo, **K. T. Nam**, A. M. Belcher, P. T. Hammond, US patent filed.

TABLE OF CONTENTS

LIST OF FIGURES

Chapter 1. Introduction

Chapter 1. 1 Introduction

The primary goal of this work is to understand biotemplating and biological self-assembly and to apply them for nanomaterials synthesis and assembly in nanoelectronics, for example, nanostructured Li ion battery electrodes. To realize our vision of a bioinspired approach, M13 bacteriophage (virus) was adopted and genetically engineered to have specific functionality. As M13 virus has been studied for over twenty years in the pharmaceutical industry, nearly all aspects of the underlying genetics in M13 virus is well known. In addition to being easily genetically engineered, M13 virus is a good study material in understanding biological mechanisms because of its simple structure organized by proteins and a single stranded DNA. The length of the M13 virus can be controlled and the functionality of each protein can be modified through simple genetic engineering. Genetically engineered M13 virus functionalized with nanomaterials can be used as basic building blocks to grow and assemble nanomaterials. Additionally, in order to demonstrate the applicability of our knowledge to other biological systems and to study the underlying mechanisms more systematically, eukaryotic yeast cells were also engineered to display short peptide sequences on their surfaces.

These approaches take advantage of the biological properties of natural materials to fabricate intelligent materials that are not created naturally. Silver nanowires and cobalt oxide nanowires were fabricated by M13 virus template whose major coat proteins are specifically functionalized with short peptides. The biological fabrication of the nanowires does not require any harmful organic solvents and the synthesis occurs in water at room temperature, thus making the synthesis process environmentally benign.

Additionally, the peptide mediated reduction of silver ions on a biological scaffold was demonstrated using short peptide expressing yeast cells. The detailed reduction mechanism was also examined. Biological assembly was newly discovered and investigated in this study. Also, by controlling the electrostatic interaction on a charged polymer surface, two dimensional monolayer assembly of M13 virus was achieved. Thereafter, the biotemplating and biological self assembly methods were applied to fabricate a nanostructured electrode for Li ion batteries. Our approach can improve battery performance parameters including charging rate and capacity. Furthermore, such batteries can be assembled in water via a biological mechanism similar to that used in nature to assemble biosystems.

Before the detailed schemes of the biological approach are introduced, this chapter describes the background of 1) biomineralization which provides inspiration for the creation of a new paradigm in designing intelligent materials, 2) biological building blocks which are useful in nanotechnology, especially in a bottom-up approach, 3) opportunity of applying a biological approach to the fabrication of energy devices. Finally, the scope and plan of the dissertation will be presented.

Chapter 1. 2 Biological Approaches Inspired by Biomineralization

Biological systems have inherently possessed the most efficient approaches and functions to satisfy various requirements for survival. Therefore biological systems continue to inspire human beings to develop state-of-the-art technology. Biomimicry is a new science that seeks to understand the biological and natural approaches and then imitates these designs to solve a specific problem.[1] For example, photosynthesis and energy harvesting by biomolecules are very efficient and thus have been investigated intensively for further applications. A well-known example is spider silk, which is waterproof and five times stronger than steel. Spider dragline silk is a flexible, lightweight fiber of extraordinary strength and toughness comparable to that of synthetic high-performance fibers. The uniquely assembled, liquid crystalline protein fiber structure can lead to improved mechanical properties. Another example is the mussel, famous its ability to adhere to marine surfaces. The liquid protein adhesive produced by mussels rapidly harden upon attaching to a surface to form a solid adhesive that mediates the stable binding to various surfaces.

Among many biological mechanisms, biomineralization is believed to provide the greatest benefits to materials technology from a biologically inspired approach. Because inorganic materials posses useful functionalities that can be manipulated easily by human beings, their conjugation with organic biomolecules can result in the development of new applications. Most advances in useful devices have resulted from the development of inorganic materials. Therefore, in order to maximize the potential of biological functions and self assembly, inorganic materials must be incorporated. Although a variety of the

conjugation techniques have been proposed and developed, none of the conventional methods are comparable to that from nature. Biological systems have inherently developed the ability to nucleate, grow and assemble nanomaterials of inorganics and metals, as evident in biomineralization. Therefore, further understanding of the interface between biomolecules and inorganics could be achieved by studying the biominerals.[2] The examples of biologically inspired approach especially by biominerals are reviewed briefly.

Biologically inspired photonic systems

Nature has developed unique and optimized optical systems depending on their need. For example, whales which need good vision in and out of the water have a chamber behind the lens where the focal length is controlled by filling or emptying the fluid. The fish eye is the best for underwater vision. Also, insects posses compound eyes where up to 10 thousands lenslets form a regular and close packed array. Spherical aberration, astigmatism and birefringence can be corrected by a different mechanism in each biological creature. Furthermore, nature's designs are superior to the human-made equivalent in many aspects. For example, current infrared sensors require a complicated cooling system for device operation, but insets exhibit the same ability without the limitation of temperature control. The growing understanding of the underlying mechanism in biological optics and the rapid progress in fabrication technology continue to inspire researchers to develop bio-mimic optical devices.[3] Some research groups utilize the unconventional soft lithography for the creation of three dimensional polymer structures which are designed for an adaptive lens. Replication of a compound eye could

also be demonstrated with well-developed semiconductor processing.[4] Examples include a planar array of gradient refractive index rods that forms a self-aligned waveguide with individual microlenses. Aizenberg et al. applied their understanding of the brittlestar, the species *Ophiocoma wendti*, to developing optical networking devices.[5] Calcite crystals are located throughout the brittelstar skeletal body and play a role as the micro compound lens patterned using soft lithography. These are just a few examples of biologically inspired photonic systems. The more we learn about nature's optics, the more we can synergistically combine our creativity in materials with nature's wisdom.

Biologically inspired structural materials

Rigid biological materials such as shells, bone, and sponge spicules have been attractive as models for synthetic composites because of their unique mechanical properties such as strength, stiffness and toughness.[6] The attractive combinations of mechanical properties of many rigid biological materials stem from the fact that they are hybrid composites, consisting of a very small volume fraction of organic components surrounding a ceramic phase. $CaCO_3$ sheets are stacked alternatively and between them are thin protein organic layers with thickness of few tens of nanometers. By mass, 98 % of the shell is occupied by inorganic $CaCO_3$ and only 2 % is protein. The resulting nacreous and lamellar structures are analogous with the brick-and-motor architecture in buildings. The ordered and aligned composites of organic and inorganic material exhibit the unusual mechanical property. The toughness of the biologically fabricated materials is much higher than those of the materials made by the conventional method. While the exact mechanism underlying the resistance to failure in rigid natural materials is still

under investigation, it is believed that a thin and tenacious organic phase is involve in the energy dissipation by many mechanisms.[7] When a force is applied, a new surface can be created and the energy is dissipated by the surface.

There are a number of investigations to mimic biological structure materials. The continuous structural laminates of certain ceramic/metallic or interemetallic/metallic composites can be considered to have their origin in nacre. Additionally, based on the brick-and motor structure design, synthesized inorganic materials were stacked by an organic glue. However, the challenge to achieve a comparable mechanical property with biologically synthesized composites still remains because the organic glue cannot show the strong adhesion property.

Metal oxide synthesis inspired by diatom

Studies of marine organisms that synthesize silicon-containing compounds have revealed their underlying molecular and genetic mechanism. The DNA sequence of these organisms was characterized and a protein sequence which may play an important role in the growth of silicate was identified. The protein was named as silicatein and assembles into filamentous structures. It was also found that constituent subunits catalyze the *in vitro* polymerization of silica from tetraethoxysilane. Interestingly, it was demonstrated that this filamentous protein assembly does not only catalyze the chemical reaction but also acts as a template for the silicate growth.[8] Interestingly, this motif was analyzed and constructed as a peptide diblock polymer which can mediate the synthesis of metal oxide.[9] Interestingly, it was demonstrated that silcatein is not only capable of the

condensation of biosilica, but is also significant for the synthesis of other metal oxide such as TiO_2, ZrO_2 and Ga_2O_5.

In chapter 1.2, three examples of the biological approaches inspired by biomineralization were described briefly. The detailed mechanism how biominerals can form by biomolecules is still under investigation. There is growing evidence that short peptide sequences may play an important role in the nucleation and growth of nanomaterials and that the assembled proteins act as an organic matrix that predetermines the organization of the grown inorganic materials. The better we understand the biomineral at the molecular level, the more benefits we can obtain.

Chapter 1. 3 Biological Building Blocks

Biological systems self-assemble precisely from various building blocks. The genetic information has been passed through generations and mutations of DNA sequences help living creature get accustomed to the varying environment. DNA produces peptides and proteins. The peptides or proteins can self-assemble into hierarchical structures such as filamentous fibers or tubes. These ordered and self-assembled structures have unique biological functions. Self-assembly of biological building blocks takes place ubiquitously at multiple length scales.[10] A variety of interactions such as hydrophobic, electrostatic and Van der Walls forces are involved in driving the self-assembly. In this chapter, representative examples of biological building blocks will be briefly reviewed.

Self-Assembly of DNA

It is well known that two complementary DNA will pair to form a double helix DNA. Branched DNA structures can be combined by sticky-ended binding. In fact, branched DNA building blocks can give rise to more diversity in the organized structure. The sticky ends can be programmed and as a result the intended hierarchical structure can be achieved. The final structure is totally predictable. N-nucleotide sticky ends lead to 4N possible different sequences. Sticky ends of sufficient length cohere by base paring alone and they can be ligated to bond covalently. Through the sticky-end concept in DNA assembly, various hierarchical structures such as ring, two dimensional tile, etc, have been successfully demonstrated.

Potential application of DNA self-assembly and scaffolding include nanoelectronics, biosensors and programmable molecular machines. Recently, DNA has been used in constructing nanomechanical devices and molecular computing systems in addition to pattern formation.[11] The combination of the functional molecule or/and the inorganic nanomaterials through the appropriate conjugation technology leads to more useful functional hybrid structures. For example, it was reported that the hybridization of single stranded DNA can be controlled by an external radio frequency magnetic field. Herein, a gold nanoparticle was attached covalently at one end of DNA. When the radio frequency magnetic filed is applied, the DNA deforms and changes its conformation and the gold nanoparticle can also respond to the external field.

Peptide assembly and nanofiber scaffold

Peptides and proteins interact and self assemble to form well-defined structures that are associated with functionalities in nature. Peptides and proteins have already been used in nature as scaffolds to produce interesting structures. The examples include collagen, keratin, pearl and shell. Peptide self-assembly is mediated by weak and noncovalent bonds such as hydrogen bonds, ionic bonds, hydrophobic interaction and van der Waals interactions.

Various kinds of peptides and proteins have been demonstrated to produce stable nanofiber structures. In fact, the formation of amyloid fibrils is known to play a role in several diseases such as Alzheimer disease. Based on the understanding of existing nanofibers in nature, synthetic nanofibers can be fabricated. The ionic self-complementary peptides with an alternating polar and nonpolar pattern can self-assemble

into beta sheet structure and nanofibers. Because their formation and size can be precisely controlled, the nanofiber scaffold can serve as a scaffold to organize the inorganics.

Nature has also inherently developed amphiphilic molecules that contain hydrophilic and hydrophobic segments. In water, these surfactant-like, amphiphilic molecules can self-assemble into nanotubes with various lengths and diameters. One of the best examples is the phospholipid in plasma membranes, which protects cellular contents from the environment. The size and shape of the organized lipid is dependent on the water environment and the relative portion of the polar and nonpolar peptides. By mimicking the underlying mechanism of the peptides nanotube formation in nature, various kinds of amphipilic biopolymers have been designed and demonstrated to form nanotube structures. Furthermore, the interconnected network can also be achieved through genetic engineering. The growth of inorganic nanomaterials inside or outside peptide nanotube result in useful nanowires or nanotubes in a controlled manner.

Ordering of Filamentous Viruses

Various kinds of filamentous viruses such as Fd, TMV, Ff, M13 can be ordered into a liquid crystalline film.[12] The same theoretical framework that was successfully developed in explaining the hydrodynamic and elastic properties of low molecular weight liquid crystal can be applied to virus liquid crystalline systems. The observed liquid crystal phases are the isotropic, nematic, cholesteric, smetic A, smetic C and crystalline phase. Many groups have been studying the virus liquid crystal as a toolkit to understand the liquid crystalline behavior. Additionally, the mixture of virus with polymers or spherical colloids can lead to ordered hybrid nanostructures.[13] Furthermore, the

successful genetic engineering at specific location on the virus enables the construction of designed building blocks for self-assembling systems.

Osanger theory was first developed and demonstrated with Tobacco mosaic virus (TMV) by observing the birefringent virus film. In Osanger theory, ordering phenomena of the filamentous viruses into the nematic phase was explained well by considering the competition between rotational and translational entropy. Rotational entropy is a maximum when the filament point in all directions. Translational entropy can be maximized when the excluded volume is a minimum. Therefore, when the rods point in the same direction, the rod-like particles have the most space to be configured in. As a result, when the anisotropy of the rods are large and the concentration is high, the translational entropy is dominant and the suspension maximize the total entropy by having the rods aligned to a preferred direction.

After the successful theory by Osanger, many groups have investigated liquid crystal ordering by using viruses. The Fraden group reported the well-controlled smectic and cholestic structure of Fd viruses.[14] The ordering structure could be controlled by changing solvent concentration, ionic strength, concentration of viruses, length of viruses and external forces. The Marvin groups also reported the formation of various liquid crystals using Fd viruses analyzed by x-ray diffraction. Along with other group's work, Belcher groups report the evidence of chiral smetic C structure for the first time.

Multifunctional building block, M13 virus

Biologists have studied M13 virus widely in order to reveal the genetic linkage between proteins and DNA. Natural M13 viruses exist everywhere and there are

abundant M13 viruses living under the sea. Because it is a simple microorganism and its functionality can be manipulated through genetic engineering, it has been demonstrated to be a good study material in investigating the interaction between inorganic materials and proteins.[15] Furthermore, different functionalities can be given to each protein located at different regions on the virus so that M13 virus offers the new opportunity in nanobiotechnology. The Belcher group has demonstrated that M13 virus can be used as biological building blocks to synthesize and assemble nanomaterials.

The end protein (p3) of M13 virus was engineered to have the peptide library and the virus library utilized to identify the material-specific peptide sequences. The method is a good way to study the interface between short peptides and inorganic materials. Furthermore, it was demonstrated that the identified peptides can mediate the growth of the specific materials as well as bind to the target inorganic surface. The identified peptide sequence can be inserted into the major coat proteins and the major coat protein engineered virus can act as a template to grow the nanowires. In addition to the ability to grow the nanomaterials, M13 virus can assemble nanomaterials. Due to their anisotropicity and homogeneity, when above a critical concentration, M13 virus can form a liquid crystalline structure, which can arrange the nanoparticles.

Chapter 1. 4. Biological Approaches in Energy Devices

We live in age of great challenges such as the energy crisis. Energy consumption is increasing rapidly, but the development of alternative energy sources has not progressed significantly. NASA's Goddard Institute for Space Studies says the greenhouse effect is already affecting our climate. The solution is in biology. Biological systems inherently possess the ability to produce and transfer existing energy into a useful energy source and store the energy. Much research is seeking to understand the fundamentals of biologically producing energy systems. To develop the energy producing system in an efficient manner, the understanding and mimicking of biological system are required. In addition to the unique ability in energy production and conversion, the ability of the biological system to synthesize and assemble of nanostructured material in an accurate way can continue to inspire the development of unique energy devices.

One well-known example is photosynthesis by biomolecules. The photon energy can be converted into ATP in the presence of chlorophyll, in the conversion of carbon dioxide and water into carbohydrates and oxygen. Plants, algae and oxyphotobacteria can produce oxygen by an oxygenic photosynthesis mechanism. Anoxygenic photosynthesis can convert carbon dioxide, hydrogen sulfide and an organic acid into the reduced form. Type I photosystems use ferredoxin-like iron-sulfur cluster proteins as terminal electron acceptors, while type II photosystems ultimately shuttle electrons to a quinone terminal electron acceptor. Artificial systems that mimic photosynthesis have been achieved by various engineering approaches.

Another interesting example is a microorganism that produces fuel such as ethanol, hydrogen and methane from organic materials. In contrast to the human designed

fuel cell in which high temperature and adequate catalysts are required, microbial fuel cells can operate at room temperature with high efficiency. Reduced fermentation products and microbe-reduced artificial mediators can yield a small electrical current. Metabolism of microorganisms can convert a wide variety of organic compounds into electricity.

Chapter 1. 5. Plan of the Dissertation

The primary goal of this work is to understand the biotemplating and biological self-assembly and to apply them for the nanomaterials synthesis and their assembly in nanoelectronics, for example, nanostructured Li ion battery electrode. To realize our vision of bioinspired approach, M13 bacteriophase (virus) was adopted and genetically engineered to have the specific functionality.

Chapter 2 describes the genetically driven ordering of the filamentous M13 virus into ring structure. One-dimensional ring structures from M13 viruses were constructed by two genetic modifications encoding binding peptides and synthesis of a heterobifunctional linker molecule. The bifunctional viruses displayed an anti-streptavidin peptide and hexahistidine peptide at opposite ends of the virus as pIII and pIX fusions. Stoichiometric addition of the streptavidin-NiNTA linker molecule led to the reversible formation of virus-based nanorings.

Chapter 3 presents the ordering of M13 viruses, highly complex biomacromolecules, driven by competitive electrostatic binding, preferential macromolecular interactions, and the rigid rod nature of the virus systems during alternating electrostatic assembly. The spontaneous formation of a two-dimensional monolayer structure of viruses atop a cohesive polyelectrolyte multilayer was achieved. This viral-assembled monolayer can be a biologically tunable scaffold to nucleate, grow and align nanoparticles or nanowires over multiple length scales.

Chapter 4 present the virus enabled synthesis and assembly of nanowires as negative-electrode materials for lithium ion batteries. The expression of cobalt ion binding peptides on the filamentous coat of M13 bacteriophage viruses facilitates the

fabrication of homogenous Co_3O_4 nanowires at room temperature. Furthermore, genetically incorporating gold binding peptides for the engineering of hybrid Co_3O_4 nanowires containing gold nanoparticles resulted in improved battery capacity. This chapter describes that biological approach using biotemplating and biological self assembly can give the technological benefits to improve the battery property.

Chapter 5 describe the spontaneous reduction of silver ions into nanostructures by yeast displaying glutamic acid (E_6) and aspartic acid (D_6) peptides on their surface. This principle was further extended to the M13 virus for fabricating crystalline silver nanowires. These insights into the spontaneous reduction of metal ions on biological scaffolds should help further the formation of novel nanomaterials in biological systems.

Chapter 1.6 References

1. M. Sarikaya, C. Tamerler, A. K. Y. Jen et al., *Nature Materials* **2** (9), 577 (2003).
2. S. Weiner, L. Addadi, and H. D. Wagner, *Materials Science & Engineering C-Biomimetic and Supramolecular Systems* **11** (1), 1 (2000).
3. L. P. Lee and R. Szema, *Science* **310** (5751), 1148 (2005).
4. D. Y. Zhang, V. Lien, Y. Berdichevsky et al., *Appl Phys Lett* **82** (19), 3171 (2003).
5. J. Aizenberg, D. A. Muller, J. L. Grazul et al., *Science* **299** (5610), 1205 (2003).
6. G. Mayer, *Science* **310** (5751), 1144 (2005).
7. S. Kamat, X. Su, R. Ballarini et al., *Nature* **405** (6790), 1036 (2000).
8. J. N. Cha, K. Shimizu, Y. Zhou et al., *P Natl Acad Sci USA* **96** (2), 361 (1999).
9. J. N. Cha, G. D. Stucky, D. E. Morse et al., *Nature* **403** (6767), 289 (2000).
10. S. G. Zhang, *Nat Biotechnol* **21** (10), 1171 (2003).
11. N. C. Seeman and A. M. Belcher, *P Natl Acad Sci USA* **99**, 6451 (2002).
12. Z. Dogic and S. Fraden, *Curr Opin Colloid In* **11** (1), 47 (2006).
13. M. Adams, Z. Dogic, S. L. Keller et al., *Nature* **393** (6683), 349 (1998).
14. Z. Dogic and S. Fraden, *Philos T Roy Soc A* **359** (1782), 997 (2001).
15. C. E. Flynn, S. W. Lee, B. R. Peelle et al., *Acta Mater* **51** (19), 5867 (2003).

Chapter 2. Genetically driven assembly of nanorings based on the M13 virus

Chapter 2. Summary

This chapter describes the genetically driven ordering of the filamentous M13 virus into a ring structure. One-dimensional ring structures from M13 viruses were constructed through two genetic modifications that encode binding peptides and lead to the synthesis of a heterobifunctional linker molecule. The bifunctional viruses displayed an anti-streptavidin peptide and hexahistidine peptide at opposite ends as pIII and pIX fusions, respectively. Stoichiometric addition of the streptavidin-NiNTA linker molecule led to the reversible formation of virus-based nanorings with circumferences corresponding to lengths of the packagable DNAs. These virus-based ring structures can be further engineered to nucleate inorganic materials and form metallic, magnetic, or semiconductor nanorings using trifunctionalized viruses.

Chapter 2. 1 Introduction

Biological self-assembly and biomolecular interactions continue to inspire novel approaches for the development of nanostructured materials[1-5]. Furthermore the remarkable ability of biomolecules to recognize and nucleate inorganic materials such as semiconductors, magnetic materials, and metals has broadened the possible applications in nanoelectronics and nanobiotechnology[6-9]. Our previous work, along with that of others[10-14], has shown that biomolecules, in our case genetically engineered M13 bacteriophage (virus), can be used as a molecular building block to nucleate and arrange quantum dots[15], template semiconductor nanowires[16,17], and build multidimensional liquid crystals and films[15,18-20]. Other self-assembling peptide and protein systems have been used to make wires[21], fibers[22], and other structures incorporating inorganic materials[23]. However, the potential of these systems for assembling devices is limited in part by difficulties in programming distinct structural size and geometric control into the self-assembling components. As discussed in Chapter 1, the various biological building blocks have been programmed to control the self assembly behavior. In this chapter, we set out to explore the possibility of genetically encoding size and shape information into self-assembling multifunctional viruses. The wild type filamentous M13 virus is approximately 6.5 nm in diameter and 880 nm in length[24]. The length of the cylinder reflects the length of the packaged single stranded DNA genome size. At one end of M13 virus, there are approximately five molecules each of protein VII (pVII) and protein IX (pIX). The other end has about five molecules each of protein III (pIII) and protein VI (pVI), totaling 10-16 nm in length. The wild type M13 virus coat is composed of roughly

2800 copies of the major coat protein VIII (pVIII) stacked in units of 5 in a helical array. Here we demonstrate the one-dimensional (1D) formation of a ring structure from a M13 virus genetically engineered to display fused functional binding peptides at each end. Ring structures of M13 viruses were constructed by two genetic modifications of the M13 virus and synthesis of a heterobifunctional linker molecule, which was designed to specifically bind each modified virus end (Figure 1).

This chapter concerns the self-assembly of a virus. This work demonstrated that, for the first time, filamentous shaped biomolecules could change their intrinsic shape into a ring structure through a process driven by biomolecular interactions. The virus based nanoring structure also demonstrated that p9 of a virus can be successfully engineered by a phagemid system. Potentially, further engineering of the major coat protein (p8) can enable the fabrication of inorganic ring structures of nanoscale dimensions.

Chapter 2. 2 Experimental

Genetic modification of M13 virus

At one end of the virus, the anti-streptavidin peptide (SWDPYSHLLQHPQ-), identified through a phage library screen for streptavidin binding[19], was displayed at the N-terminus of pIII. The anti-streptavidin sequence was encoded in the M13 virus genome, thus, all copies of the pIII minor coat protein on the engineered virus display the anti-streptavadin peptide. At the other end of the virus, a hexahistidine peptide (AHHHHHH-), which binds strongly to Ni(II)-nitrilotriacetic acid complex (Ni-NTA), was fused to the N-terminus of pIX. A genetically encoded hexahistidine peptide and a flexible amino acid spacer sequence were fused upstream of M13 virus pIX gene in a pAK derived phagemid (ref 14, Mao 2003) by PCR cloning techniques. The mature protein sequence of expressed His_6-pIX was AHHHHHHGQGGGVDMSVLVYSFASFVLGWCLRSGITYFTRLMETSS after cleavage of the pelB leader sequence in *E. coli*, as confirmed by DNA sequencing. These bifunctional viruses are easily amplified to large quantities using standard bacterial amplification procedures.

For the amplification of bifunctional viruses where p3 and p9 was engineered, the bacterial amplification procedure was utilized. Tetracycline and Chloramphenicol was used as antibodies when E. Coli was amplified. The volume ratio of the antibodies is 1:1000 compared to the total LB solution. When the O.D value reached 0.5, the virus that has the antistreptavidin peptide sequence was added, and IPTG was used to induce the expression of the His6 proteins through the plasmid inside the bacterial cell.

The engineered viruses were produced using a phagemid system[24], which used a plasmid separate from the M13 genome to express the engineered His_6-pIX fusion. Single stranded DNA produced from this plasmid inside the *Escherichia coli* host packages into viruses, called phagemids, as does the M13 genome. Since the length of the virus is proportional to the size of its packaged DNA, the phagemid-based viruses are typically observed to be 300-600 nm in length, shorter than wild type M13 viruses. In this phagemid expression system both wild-type and His_6-pIX were produced, and the resulting virus may display between zero and five copies[24] of the his-tagged pIX per virus. The dual-end modified viruses were amplified by infection of ER2738 *E. coli* (New England Biolabs) harboring the His_6-pIX phagemid with the anti-streptavidin-pIII containing M13 virus, purified from centrifuge clarified supernatant by PEG-fractionation, and resuspended in Tris buffered saline, pH 7.5.

Synthesis of linker molecule

A linker molecule consisting of streptavidin conjugated with Ni-NTA was also synthesized (Figure 1b). A NTA ligand (Qiagen) bearing a primary amine was reacted with carboxylate groups on streptavidin (New England Biolabs) in the presence of EDC catalyst, then charged with Ni, and purified. Streptavidin (1.5 mg/mL) dissolved in 1 mL 0.1 M MES [2-(N-morpholino) ethane sulfonic acid] and 0.5 M NaCl (pH 6.0), was activated by adding 0.01M EDC [1-Ethyl-3-(3-Dimethylaminopropyl)carbodiimidie Hydrochloride] and 0.01M Sulfo-NHS (N-Hydroxysulfosuccinimide). After 15 minutes at room temperature, EDC was quenched with 2 uL of 2-mercaptoethanol. The buffer was exchanged to sodium phosphate buffer (0.3 mL, 0.1M, pH 7.5) using a 10 kDa-cutoff

spin column (Microcon). NTA ligand was added and after 3hrs at room temperature, the buffer was exchanged to Tris Buffered Saline (pH 8.0). The conjugated NTA-streptavidin was incubated for 5hr in $NiSO_4$ (5 mM in 0.5 mL TBS), spin purified again, and dissolved in distilled water. Since the linker must bind both ends of the virus, heterobifunctionality was important in order to prevent saturation of binding sites on the linker by binding peptides displayed multivalently at a single end of the virus.

AFM observation

Atomic Force Microscopy (AFM) images of virus ring structures on mica substrate observed with a NanoscopeIV (Digital Instruments) in tapping mode under dry condition. Freshly cleaved mica was silanized by dipping it in a mixed solution of Methanol (10 mL) and 3-aminopropultriethoxysilane (0.5 mL) for 40 minutes. After the incubation, it was dipped in methanol for 10 minutes and in distilled water for 5 minutes. After the virus based nanorings were formed in solution, 100 uL solution was dropped on mica. After the incubation for 30min, the mica was washed with the distilled water three times. After drying in air, the mica was observed by AFM. Height and amplitude signals were simultaneously recorded. Height images were flattened to eliminate background curvature.

TEM analysis and gold conjugation

Virus were labeled by mixing 10 uL of 1:100 diluted anti-fd bacteriophage antibody (Sigma-Aldrich, 7mg/mL) with 10 uL of anti-rabbit 10 nm gold conjugate (Sigma-Aldrich,$1.4x10^{13}$ particles/mL) for 1 hour, then adding 10 uL of 1:1 virus-linker

suspension. Virus ring structures conjugated with gold nanoparticles were adsorbed on carbon coated TEM grids (Ted Pella). For the adsorption, the virus ring containing solution was dropped on parafilm, and one TEM grid was placed on the droplet for 10 minutes. Then, the TEM grid was put on a droplet of water for 2 minutes. Water of the washed TEM grid was soaked by filter paper. TEM grid was observed by JEOL 200CX with an accelerating voltage of 200 kV.

Bifunctional M13 virus

Genetic modification of p9 proteins to yield six histidines caused the length of the M13 virus to become shorter, as observed in AFM images. The length of the virus is proportional to the size of its packaged DNA, the phagemid-based viruses are typically observed to be 300-600 nm in length, shorter than wild type M13 viruses. In this phagemid expression system both wild-type and His_6-pIX were produced and the resulting virus may display between zero and five copies of his tagged p9. The AFM image and the histogram of the measured virus length are shown in Figure 2.2.

Linker Molecule Synthesis

Before observing the nanostructures, synthesis of the linker was verified using Matix Assisted Laser Desorption Ionization Time of Flight (MALDI-TOF) mass spectrometry on a Voyager DE-Star instrument in linear mode. The MALDI data is shown in Figure 2.3. Streptavidin is a tetrameric protein made up of four identical subunits each with a single biotin binding site[25]. The approximate total molecular weight of the streptavidin used was 52.8 kDa, corresponding to a mature truncated form of

streptavidin. The intensity distribution indicated that the streptavidin was fully dissociated into monomer subunits, and momomer, dimer, trimer and tetramer were present, as seen by others[26]. In the case of the NiNTA-streptavidin linker molecule, the peak maximum corresponding to tetramer was shifted by approximately 1.2 kDa, and monomer by about 0.3 kDa. Considering the additional 301.7 Da mass of a single conjugated Ni-NTA, each monomer of streptavidin appeared to have on average one Ni-NTA molecule attached. However, if a stochastic distribution of conjugated products was present, they were not resolved in the mass spectra.

Chapter 2.3 Results & Discussions

Virus Based Ring

The viruses were observed to form a ring structure when the inter distance of each M13 virus in solution was greater than a few times the virus length and the relative concentration of the M13 virus to NiNTA-streptavidin was 1:1 (10^{11} phage/mL: 10^{11} molecules/mL). The bifunctional virus (in 1 mM Tris HCl, 1.5 mM NaCl, pH 7.5) and linker molecule (in H_2O) were stochiometrically combined, mixed by vortexing, and incubated at 23 °C for one day. Figure 2.4 shows Atomic Force Microscopy (AFM) images of virus ring structures on mica substrate observed with a NanoscopeIV (Digital Instruments) in tapping mode. The virus-based rings were found scattered over a large area of the sample. The radii of rings predominantly ranged between 60 nm and 90 nm. The range of circumferences observed corresponded to the size of packagable DNA from the phagemid plasmid and virus genome. Additional engineering of the phagemid system to package a single DNA or of the viral genome to incorporate the modified His_6-pIX gene should lead to a greater monodispersity of ring structures.

The ring formation verifies the successful engineering of the pIII and pIX to generate a bifunctional M13 virus. This to our knowledge is the first engineered bifunctional phage. Other experiments were performed to verify the requirement of the engineered components to form the rings. A monofunctionalized virus displaying only the anti-streptavidin peptide on pIII was stoichiometrically mixed 1:1 with linker (10^{11} phage/mL: 10^{11} molecules/mL). Also, the bifuntional virus was mixed 1:1 with streptavidin lacking the NiNTA modification. Neither of these control samples formed

rings, and only linear viruses were observed by AFM. Thus, modified pIX on the virus and the NiNTA functionalization of the linker were essential to ring formation. Earlier experiments identifying anti-streptavidin peptides displayed on pIII viruses and attaching streptavidin conjugates to such viruses have demonstrated the importance of a displayed peptide for binding streptavidin[19,27].

Ring formation was also observed by Transmission Electron Microscopy (TEM) on a JEL 200CX instrument operating at 200 kV, as shown Figure 2.5a. The darker region of about 5 nm (indicated with the arrow in upper part of ring) was believed to be the linker. The size of the observed ring by TEM was similar to that of the ring structure in AFM image. Antibody labeling was used to enhance the contrast of the virus rings for TEM imaging (Figure 2.5b). A polyclonal pVIII primary antibody was used to bind the major coat of the virus and anti-rabbit IgG secondary antibody conjugated to 10 nm gold nanoparticle was used as the label. The large effective diameter of the antibody conjugated gold particles potentially distorts the size of the observed virus rings. However, ring shaped assembly of gold nanoparticles were observed in the sample.

To form a ring, the two ends of the virus must meet and be held together via the linker molecule. An increase of strain energy and some decrease in entropy would accompany this process. Thermal fluctuation, mechanical forces induced by vortexing or hydrodynamic fluid motion including Brownian motion may contribute to overcoming the required activation energy to bend the virus into a ring. Once formed, the ring structure is believed to be stable due to exceptionally strong binding between the displayed peptides and the linker. In fact, the dissociation constant (K_d) of His_6 to Ni-NTA has been measured at pH 8 to be 10^{-13} M[31]. This is stronger than most antibody

bindings, of which the K_d's range from 10^{-7} M to 10^{-10} M. The binding of streptavidin and anti-streptavidin peptide, with its HPQ biotin-like motif, is expected to be slightly weaker than that of streptavidin and biotin, which has a K_d of 10^{-15} M[32]. Furthermore, avidity effects should strengthen interaction since multiple copies of the binding peptides were displayed at each end of the virus and the linker molecule possesses on average four binding sites for each peptide.

The persistence length of virus has been known to be 2.2 μm by TEM. Persistence length is defined as the length over which correlations in the direction of the tangent are lost, or in another words, the distance we would hypothetically travel from one end of the chain to reach a 90 degrees bend at the opposite end. Therefore, when the length of a macromolecule is much less than its persistent length, its shape could be assumed to be straight, not bent. Therefore, M13 virus has been considered as the straight and rigid biomacromolecule because the length of virus is much less than its persistent length. Total energy was calculated by considering the binding energy between the tips of the virus and linker molecule and the bending energy which is associated with persistence length (λ) and virus length (L). The total energy can be expressed as follows.

$$\Delta G = \Delta E(binding) + \Delta E(bending)$$
$$= -kT \ln \frac{1}{K_d} + \frac{1}{2} kT\lambda \int_0^L \frac{1}{\rho^2(s')} ds'$$

The persistence length was assumed to be 2 or 1.5 μm and the dissociation constant was varied from 10^{-12} to 10^{-15}. The result is shown in Figure 2.6. Neither assumption can verify the formation for the virus-based ring. The result suggests that the persistence length could be much shorter than the previously known data. In fact, recently our group measured the persistence length of virus to be 1.2 μm via a optical trapping method.

This virus-based ring structure is expected to function as a biological template for the nucleation and formation of metalized, magnetic, or semiconductor nanorings using a trifunctionalized virus. Magnetic ring structures have unique magnetic properties[29] and are of interest for use as a magnetic data storage device[30]. Modification of the pVIII with peptides that nucleate ZnS, CdS, or FePt nanowires has already been demonstrated[16,17,28]. Incorporating pVIII display into the bifunctional viruses by changing conditions of virus amplification will enable nucleation and ring formation by the viruses.

Hierarchical assembly of viruses

When the concentration of the virus was high enough for multiple viruses to collide with a linker, linear or radial linkages of viruses were observed. Virus and linker were mixed at a ratio of 10:1 (10^{12} units/mL: 10^{11} units/mL) and imaged by AFM, as shown in Figure 2.6. The resultant structures (Figure 2.6a) can be explained through the presence of multiple binding sites on the linker. NiNTA-Streptavidin was expected to have 4 binding sites for the anti-streptavidin peptide, inferred from the known tetrametric structure of the biotin-streptavidin complex[33]. Additionally as determined by mass spectrometry and shown schematically in Figure 2.6b, each native linker had on average a total of four Ni-NTA ligands and thus multiple binding sites for the His_6 peptides. Binding of anti-streptavidin or His_6 peptide of one virus and anti-streptavidin or His_6 of another virus to the same linker molecule caused M13 virus to arrange linearly as shown in Figure 4b. When the virus concentration (10^{12} phage/mL) is greatly exceeded by linker (10^{13} molecules/mL), all phage displayed binding peptides were seemingly passivated with linker such that viruses remained independentlu. As a result, by simply controlling

the concentration of the virus and the linker in this system, various self-assembling structures were achieved.

Reversible formation of the virus based ring as a switch

Ring formation was designed to be reversible through regulation of His_6 – NiNTA binding via control over free imidazole concentration[34]. The sample was prepared 1:1 virus to linker as in Figure 2.4, then imidazole was added to a final concentration of 50 mM (5 uL virus suspension + 5 uL 100 mM imidazole in H_2O) and samples imaged by AFM (Figure 2.7). Indeed, when imidazole was added to the ring-forming sample (Figure 5a), no rings were observed (Figure 2.7b). Furthermore, addition of biotin to a final concentration of 5 mM (5 uL virus suspension + 5 uL 10 mM biotin in H_2O) to the sample in Figure 5a also produced only linear viruses (Figure 2.7c). Combined, these results demonstrate that ring formation is dependent upon highly specific binding of the virus-displayed peptides to polyhistidine and biotin binding sites on the linker. This and other reversible biomolecular interactions may enable engineered virus to function as a biomolecule based switch, which is similar in concept to a supramolecular switch[35].

Chapter 2. 4 Conclusion

Similar systems may be constructed which genetically incorporate both binding domain and binding site functions directly into the virus. Heterofunctional viruses may allow us to do several things, such as bind or grow different materials in spatially distinct areas, assemble multiple different viruses in specific orders, and regulate specific individual interconnects. We expect that more complex assemblies and arrangements of biomolecules may be achieved by developing additional "directionally interconnecting" components that capitalize upon the diversity and specificity of biomolecular recognition.

Chapter 2.5. References

1. S. Mann, *Biomimetic Materials Chemistry*; VCH: New York, 1996.
2. P. Ball, *Nature* ***413***, 667 (2001).
3. N. C. Seeman, *Nature* ***421***, 427 (2003).
4. C. E. Flynn, S.-W. Lee, B. R. Peelle, A. M. Belcher, *Acta Mater.* (2003)
5. C. M., Niemeyer, M. Adler, S. Gao, L, Chi, *Angew. Chem. Int. Ed. Engl.* ***39***, 3055 (2000).
6. S. Brown, *Nature Biotechnol.* ***15***, 269 (1997).
7. S. R. Whaley, D. S. English, E. L. Hu, P. F. Barbara, A. M. Belcher, *Nature* ***405***, 665 (2000).
8. S. Mann, W. Shenton, M. Li, S. Connolly, D. Fitzmaurice, *Adv. Mater.* ***12***, 147 (2000)
9. S. Nygaard, R. Wendelbo, S. Brown, *Adv. Mat.* ***14***, 1853 (2002).
10. T. Douglas, M. Young, *Nature* ***393***, 152 (1998).
11. W. Shenton, T. Douglas, M. Young, G. Stubbs, S. Mann, *Adv. Mater.****11***, 253 (1999)
12. M. Knez, A. M. Bittner, F. Boes, C. Wege, H. Jeske, E. Mai, K. Kern, *Nano Lett.* ***3***, 1079 (2003).
13. Z. Li, S. W. Chung, J. M. Nam, D. S. Ginger, C. A. Mirkin, *Angew. Chem. Int. Ed. Engl.* ***42***, 2306 (2003).
14. E. Dujardin, C. Peet, G. Stubbs, J. N. Culver, S. Mann, *Nano Lett.* ***3***, 413-417 (2003).
15. S.-W. Lee, C. Mao, C. E. Flynn, A. M. Belcher, *Science* ***296***, 892 (2002).
16. C. Mao, C. E. Flynn, A. Hayhurst, R. Sweeney, J. Qi, J. Williams, G. Georgiou, B. Iverson, A. M. Belcher, *Proc. Natl. Acad. Sci. USA* ***100,*** 6946 (2003).
17. C. E. Flynn, C. Mao, A. Hayhurst, J. L. Williams, G. Georgiou, B. Iverson, , A. M. Belcher *J. Mater. Chem.* **13** (2003)
18. S.-W. Lee, B. M. Wood, A. M. Belcher, *Langmuir* ***19***, 1592 (2003).
19. S.-W. Lee, S.-K. Lee, A. M. Belcher, *Adv. Mater.* ***15***, 689 (2003).
20. C. E. Fowler, W. Shenton, G. Stubbs, S. Mann, *Adv. Mater.* ***13***, 1266(2001).

21. T. Scheibel, R. Parthasarathy, G. Sawicki, X. M. Lin, H. Jaeger, S. L. Lindquist, *Proc. Natl. Acad. Sci. USA* ***100***, 4527 (2003).

22. J. D. Hartgerink, E. Beniash, S. I. Stupp, *Science* ***294***, 1684 (2001).

23. M. Reches, E. Gazit, *Science* ***300***, 625 (2003).

24. B. K. Kay, J. Winter, J. McCafferty, *Phage Display of Peptides and Proteins: A Laboratory Manual*; Academic Press: San Diego, 1996.

25. P. C. Weber, D. H. Ohlendorf, J. J. Wendoloski, F. R. Salemme, *Science* ***243***, 85 (1989).

26. L. Cohen, K. Strupat, F. *J.* Hillenkamp, *Am. Soc. Mass Spectrom.* ***8***, 1046 (1997).

27. J. J. Devlin, L. C. Panganiban, P. E. Devlin, *Science* ***249***, 404 (1990).

28. B. D. Reiss, C. Mao, D. J. Solis, R. Y. Sweeney, K. S. Ryan, A. Aggarwal, T. Thomson, A. M. Belcher, *Adv. Mater* (2004).

29. F. J. Castano, C. A. Ross, C. Frandsen, A. Eilez, D. Gil, H. I. Smith, M. Redjdal, F. B. Humphrey, *Phys. Rev. B* ***67***, 184425 (2003).

30. J. Zhu, Y. Zheng, G. *J.* Prinz, *Appl. Phys.* ***87***, 6668 (2000).

31. J. Schmitt, H. Hess, H. G. Stunnenberg, *Mol. Biol. Rep.* ***18***, 223 (1993)

32. N. M. Green, *Adv. Protein Chem.* ***29***, 85 (1975).

33. W. A. Hendrickson, A. Pahler, J. L. Smith, Y. Satow, E. A. Merritt, R. Phizackerley, P. *Proc. Natl. Acad. Sci. USA* ***86***, 2190(1989).

34. E. Hochuli, *Genet. Eng.* ***12***, 87(1990).

35. J. M. Lehn, Supramolecular *chemistry : concepts and perspectives*; VCH: Weinheim ; New York, 1995.

Figure 2.1 Schematics of the approach (a) Schematic representation of engineered M13 virus. His_6 peptide displayed as pIX fusion shown in red, anti-streptavidin peptide displayed as pIII fusion shown in blue. (b) Tetrameric streptavidin shown in blue conjugated with four nickel-nitrilotriacetic acid (Ni-NTA) groups.

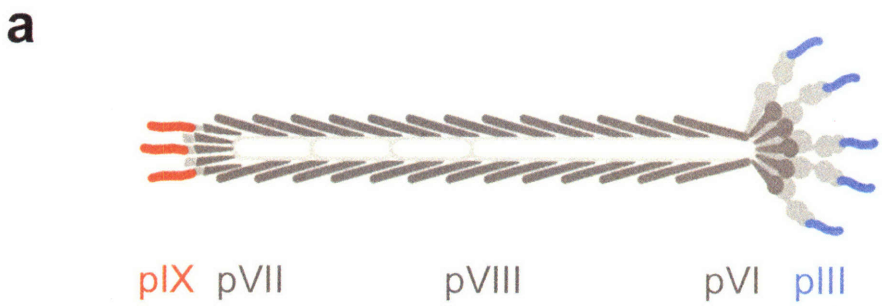

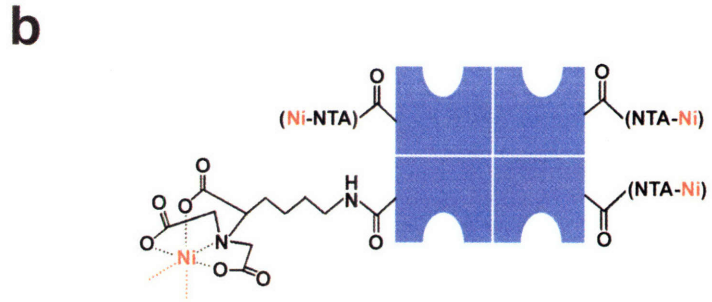

Figure 2.2. AFM image of the engineered virus and histogram of the virus length.

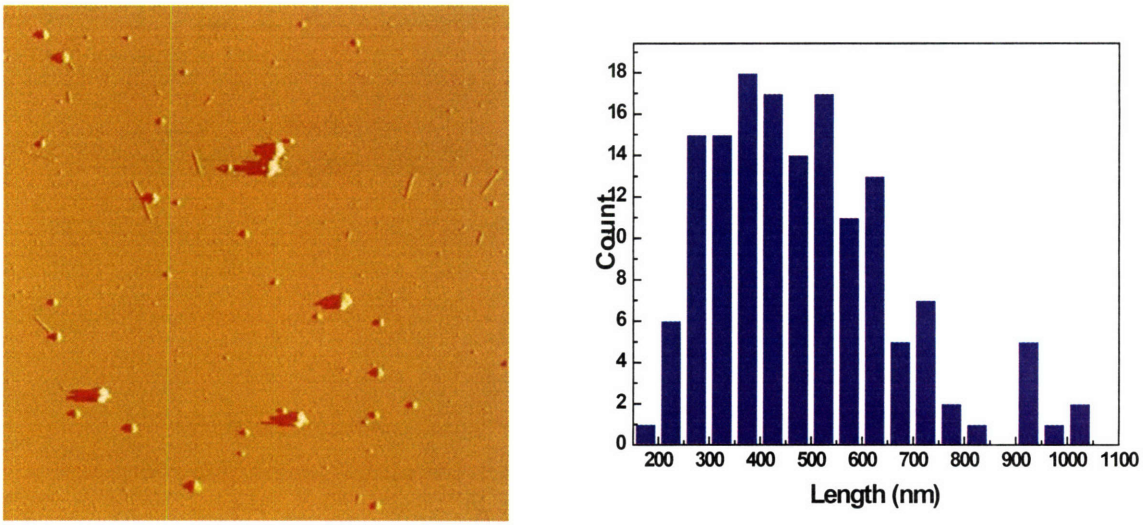

Figure 2.3 MALDI data of linker molecule and streptdavidin.

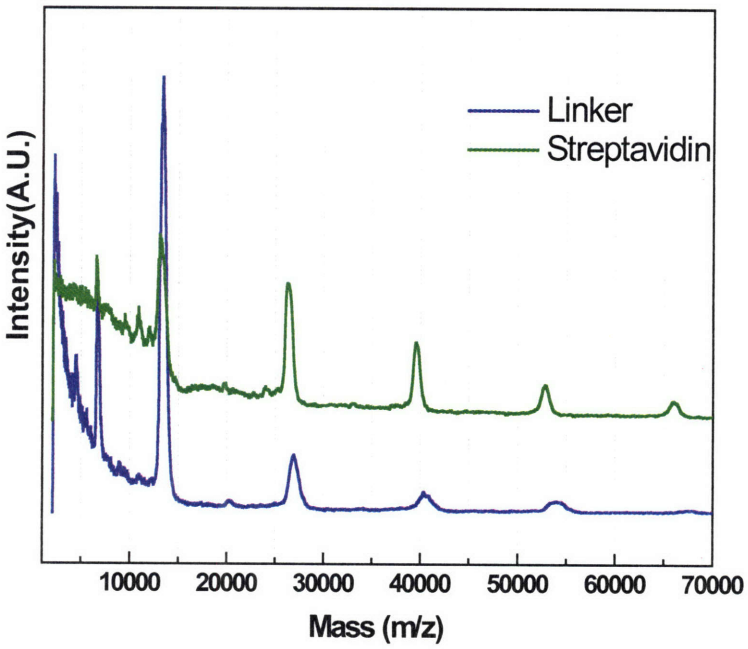

Figure 2.4 M13 virus-based ring structures observed by AFM on mica surface.

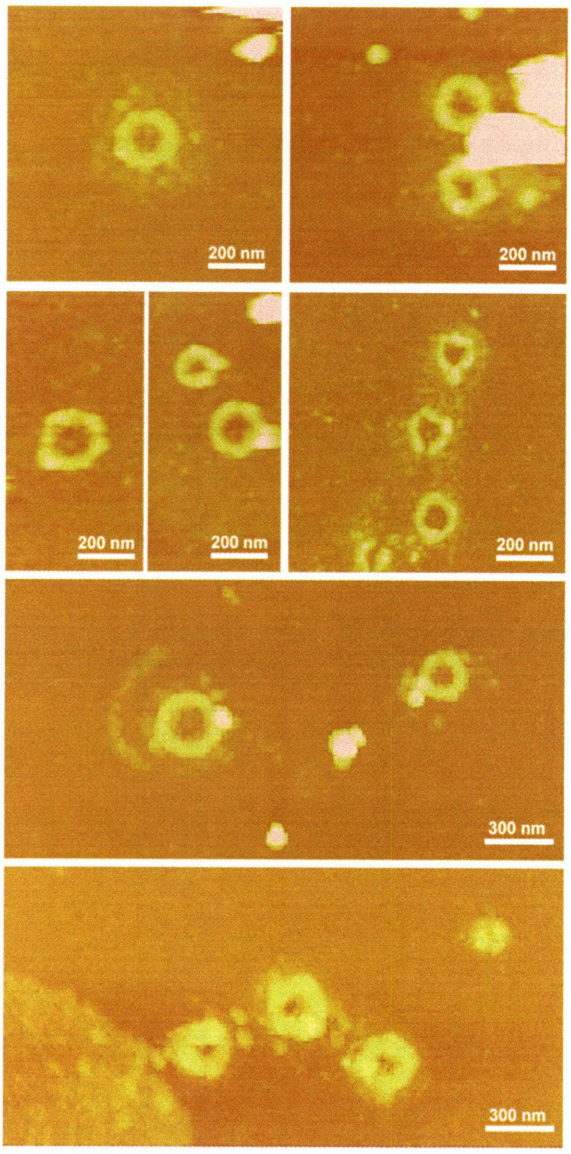

Figure 2.5 TEM image of the virus based ring (a) TEM image of an individual virus-based ring structure stained with 2% uranyl acetate. The arrow indicates the darker region believed to be the linker. (b) TEM image of a virus-based ring structure where virus is labeled with antibody conjugated gold nanoparticles.

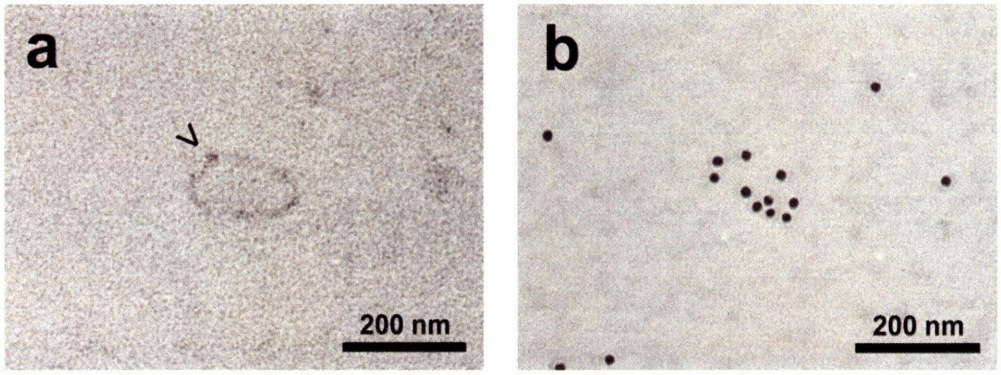

Figure 2.6. The bending energy of the virus based ring and the binding energy between the proteins and the linker molecule.

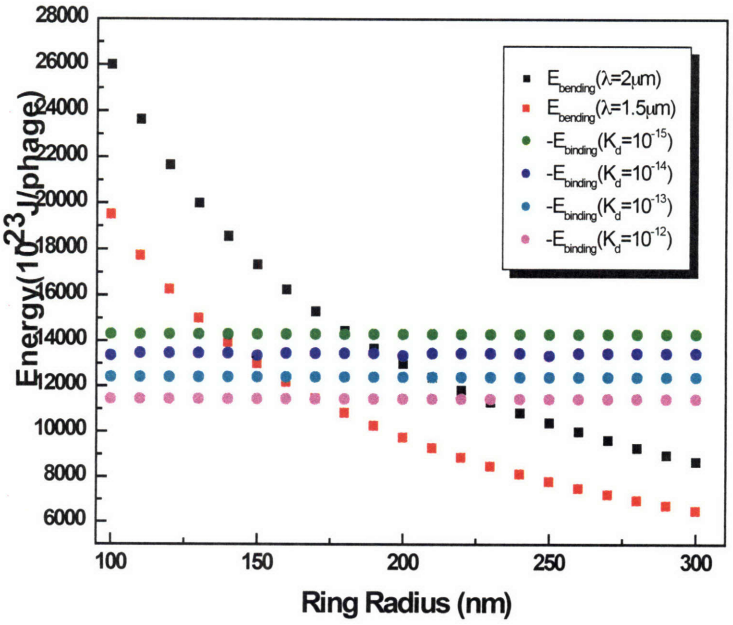

Figure 2.7 AFM image of engineered phage mixed with linker molecule at different stochiometric ratios. At 10:1 virus:linker, (a) radially aggregated viruses and (b) linearly linked viruses were observed.

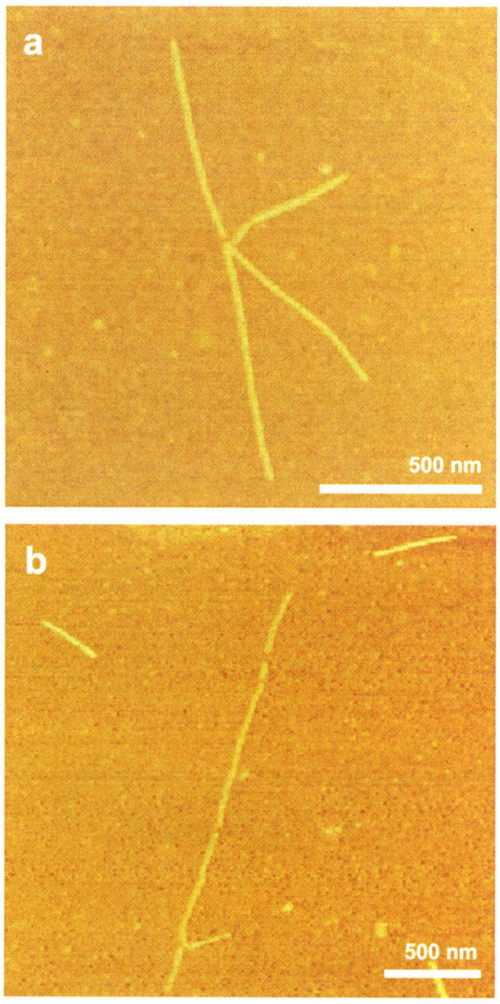

Figure 2.8 Engineered phage mixed 1:1 with linker molecule imaged by AFM. (a) Virus based ring structures were observed. (b) However, after addition of 50 mM imidazole to the same suspension only linear viruses were observed. (c) Linear viruses were also observed with addition of 5 mM biotin to the suspension.

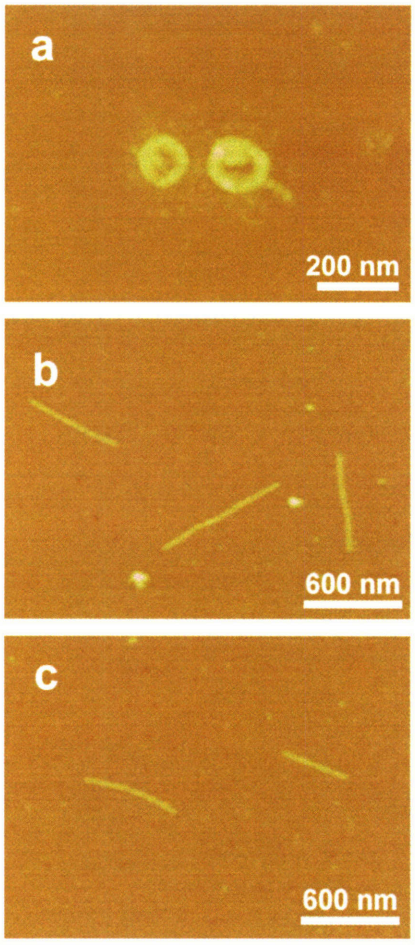

Chapter 3. Spontaneous assembly of viruses on multilayered polymer surfaces

Chapter 3. Summary

This chapter presents the ordering of M13 viruses, highly complex biomacromolecules, driven by competitive electrostatic binding, preferential macromolecular interactions, and the rigid rod nature of the virus systems during alternating electrostatic assembly. The spontaneous formation of a two-dimensional monolayer structure of viruses atop a cohesive polyelectrolyte multilayer was achieved. This viral-assembled monolayer can be a biologically tunable scaffold to nucleate, grow and align nanoparticles or nanowires over multiple length scales. This system represents an interface that provides a general platform for the systematic incorporation and assembly of organic, biological and inorganic materials.

Chapter 3.1 Introduction

Two-dimensional ordering of nanomaterials on a substrate has many potential implications in various applications. Because current integrated circuit devices are patterned in two dimensions, the 2D controllability of nanomaterials is important for integration. Additionally, two dimensionally assembled structures can provide unique optical and magnetic properties as demonstrated by other research groups. If nanowires can be aligned into 2D patterns, the impact would be tremendous in many applications. This ability also would provide a fundamental strategy in designing building blocks to render hierarchical supramolecular self-assembly. This versatility arises from their high geometrical anisotropy (aspect ratio of 10~100) along with unique material properties.

The conventional method to assemble anisotropic materials such as nanowires is Langmuir-Blodgetts assembly. It takes place at the interface of air and water. For the assembly, the surface of the target materials need to be modified to have hydrophobicity for segregation and external forces such as flow, electric field and physical confinement are required for exceeding the critical concentration and improving the ordering. Such requirements sometimes limit the scope the potential applications of the technique.

The required ingredients for ordering nanoscopic to macroscopic systems are the molecular mobility required for dynamics and a thermodynamic or kinetic driving force[1-3]. On a nanoscopic scale, for example, specific covalent interactions within functionalized molecules determine the hierarchical structures of supramolecules[4,5] and a rearrangement process toward equilibrium between chains in block copolymers leads to final phase separated morphologies[6]. On a macroscopic scale, fluidity facilitates

ordering; capillary interactions can produce a complex array of small objects on the water surface[7] and the convective flow of mixed granules leads to granular separation where larger bodies of grain eventually replace smaller ones, a phenomenon called the 'Brazil-nut effect' [8,9]. Electrostatic interactions of repulsion and attraction that are ubiquitous in nature also can be utilized to induce molecular mobility for ordering, exemplified by separations as demonstrated in electrophoresis[10,11], or organization as in biomolecular self-assembly[12,13].

To find a way to assemble the filamentous virus, we turned to biology. The charge driven assembly of filamentous actin protein inspired us to develop a new technique to assembly our anisotropic nano building blocks. Actin is a globular structural protein that polymerizes in a helical fashion to form an actin filament. These form the cyoskeleton. Actin filaments provide mechanical support for the cell and enable cell movement. The responsive and dynamic assembly of actin filaments is important for cell motility. It was also found that the charged linker molecules are playing an important role to determine the assembled structure from nematic to smetic. Generally, for liquid crystalline assembly, the concentration of the target materials should be higher than the critical concentration because the increase in translational entropy should be higher than the decrease in rotational entropy. However, with the help of the charged linker molecules, the charged actin filaments can assemble into the various morphology of liquid crystal even at low concentration. The positively charged molecules can compensate the repulsive interaction of the negatively charged actins and act as a linker whose concentration determine the assembly behavior of actins. The charged driven assembly

that exists in biology inspired the lesson that charge control can induce the ordering of charged biomacromolecules.

In order to control the charge, an electrostatic layer-by-layer assembly technique (LBL) was adopted. LBL allows the adsorption of multiply charged species to create nanometer scale films that form an effective ionically crosslinked network. The use of LBL enables the creation of ultrathin functional films and highly tunable surfaces through the control of electrostatic interactions. Layer-by-layer assembly and deposition construct the polyelectrolyte multilayer of charged polymers. During the deposition, a suitable substrate is dipped back and forth between baths of positively or negatively charged polyelectrolyte solutions. During each deposition, the charged polyelectrolyte is adsorbed and the surface charge is reversed. The main advantages of polyelectrolyte multilayer are the ability to coat conformably, the low cost, and the environmentally benign process.

For a polymeric pair for LBL assembled film, we used linear polyethylenimine (LPEI) as a cation and polyacrylic acid (PAA) as an anion. This pair exists as weakly charged state in solution, thus the degree of ionization of the polymeric chains can be readily manipulated by pH of the solution. Noticeably, there is strong molecular interdiffusion in this pair driven by mobile free chains of LPEI, as confirmed by the superlinear growth in film thickness during LBL deposition. Therefore, a mobile nature of cationic LPEI species can be directly employed for inducing the surface mobility of negatively charged M13 viruses.

We discovered that the electrostatically induced interdiffusion between weakly charged polyelectrolytes drives the separation and 2D liquid crystal (LC) ordering of virus particles during alternating electrostatic assembly with complementary

polyelectrolytes. The idea that randomly arranged supermolecular species incorporated in a network medium can ultimately create ordered structures at the surface may be counterintuitive. However, such order can be accommodated by regulating dynamic and equilibrium driving forces. We present the ordering of M13 viruses, highly complex biomacromolecules, driven by competitive electrostatic binding, preferential macromolecular interactions, and the rigid rod nature of the virus systems during alternating electrostatic assembly. The steric constraints inherent to the competitive charge binding between M13 viruses and two oppositely charged weak polyelectrolytes leads to interdiffusion and the virtual "floating" of viruses to the surface. The result is the spontaneous formation of a two-dimensional monolayer structure of viruses atop a cohesive polyelectrolyte multilayer. In addition, because the genome of the M13 virus is easy to manipulate, the virus can be coded to grow and assemble specific inorganic materials, thus forming an ordered array of self-assembling nanowires. We demonstrate that this viral-assembled monolayer can be a biologically tunable scaffold to nucleate, grow and align nanoparticles or nanowires over multiple length scales. This system represents an interface that provides a general platform for the systematic incorporation and assembly of organic, biological and inorganic materials.

In addition to the floating induced ordering virus, it was also discovered that viruses themselves assemble through liquid crystalline ordering on the polymeric surface of polyelectrolyte multilayers. Viruses are directly captured on the charged surface of the patterned polymeric template via electrostatic attraction and then ordered into closely packed monolayer structures through the subsequent mobility provided by underlying PEM patterns. Leveraging the ordering mobility directly from the patterned template

provides excellent advantages in that target molecules can be spontaneously organized into highly ordered and densely packed structures without any help from external flow or additional chemical functionality.

Chapter 3.2 Experimental

LBL film assembly

LPEI (25,000 M_W and 250,000 M_W) (Polysciences) and PAA (90,000 M_W, 25% aqueous solution) (Polysciences), were used as received and prepared as 0.02 M solutions based on the repeat-unit molecular weight in Milli-Q water. The pH of the LPEI and PAA solutions of weakly charged polyelectolytes were adjusted to 5.0. LPEI/PAA multilayer thin films were made by conventional LBL method by using a HMS programmable slide stainer (Zeiss). For the floating induced ordering, 3.5–5.5 bilayers of LPEI/PAA were applied on the silicon substrate. To produce a relatively thick layer of film (usually thicker than 100 nm), more than 10.5 bilayers of LPEI/PAA were deposited. In order to make a free standing film (Fig. 5a), 80.5–100.5 bilayers of LPEI/PAA were prepared on the Teflon-AF (DuPont) coated silicon substrate.

M13 virus assembly

The viruses were dissolved in water to have a diluted concentration (10^{10} phages / ml) and the solution pH was adjusted by adding 0.01 M HCl or 0.01 M NaOH. Then, 1 ml of the virus solution was dropped on the prepared LBL films of LPEI/PAA (2 cm × 4 cm). After incubation for 30 minutes, virus assembled film was rinsed with Milli-Q water and dried by blowing with nitrogen.

M13 virus genetic engineering

The p8 library was constructed by fusing eight random amino acids into the N-terminus of all the 2700 copies of the p8 proteins. It provides a random population of 10^7–10^8. Through the use of general biopanning technique by exposing the p8 libraries to GaN, the peptide sequences which have the binding affinity for GaN was evolved and identified. After each round of selection and washing, the tightly bound phage clones were eluted with low pH and amplified using bacterial medium (*Escherichia coli* strain ER2738, New England Biolabs).

Surface Characterization

The virus-ordered surface was characterized with AFM (Digital Instruments, Dimension 3100) in tapping mode at an amplitude set point of 0.8 V under dry condition. In order to obtain high-resolution images, supersharp silicon probe (Pacific Nanotechnolog, SSS-NCH) were used to capture the image. Height and phase images were taken at scanning rates of approximately 1.5 Hz.

Vapor-assisted capillary force molding:

PDMS molds were fabricated by thermal casting prepolymer (Sygard 184, Dow Corning) against complimentary relief structures of silicon master prepared by a photolithographic method. For thermal curing of the PDMS molds, a 1:10 ratio of curing agent and the PDMS prepolymer were mixed and incubated at 70 °C for 3 hrs. Cured PDMS molds were then peeled from the master and cut into desired sizes. For a vapor-assisted capillary molding, prepared sample of LPEI/PAA film was placed in a mildly heated humid chamber (70~80 °C, 100% relative humidity) for 0.5 hr to soften the film

prior to contact with PDMS mold. Then, the PDMS mold was placed onto the vapor-soaked polymeric film with a slight pressure of a few bars to promote the capillary molding. After 2 hrs of molding, the PDMS mold was detached from the sample surface and the replicated patterns of polyelectrolyte multilayer were left on the surface. To remove very thin layers of polymer under mold contact regions, the patterned surface was treated with 30 sec of plasma cleaning.

Chapter 3.3 Results & Discussions

The electrostatic layer-by-layer assembly technique (LBL) allows the adsorption of multiply charged species to create nanometer scale films that form an effective ionically crosslinked network[14-16]. The use of LBL enables the creation of ultrathin functional films and highly tunable surfaces through the control of electrostatic interactions; the assembly process has the added advantage of strong compatibility with biomolecular species without loss of biological function. We chose to use this assembly process as a means of incorporating genetically engineered M13 virus particles to create cohesive thin films, thus allowing the coupling of virus functionality and thin film characteristics such as conductivity, electrochemistry, and biodegradability depending on choice of polyion[17]. Although such multilayer systems are generally considered random, kinetically frozen networks, the complete rearrangement of the films examined here can be induced through interdiffusion of polyelectrolytes during adsorption. Remarkably, the competitive interdiffusion that usually leads to disorder and disruption in electrostatically assembled thin films, is harnessed to achieve spontaneous ordering of virus particles during the assembly process; this finding is particularly surprising given the high molecular weight nature of this viral macromolecule (about 14,000,000 M_w).

Linear-polyethylenimine (LPEI, 25,000 M_w), which is widely accepted as a biocompatible polymer[18], was used as the polycationic building block and anionic polyacrylic acid (PAA, 90,000 M_w) was used as a counter ion[19]. Recent investigations have revealed that reversible interdiffusion can take place within LBL's consisting of certain pairs of weak polyelectrolytes; such multilayers typically exhibit the characteristic

of superlinear growth[20,21]. We have found that the LPEI/PAA polyelectrolyte pair is a strong candidate for this interdiffusion behavior (Fig. 3.1a), and also exhibits good film processibility due to its ultra-flat surface roughness during deposition (mean roughness less than 1 nm). The M13 virus is a filamentous and negatively charged virus[22]. The inherent monodispersity and anisotropic nature of the M13 virus inspired us to extend our successful realization of a 3D liquid crystal solution at high concentration to a large area two-dimensional thin film surface assembly. Additionally, the different locations of proteins (Fig. 3.1b, p3 and p8 coat) on viruses and programmable protein functionalities via genetic engineering make viral systems an attractive toolkit for synthesis and assembly of nanoparticles and nanowires[23,24]. The proteins at pIII in the head group and pVIII around the capsid body of virus can be genetically engineered to have specific function with biological or inorganic materials. The virus structure was constructed from the crystal structure of p8 protein (Protein Data Base No.:1ifj). In particular, the recent advances in modifying the major coat protein of the virus enables us to facilitate peptide interactions with inorganic ions for further biomineralization, as well as the control of surface charge density of the virus[25].

This interdiffusion-induced viral assembly process is schematically depicted in Figure 3.2a. Negatively charged M13 viruses are randomly deposited on the positively charged top surface of very thin LPEI/PAA multilayers (less than 10 nm) by electrostatic interactions (step 1). The PAA competes with the viral macromolecule for more favourable electrostatic interactions with LPEI, driving a separation process that forces the virus to the surface (step 2). Finally, mutually repulsive interactions due to the liquid-crystalline behaviour between virus molecules induce a spontaneous ordering process on

the surface that results in an ordered viral monolayer structure (step 3, Fig. 3.2c). In figure 3.2c, viruses are initially adsorbed on 4.5 bilayers of LPEI/PAA (Hereafter, it will be denoted as $(LPEI/PAA)_n$, n is a deposition number) under the same pH condition, then additional $(LPEI/PAA)_{5.5}$ layers are deposited onto the virus and promote the ordering of virus. Some aspects of this process have analogies, interestingly, to Langmuir-Blodgett assembly techniques, which are driven by hydrophobic interactions[26,27]. However, the use of the polyelectrolyte-biomacromolecule interface used here offers many advantages over techniques exploiting air-water interfaces. In particular, because our biomolecules are easily manipulated at the DNA level to produce the desired chemical functionality, there is no need to attach a specific functionality for hydrophobicity, charge or segregation. Simple modifications in the DNA sequence allow us to manipulate the intrinsic charge properties of the constituents, which yields an additional degree of tunability in this system. In addition, the layer-by-layer adsorption process has been shown to be easily scalable up to meter length scales, in contrast to the more difficult manipulation of materials at liquid-air interfaces. In conventional polyelectrolyte multilayer (PEM) systems, strong charge binding between ion pairs yields an ionically crosslinked network in which the mobility of polymer chains is significantly limited; in such cases, the intermixing or diffusion of polyions[20] within the interior of the PEM film during multilayer construction is not facilitated. Adsorption of a charged virus monolayer within such a system would only generate irreversible charge binding and lead to a randomly stacked virus layer (Fig. 3.2b), which is similar to the case of stacked single-wall carbon nanotube layer within PEM film[28]. Images are 3×3 μm^2 (Inset illustrates the magnified image of 800×800 nm^2) and *Z*-range is 30 °. When one of the

polyelectrolytes is able to interdiffuse into the multilayer, however, it is possible to "unlock" these electrostatic crosslinks through competitive interactions.

To investigate this interdiffusion and ordering process, we monitored the buildup process for a series of polyelectrolytes atop an already adsorbed viral stack (Fig. 3.3). A thin base polyelectrolyte multilayer (less than 5 nm thick) was first deposited onto a silicon substrate; onto this multilayer, viruses were directly adsorbed from a dilute buffer solution. Finally, LPEI and PAA were alternately adsorbed on top of the viral layer using the same adsorption conditions as for the base layer, and the topography of the thin film was monitored systematically with increasing deposition number using tapping mode atomic force microscopy. It is clear that the originally adsorbed viral layer is highly disordered (Fig. 3.3a). When the first LPEI layer is deposited atop these viruses, it appears that some of the viruses are able to diffuse to the surface through the top LPEI layer (Fig. 3.3b). On the contrary, counter-ionic PAA deposition completely blankets the virus particles, resulting in a structure in which the viruses are buried under the surface (Fig. 3.3c). This process implies that LPEI plays a key role in driving the interdiffusion where it diffuses into the underneath of virus layer during LPEI deposition and it diffuses out to the overlaying virus layer and forms globular complex with PAA during PAA deposition. Accordingly, when LPEI is once again adsorbed, interdiffusion and complexation exchange processes between LPEI and PAA chains both at the surface and throughout the interior of the film take place, leading to the freeing of more viral particles from the original adsorbed layer within the film. This alternating process of preferential complexation, displacement of viruses and repeated deposition of polyelectrolyte increases the surface concentration of the virus, driven by competitive electrostatic

interactions (Figs. 3.3d and 3.3e). Interestingly, after each deposition, the number of "floating" viruses freed from the PEM matrix and accumulated at the surface is increased, and the size of the PAA globules becomes larger after each PAA adsorption step because the number of free chains of LPEI that can participate in the interdiffusion process increases, yielding an exponentially growing thin film[21]. Finally, after the deposition of additional layers, the viruses form a close-packed monolayer (Fig. 3.3f).

Stepwise AFM observations indicate that LPEI is the mobile species within the film that drives the interdiffusion through its preferential binding with PAA versus the virus coat. More importantly, it enables the direct visualization of the interdiffusion process within the PEM down to the nanometer thickness regime. In this case, the viruses act as effective tagging agents, which can be compared with the conventional fluorescence labeling and confocal microscopy technique relevant to micrometer scale systems[20]. Separate ongoing work in our group with dye-conjugated LPEI also supports the fact that LPEI can undergo interdiffusion during the adsorption process in the construction of LPEI/PAA multilayer thin films[29]. The reasons for preferential charge binding with PAA as opposed to the negatively charged viral coats might be considered due to differences in charge density and chain conformation. At approximately pH 5, the charge density of the capsid body of the M13 virus ($1 \sim 1.5$ e^- / subunit)[30,31] is lower than the surface charge density of LPEI ($3 \sim 4$ e^- / nm)[32]. This mismatch in charge distribution between LPEI and the virus molecules, as well as steric constraints introduced by the rigidity of the virus that restrict the ability to maximize charge-charge contacts, result in competitive exchange of the virus with PAA. To test the concept of LPEI as the mobile species, and examine the impact of molecular chain size on interdiffusion based on

polymer dynamics using the generalized reptative polymer chain model[33], we replaced the LPEI used in the above experiments with LPEI with ten times higher molecular weight (250,000 M_w). The reduced mobility of the larger molecular weight LPEI species resulted in the effective blocking of chain interdiffusion by LPEI within the PEM, and thus the virus could not effectively undergo the spontaneous ordering process during assembly.

The mesophase ordering of the viruses at the top surface is entropically driven and electrostatically regulated. Generally, in solutions of highly concentrated viruses, liquid crystalline ordering such as smectic or nematic phases are induced by the entropic excluded-volume (depletion) effect because the interparticle potential is dominated only by "steric hard-rod repulsion" [22,34,35]. However, in our case, electrostatic interactions between the viruses and the PEM also contribute to the entropic ordering process by compensating or shielding the overall repulsive charge between viruses. Similar ordering processes for charged species were reported experimentally in the ordered complexation in DNA/liposome system by x-ray scattering analysis[36] and theoretically in the responsive LC behavior of actin filaments in the cytoskeleton[37]. To maximize the entropic state of the viruses and their electrostatic attractions with the underlying PEM, the virus molecules arrange in non-overlapping, close packed monolayer structures with optimized order. The random initiation and non-directional propagation of ordering ultimately leaves topological defects (Figs.3.2c and 3.3f)[38]. The typical singularity defects of LC disclinations were observed; Möbius defects of strength $s = \pm 1/2$ and spiral defects of $s = \pm 1$. The removal of these ordering defects and unidirectional orientation of the viruses by application of an external shear force is also being investigated. The

major coat protein sequence (p8) of the virus and the pH of the virus solution can manipulate the surface charge of M13 virus, determining the assembly behaviour. Dramatic potential changes of the virus within a narrow pH region (Fig. 3.4a) enables us to control the initial number of disordered adsorbed viruses, which results in final ordering densities ranging from 1 to 100 viruses / μm^2 (Figs. 3.4b–4d). For zeta potential measurement, each point of potential value was obtained by averaging 10 measurements. In figure 3.4b-4d, $(LPEI/PAA)_n$ was deposited at pH 5.0 and viruses were adsorbed at different pH values. Densely close packed structure as shown in **b** (pH 4.8, 60 viruses / μm^2), the loosely packed in **c** (pH 5.15, 25 viruses / μm^2) and the sparsely ordered in **d** (pH 5.5, 10 viruses / μm^2) can be obtained because the stronger repulsive interaction at higher pH results in less adsorbed viruses.

Inorganic crystal nucleation or nanoparticle binding from the two dimensionally ordered virus scaffold enables the assembly of dense, highly ordered and nanostructured hybrid monolayers even on free-standing polymer films (Fig. 3.5a), which is a prerequisite for the realization of practical devices in nano-electronics, magnetics and optics. To illustrate the versatility of this system we assembled nanowire-monolayers that were composed of a noble metal, a transition metal and semiconductor material. Three strategies were used for the formation of these nanowire arrays. The first was utilization of the electrostatic interactions for binding cationic nanoparticles to a negatively charged virus layer. The second involved peptide-mediated biomineralization of metal ions. The third involved phage selected from a 100 % display library for a peptide sequence on the viral coat that was specific to bind to GaN. To date, biomolecular scaffolds such as DNA, lipids and proteins have been used to fabricate

nanowires or arrays of nanoparticles[39-41], which act as individual building blocks. However the potential of these systems is limited in part due to difficulties in organizing the individual blocks over large length scales and limitations in the variety of inorganic materials that can be used.

Figure 3.5b shows that 5 nm cationic Au nanoparticles were arrayed along the M13 virus scaffold when the virus scaffold was modified to express a tetraglutamate sequence as an N terminal protein fusion (p8). The same tetraglutamate M13 virus was used to nucleate cobalt nanowires by incubation of cobalt ions with the 2D ordered virus scaffold, followed by reduction with $NaBH_4$ (Fig. 3.5c). The carboxylic acid side chain of glutamic acid is capable of binding positive cobalt ions by an ion exchange mechanism. To form GaN monolayers (Fig. 3.5d), we used the method of phage selection from a random octamer peptide display p8 library. We have previously shown that M13 phage virus display can be used to specifically bind nanobiological materials[23,42]. A solution of GaN nanoparticles was incubated with GaN specific phage in a 2D ordered array resulting in a densely packed film of GaN wires. The GaN virus nanowire film was imaged with AFM and maintains the fluorescent properties of the GaN nanoparticles.

An advantage of this method is that it can provide a tool for the construction of quantitatively scalable and functionally controllable biomolecular surfaces on this flexible polymer film. The film thickness can be varied from 10 nm to tens of microns. In addition, the polyelectrolyte multilayer film can be doped with broad range of materials, from conducting and redox active polymers to biologically compatible materials. The flexibility, variety of inorganic materials that can be grown, and the low

cost of synthesis and assembly of these materials systems will enable many potential technological applications, including chemical and biological sensors, power devices, and catalytic reactive membranes. Applications that we are currently investigating include the synthesis and assembly of thin film electrode materials on ionically conductive multilayers form light weight, flexible, Li ion batteries, solar cells and light emitting diodes.

Figure 3.6 shows the schematic illustration and the representative result of direct virus assembly (Figs. 3.6C and D), which is fundamentally inspired by the previous method of interdiffusion-induced virus ordering. The motivation of this development arises from one simple question. If one could utilize the polymeric interdiffusion in axial z-direction for the ordering of virus molecules, it can also be applicable to the lateral plane of x,y-directions due to the isotropic nature of molecular diffusion. When charged virus molecules are applied on a very thin layer of oppositely charged surface of PEM (less than 10 nm) as presented in Fig. 3.6A, they are electrostatically bound but frozen on the surface due to the lack of surface mobility, which arised from their bulk (thickness of virus ~ 7 nm) in comparison with the underlying film thickness (Fig. 3.6B). In the previous study, additional deposition of polyelectrolytes is needed to induce polymeric interdiffusion in the z-direction and to provide the mobility for viruses for further monolayer assembly. Alternatively, when being applied on a relatively thick layer of PEM (usually thicker than 100 nm) as depicted in Fig. 3.6C, it is anticipated that the increased surface mobility of underlying polymer can directly drive the ordering of viruses (Fig. 3.6D). The underlying PEM can thus provide molecular mobility as well as electrostatic affinity for ordered viral assembly.

The result of the direct assembly is a densely packed monolayer structure of viruses as shown in Fig. 3.6D. Surface adsorbed viruses are vigorously mobile on the polyelectrolyte multilayer and spontaneously rearrange to form a closely packed monolayer structure, with aid from their inherent liquid-crystalline nature. This ordering proceeds until the electrostatic equilibrium between the charged viruses and polymeric surface is reached. Above the equilibrium point, the excess virus molecules supplied by solution is automatically excluded from surface binding due to the electrostatic repulsion with pre-assembled viruses, which enables the quantitative control over assembly density depending on the surface charge density of virus molecules. As compared to the previous method described earlier in this chapter, this technique is advantageous because it allows an independent procedure in LBL deposition and virus incorporation for a final ordered structure. Therefore, by utilizing the patterned structures of PEM as a template for selective binding, it is possible to accomplish the construction of a patterned assembly of viruses in a reliable way.

The virus patterning was also successfully demonstrated by vapor assisted capillary force molding. Detailed observation by atomic force microscope (AFM) on the virus assembled PEM pattern shows that viruses can be uniformly ordered into a monolayer structure as shown in Fig. 3. We demonstrated two types of representative patterns (line in Fig. 3A and dot in Fig. 3B), which are potentially useful for the construction of high density interconnected or arrayed structures in electronic and biological applications. Swollen by virus solution during virus assembly process, as discussed earlier, PEM patterns were deformed to have rounded curvatures, leading to the formation of cylindrical waves of line patterns and checkerboard-like droplets of dot patterns (Figs. 3A

and B). Interestingly, the shape of the individual dot shows volcano-like droplet instead of hemi-spherical one that was expected for an ideal swelling case. It was attributed to the relatively high surface-to-volume ratio of the dot pattern in the original PDMS mold, which caused the swelling-induced (or drying-induced, in reverse) stress and consequent surface wrinkles around the center of the pattern. Phase mode AFM images in Figs. 3A and B reveal that the virus molecules are selectively collected on the patterned PEM surface with a well-ordered monolayer structure. Closer observation on the images shows minimal non-specific adsorption of viruses on the silicon substrate between patterns.

Chapter 3.4 Conclusion

In this chapter, the spontaneous ordering of M13 viruses on the polyelectrolyte multilayer was demonstrated. Inspired by the charge driven assembly in biology, this approach provides a new method for the assembly of anisotropic nanomaterials. This approach also offers a new platform to utilize the interfaces of polymers, biomacromolecules, and inorganic materials. By utilizing the interdiffusion phenomena of oppositely charged polymers, the mobility of the viruses could be enhanced in polymer matrix, resulting in two-dimensional liquid crystalline ordering. This newly developed ordering mechanism could lead to interesting new technologies including self-assembled electrochemical devices and biosensors.

Chapter 3.5 References

1. G. M. Whitesides , B. Grzybowski, *Science* **295**, 2418 (2002).
2. T. Shinbrot, F. J. Muzzio, *Nature* **410**, 251 (2001).
3. P. Ball, *The Self-Made Tapestry: Pattern Formation in Nature* (Oxford, New York, 2001).
4. J. D. Hatgerink, E. Beniash, S. I. Stupp, *Science* **294**, 1684 (2001).
5. S. Park, J. H. Lim, S. W. Chung, C. A. Mirkin, *Science* **303**, 348 (2004).
6. F. S. Bates, G. H. Fredrickson, *Phys. Today* **52**, 32 (1999).
7. N. Bowden, A. Terfort, J. Carbeck, G. M. Whitesides, *Science* **276**, 233 (1997).
8. H. M. Jaeger, S. R. Nagel, R. P. Behringer, *Rev. Mod. Phys.* **68**, 1259 (1996).
9. M. E. Möbius, B. E. Lauderdale, S. R. Nagel, H. M. Jaeger, *Nature* **414**, 270 (2001).
10. M. J. Gordon, X. Huang, S. L. Pentoney, R. N. Zare, *Science* **242**, 224 (1988).
11. J. Han, H. G. Craighead, *Science* **288**, 1026 (2000).
12. C. M. Niemayer, *Angew. Chem. Int. Ed.* **22**, 4128 (2001).
13. G. M. Whitesides, J. P. Mathias, C. T. Seto, *Science* **254**, 1312 (1991).
14. G. Decher, *Science* **277**, 1232 (1997).
15. F. Caruso, R. A. Caruso, H. Möhwald, *Science* **282**, 1111 (1998).
16. Z. Tang, N. A. Kotov, S. Magonov, B. Ozturk, *Nat. Mater.* **2**, 413 (2003).
17. P. T. Hammond, *Adv. Mater.* **16**, 1271–1293 (2004).
18. S. C. De Smedt, J. Demeester, W. E. Hennink, *Pharm. Res.* **17**, 113 (2000).
19. D. M. DeLongchamp, P. T. Hammond, *Chem. Mater.* **15**, 1165 (2003).
20. C. Picart,*et al. Proc. Nat. Acad. Sci. USA* **99**, 12531 (2002).
21. P. Lavalle *et al. Macromolecules* **35**, 4458 (2002).
22. M. Adams, Z. Dogic, S. L. Keller, S. Fraden, *Nature* **393**, 349 (1998).
23. S. W. Lee, C. Mao, C. E. Flynn, A. M. Belcher, *Science* **296**, 892 (2002).
24. C. Mao *et al. Science* **303**, 213 (2004).
25. Y. Huang *et al. Nano Lett.* **5,** 1429 (2005).
26. D. Whang, S. Jin, Y. Wu, C. M. Lieber, *Nano Lett.* **3**, 1255 (2003).
27. P. Yang, *Nature* **425**, 243 (2003).
28. A. A. Mamedov *et al. Nat. Mater.* **1**, 190 (2002).

29. N. Zacharia, D. M. DeLongchamp, M. Modestino, P. T. Hammond (in preparation).

30. K. R. Purdy, S. Fraden, *Phys. Rev. E* **70**, 061703 (2004).

31. K. Zimmermann, H. Hagedorn, C. C. Heuck, M. Hinrichsen, H. Ludwig, *J. Biol. Chem.* **261**, 1653 (1996).

32. R. Mészáros, L. Thompson, M. Bos, P. de Groot, *Langmuir* **18**, 6164 (2002).

33. T. P. Russell *et al. Nature* **365**, 235 (1993).

34. J. Herzfeld, *Acc. Chem. Res.* **29**, 31 (1996).

35. Z. Dogic, S. Fraden, *Phys. Rev. Lett.* **78**, 2417–2420 (1997).

36. J. O. Rädler, I. Koltover, T. Salditt, C. R. Safinya, *Science* **275**, 810 (1997).

37. I. Borukhov, R. F. Bruinsma, W. M. Gelbart, A. J. Liu, *Proc. Nat. Acad. Sci. USA* **102**, 3673 (2005).

38. H. R. Brand, P. E. Cladis, H. Pleiner, *Macromolecules* **25**, 7223 (1992).

39. M. G. Warner, J. E. Hutchinson, *Nat. Mater.* **2**, 272 (2003).

40. S. Mann *et al. Science* **261**, 1286 (1993).

41. M. M. Murr, D. E. Morse, *Proc. Nat. Acad. Sci. USA* **102**, 11657 (2005).

42. S. R. Whaley, D. S. English, E. L. Hu, P. F. Barbara, A. M. Belcher, *Nature* **405**, 665 (2000).

Figure 3.1 **Materials used in this study. a**, A sketch of superlinear thickness growth in LPEI/PAA layer-by-layer assembly system. b, Schematic presentation of engineered M13 virus and its functional groups.

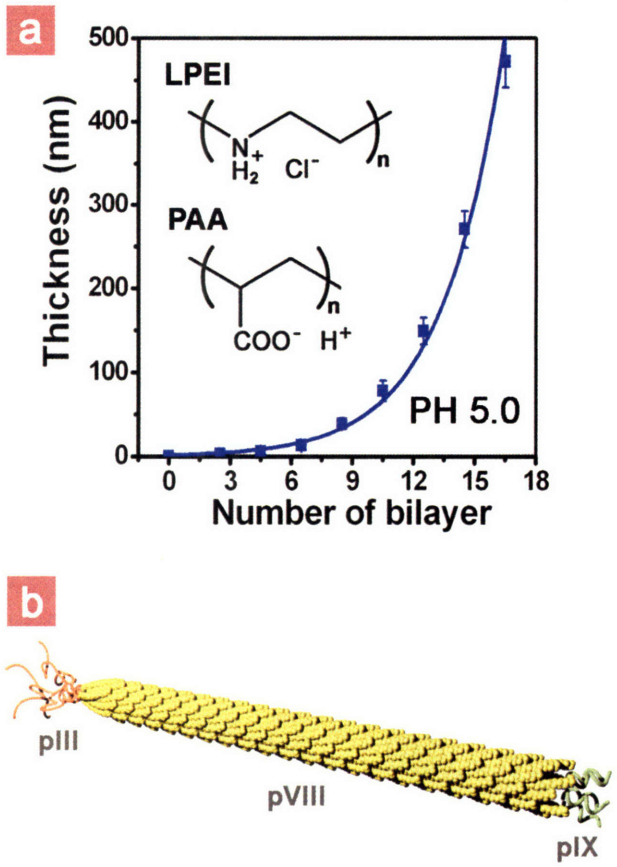

Figure 3.2 A schematic strategy of viral monolayer assembly and AFM demonstration of disordered state and the ordered monolayer state of M13 virus. **a**, An experimental procedure for monolayer assembly of M13 virus on the polyelectrolyte multilayer of LPEI/PAA. **b**, Phase mode atomic force microscopy (AFM) image of randomly stacked and aggregated structure of M13 viruses on 5.5 bilayers of strong PEM of polydiallylamine hydrochloride and polystyrene sulfonate. **c**, Phase mode AFM image of closely-packed monolayer of M13 virus on weak PEM (deposited at pH 5.0) of LPEI and PAA.

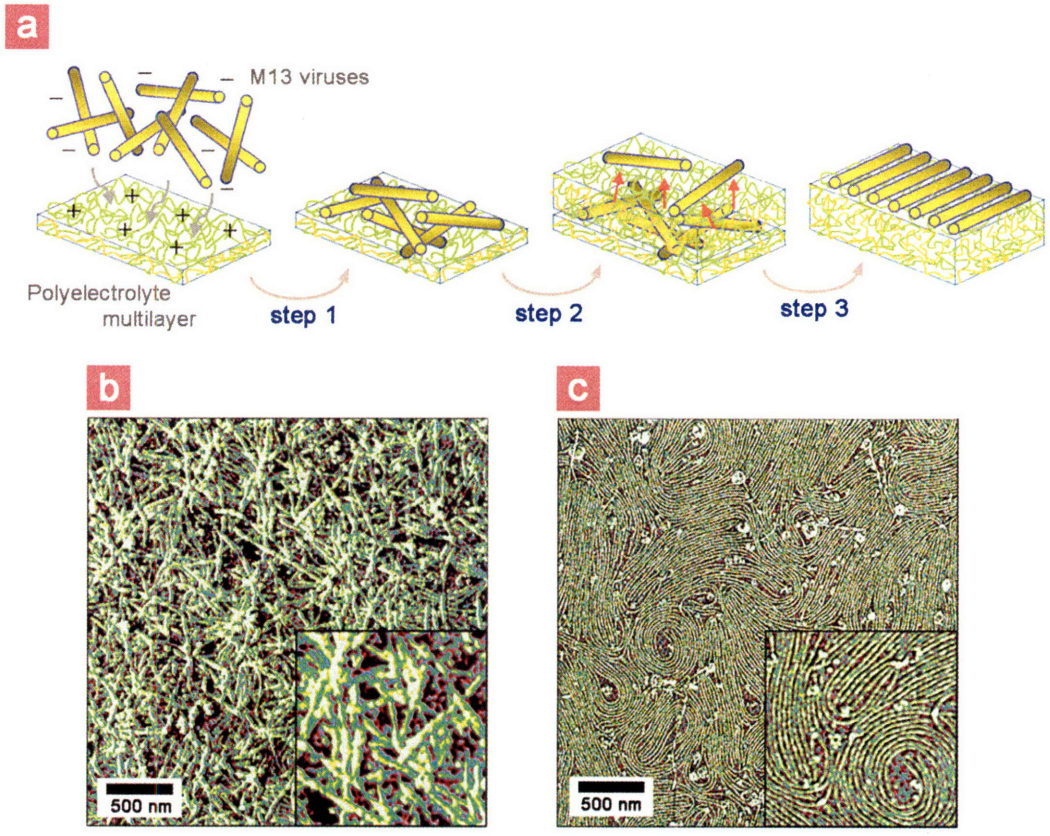

Figure 3.3 A series of images to investigate the interdiffusion process in the LPEI/PAA system. 1.5 × 1.5 μm^2 height mode AFM images are presented (*Z*-range: 20 nm). All of species are deposited at pH 5.0. **a**, Initial disorderly adsorbed viruses on $(LPEI/PAA)_{3.5}$. **b–e**, Alternating depositions of LPEI and PAA onto the prepared virus layer of **a**. **f**, After additional deposition of $(LPEI/PAA)_{4.5}$ onto the surface of **e**. Highly ordered and closely-packed monolayer of M13 virus is obtained on the surface.

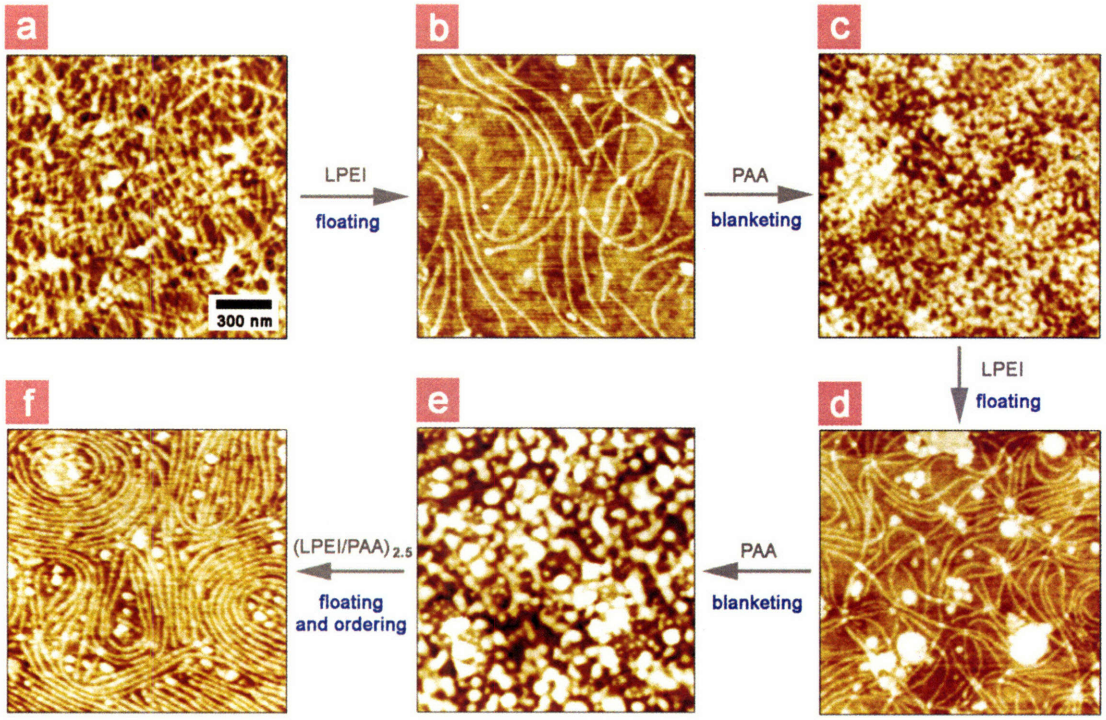

Figure 3.4 Density control in an electrostatically regulated viral monolayer. **a**, Zeta potential-pH dependence of M13 virus and a brief description for the assembly behaviour of the floated virus on top of PEM. **b–d**, Phase mode AFM images for 1.0 × 1.0 μm^2 size (*Z*-range: 30 °).

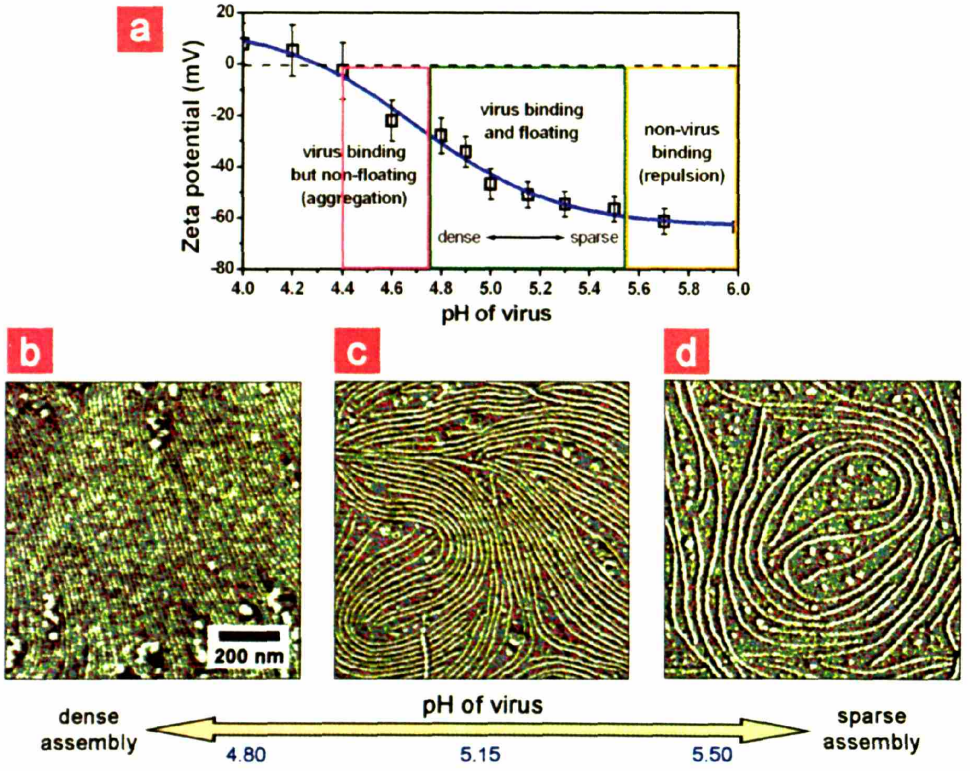

Figure 3.5 Demonstration of templated biomineralization on virus monolayer. The size of phase mode AFM images in **a**, **b**, **c** is 1.5 × 1.5 μm^2 and *Z*-range is 30 ° (Inset shows the magnified image of 400 × 400 nm^2). **a**, Assembled virus monolayer template for growing materials. Viruses are assembled at pH 5.1 on a $(LPEI/PAA)_{100.5}$ flexible free standing film. **b**, AFM and transmission electron microscope (TEM) images of gold nanoparticles attached virus monolayer. 5 nm cationic gold particles were incubated on negatively charged M13 virus. Inset shows the alignment of particles along the M13 virus. Gold attached viruses were collected for TEM imaging by dissolving the substrate polymer layer. **c**, AFM and TEM images of cobalt nucleated virus nanowires. The nucleation of cobalt increased contrast in the phase mode AFM image. Inset AFM image shows that cobalt coated virus is about 16nm in width, which is nearly two times the width of virus in **a**. **d**, AFM (5 × 5 μm^2) and fluorescence images of the GaN virus nanowire films.

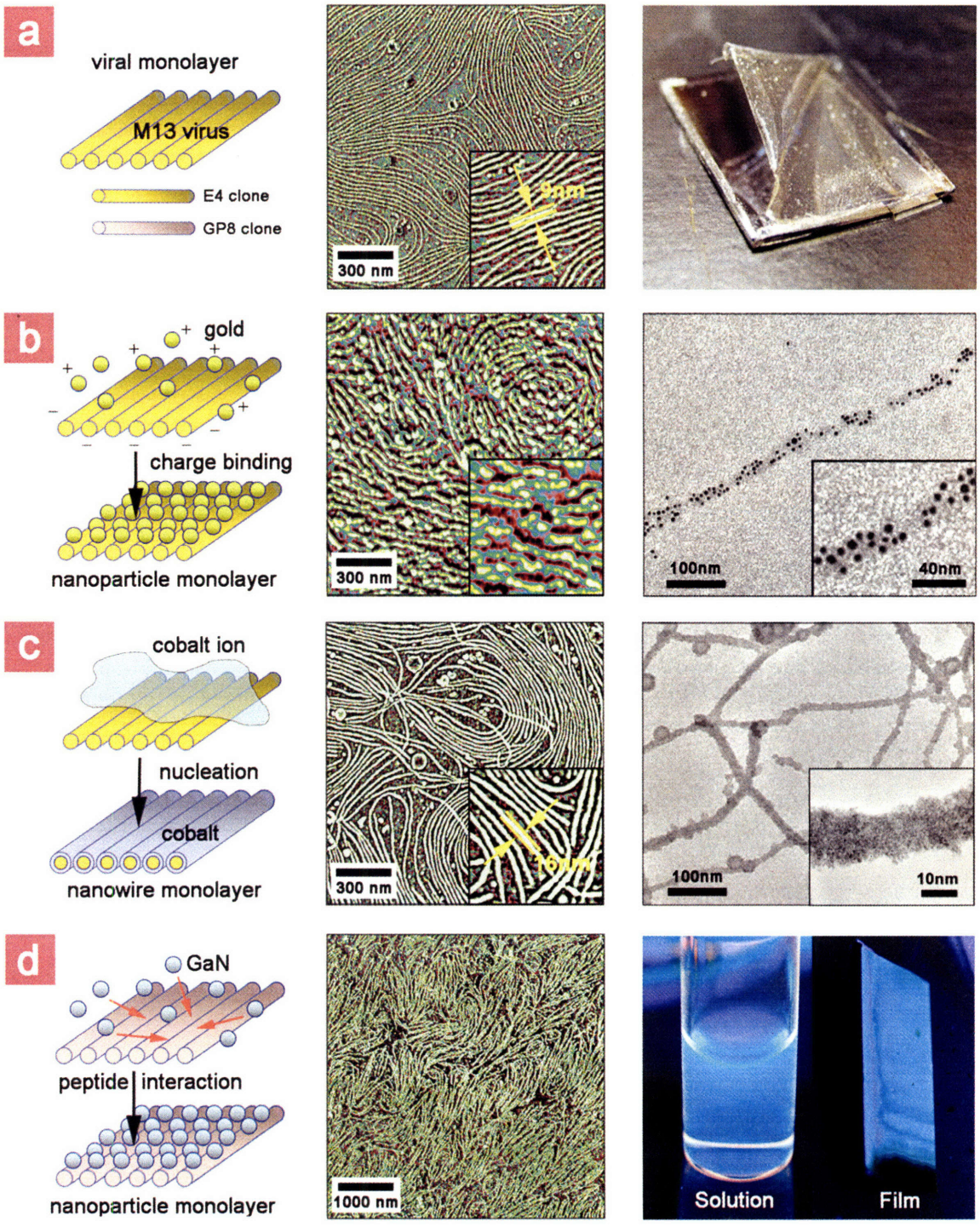
a
viral monolayer
M13 virus
E4 clone
GP8 clone
9nm
300 nm
b
gold
charge binding
nanoparticle monolayer
300 nm
100nm
40nm
c
cobalt ion
nucleation
cobalt
nanowire monolayer
300 nm
100nm
10nm
d
GaN
peptide interaction
nanoparticle monolayer
1000 nm
Solution
Film

Figure 3.6 Comparison between low-mobility and high-mobility surface of polyelectrolyte multilayer on virus adsorption and ordering. (A) Scheme for random virus adsorption on very thin and mobility-deficient PEM surface. (B) Height-mode atomic force microscopic (AFM) image for A (scan size = 3×3 μm^2, *Z*-range = 20 nm). Viruses are adsorbed on 3.5 bilayers of LPEI and PAA of 8 nm thickness. (C) Scheme for directly ordered viral assembly on relatively thick and mobility-rich PEM surface. (D) Height-mode AFM image for C (scan size = 3×3 μm^2, *Z*-range = 5 nm). Viruses are adsorbed on 10.5 bilayers of LPEI and PAA of 130 nm thickness.

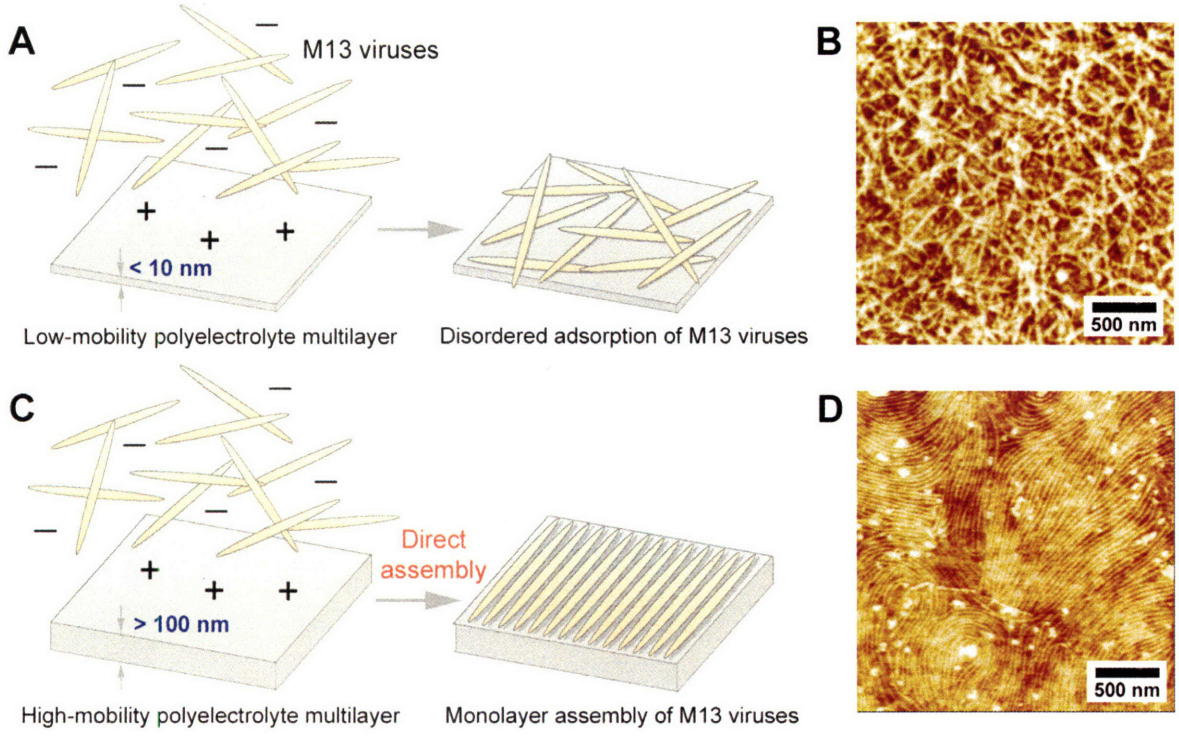

Figure 3.7 AFM images of patterned assembly of viruses on mobility-enhanced polyelectrolyte multilayer template. (A, B) Assembled viruses on 1.5 μm line-and-space pattern in A and 1.5 μm spaced dot array in B. Three-dimensional AFM image (top, scan size = 6×6 μm^2, *Z*-range = 300 nm) and magnified phase-mode AFM image (bottom, scan size = 3×3 μm^2, *Z*-range = 40 degrees) are presented and insets of yellow line indicate the cross-sectional contour of each of patterns. (C) Phase-mode AFM image of highly aligned viruses at 1.5 μm line-and-space pattern (scan size = 2×2 μm^2, *Z*-range = 40 degrees). (D) Phase-mode AFM image of randomly ordered viruses at 1.0 μm line-and-space pattern (scan size = 3×3 μm^2, *Z*-range = 40 degrees).

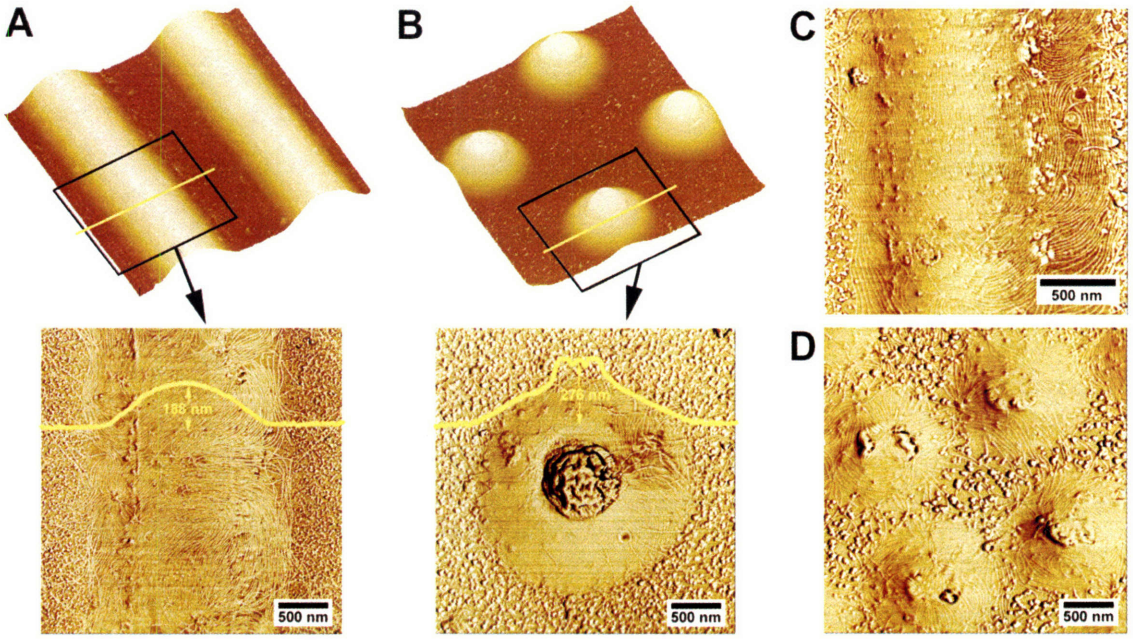

Chapter 4. Virus enabled synthesis and assembly of nanowires for lithium ion battery electrodes

Chapter 4. Summary

The virus enabled synthesis and assembly of nanowires as negative-electrode materials for lithium ion batteries is presented in this chapter. The expression of cobalt ion binding peptides on the filamentous coat of M13 bacteriophage viruses facilitates the fabrication of homogenous Co_3O_4 nanowires at room temperature. Furthermore, genetically incorporating gold binding peptides for the engineering of hybrid Co_3O_4 nanowires containing gold nanoparticles resulted in improved battery capacity. Combining the virus templated synthesis at the peptide level and our methods for the control of two dimensional assembly of viruses on polyelectrolyte multilayers provides a systematic platform for integrating these nanomaterials to form thin, flexible Li ion batteries. This chapter describes a biological approach involving biotemplating and biological self-assembly that can improve battery properties.

Chapter 4.1 Introduction

The environmental concern about air pollution from car emissions and the economic aspects about the increasing oil price are calling for the replacement of modern cars with hybrid and electric cars. However, the use of these alternative, environmentally benign cars is hindered by the limited performance of their power sources. For example, electric cars use nickel cadmium or lead acid batteries, which have low energy density and limited cycle life. In addition, nickel cadmium or lead acid batteries are detrimental to the environment and pose health hazards. Therefore, it is necessary to develop advanced energy storage devices with higher power and capacity than currently available, using environmentally benign materials. A promising solution for electric vehicles is the use of lithium ion batteries that are highly desirable in terms of cost, energy efficiency, weight and volume. In fact, lithium ion batteries have been widely used in small portable devices such as mobile phones, laptop computers, and handheld electronics. However, their performance characteristics need to be further improved before they can be used to power motor vehicles in addition to small devices. We need lightweight and high-power batteries that can continue to deliver the current for longer time.

A great number of research initiatives have been conducted to develop a high performance battery; however, several challenges still remain. One of the biggest challenges is associated with the synthesis of electrode materials. The intrinsic property of the cathode and anode materials determines the most important characteristics of a lithium ion battery including the cell voltage, the cell capacity and the cell stability. Therefore, to date, much works has been focused on discovering new compositions for electrochemically active materials. Yet, researchers have also realized that the

morphology and texture of the materials are also very critical factors. There is also growing evidence that nanostructured materials can improve electrochemical properties. However, it has been difficult to synthesize homogeneous nanomaterials with controlled texture using currently available technique.

Another concern is related to the assembling batteries. Building batteries, like building many things, requires precise assembly. The smaller the battery, the more challenging the assembly. Current manufacturing techniques involve arranging nanoparticles, nanotubes, or nanowires on surfaces using expensive, high-temperature methods. With current assembly techniques, more than half the weight and size of batteries come from supporting materials that contribute nothing to storing energy; and this leads to decreased energy density, a vital quality for batteries. A lack of energy density - the amount of charge a battery of a given size can usefully carry - is what has hampered development of electric cars, since existing batteries are generally too heavy and too week to compete with gasoline as an energy source.

The advent of nanoelectronics and the resulting need for Li ion batteries of corresponding size are driving the development of nanoscale components and methods for their assembly. Nanodimensional materials, such as nanoparticles, nanotubes [1,2] and nanowires[3], as well as several assembly methods, using lithography, block copolymer[4], or layer-by-layer deposition [5], have been introduced for constructing dimensionally small batteries. Vacuum technology based synthesis or solution based synthesis of nanomaterials have been developed and investigated intensively over the last decade. The synthesized nanomaterials could be assembled using a variety of methods. A top-down approach based on lithography and etching is the typical strategy and a bottoms-up

approaches based on self-assembly has been applied here to construct the dimensionally small battery. In addition to their utility in nanoelectronics, there is also growing evidence that nanostructured materials can improve the electrochemical properties of Li ion batteries compared to their bulk counterparts[6]. For example, according to the recent report, TiO_2 nanowires presents better electrochemical properties including higher capacity though exact mechanism is still under investigation. Additionally, it has been reported that the nanostructure of electrodes can improve the rate capability of the battery because the diffusion path of Li ion can be shortened by the nanostructure, resulting in an increase of diffusion kinetics. In fact, interdigitated structures of cathode and anode are considered to be the ideal structures where a larger surface area of each electrode can be exposed to its counter electrode and less volume of electrolyte is required so that the energy density of battery can be maximized. Many experimental results suggest that a nanostructured battery can present near-ideal battery properties. However, the potential disadvantages of nanomaterials for bateries should be considered and overcome through appropriate solutions. Previous research reports the harmful effects of nanomaterials on battery characteristics. In particular, it has been reported that nanostructured electrodes can dissociate and degrade the liquid electrolyte by catalytic reactions, resulting in the decrease of the battery's long-term stability.

Therefore, in order to attain this maximum potential and minimize the possible disadvantage of nanomaterials, monodisperse, homogeneous nanomaterials and hierarchical organization control are needed. The controlled synthesis of uniform nanomaterials as well as the development of new methods to assemble the synthesized nanomaterials is important. Thus we set out to explore the possibility of implementing

biotemplating and biological self assembly for battery electrode synthesis and their assembly in Li ion batteries. As a solution, we demonstrate the technological advantage of biologically inspired designs for synthesizing and assembling lithium ion battery electrode through the use of a multifunctional virus template.

Bio-systems have inherently developed very specific molecular recognition patterns that can be manipulated through genetic control and can be used to exert molecular scale control over inorganic materials nucleation, growth, and stability, analogous to the process of biomineralization[7-9]. Furthermore, due to the remarkable capability[10-13] of biological molecules to self assemble at multiple length scales, the opportunity exists for designing novel nanomaterials via genetic modification and then constructing the hierarchically assembled structures for Li ion batteries. Here we demonstrate the technological advantage of biologically inspired design for nanostructured Li battery electrodes by utilizing the genetically engineered M13 bacteriophage virus as a multimaterial template and scaffold. As parent abalone shells inherit the genetic information for shell growth to children abalone shells, we have given genetic information (DNA) to M13 viruses to fabricate Li ion battery. The schematic of our idea is described in Figure 4.1. As reviewed in Chapter 1, harvesting energies produced by biological systems can be effective when inorganic nanomaterials are conjugated with biomolecules at specific positions. Therefore, our study of the interface between inorganic materials and peptides can provide the foundation for the bio-energy harvesting research. To realize our idea, we have chosen the M13 virus as a model system.

The M13 virus was exploited to template the growth and assembly of nanomaterials for lithium battery electrodes (Figure 4.2). The M13 virus consists of approximately 2700 major coat proteins (p8) helically wrapped around its single stranded DNA, and of minor coat proteins (p3, p6, p7, and p9) at each end of the virus. The functionality of these subunit proteins can be modified specifically through additions in the M13 genome. Modification of the major coat proteins as well as minor coat proteins at the virus ends has been successfully demonstrated to form functional heterostructured templates for precisely-positioned nanomaterials[14,15]. Furthermore, the intrinsically anisotropic virus structures are well-suited for the growth of monodisperse, highly crystalline nanowires[16] and promising as elements of well ordered nanostructure as demonstrated in 3D liquid crystal film [17,18] . Here, we demonstrate the first 1) synthesis of virus-templated cobalt oxide, Co_3O_4, nanowires for electrodes (Fig. 4. 2A), 2) synthesis of hybrid Au-Co_3O_4 nanowires electrodes (Fig. 4.2 B) and 3) virus based self assembly of a Li ion battery utilizing electrostatic layer-by-layer assembly (Fig. 4.2 C). Co_3O_4 was chosen as one of a family of new lithium-active compounds with extremely large reversible storage capacity arising from displacement reactions [19], approximately three times larger than the capacity of carbon-based anodes currently used in commercial batteries.

Predictive based design was used for engineering the virus to satisfy the multifunctional purpose of electrode formation and assembly with a polymer electrolyte for the Li ion battery (Fig. 4.2). Tetra-glutamate (EEEE-) was fused to the N-terminus of each copy of the major coat p8 protein with one hundred percent expression. This clone, named the E4 clone, was designed with three distinct purposes. First, it can serve as a

general template for growing nanowires through the interaction of the glutamate with various metal ions, in our case, cobalt ion (Virus Biotemplating in Fig. 4.2). Carboxylic acid, the side chain of glutamate, binds positive metal ions via ion exchange, as demonstrated in polymeric templates [20]. Glutamate is also believed to be important in biomineralization, as evident in its role in specific proteins that regulate the nucleation of biominerals in nature. Second, tetra-glutamate acts as a blocking motif for the gold nanoparticles, due to the electrostatic repulsion between negatively charged glutamate and negatively charged gold nanoparticles (Protein Engineering in Fig. 4.2). A previous study [21] revealed that the existence of glutamate in peptide sequences decreased the binding affinity to gold films while hexa-glutamate had no interaction with gold films. Therefore, tetra-glutamate reduces non-specific gold nanoparticle binding to phage, thereby increasing the specificity of a gold specific peptide to bind gold in low concentration, which is necessary for realizing hybrid nanowires of gold nanoparticles and cobalt oxide. Lastly, the E4 clone is ideally suited for electrostatically driven assembly with a charged polymer (Assembly Engineering in Fig. 4.2). E4 is more negatively charged than wild type virus, enabling a favorable interaction with the positively charged electrolyte polymer. Zeta potential measurements of the E4 clone reveal a dramatic potential change between pH 4.5 and pH 5.5, thus enabling a certain degree of charge control.

Chapter 4.2 Experimental

Genetic engineering of M13 virus

To display tetraglutamic acid (-EEEE) on the n-terminus of the p8 protein on M13 bacteriophage (producing so-called E4 phage), a small DNA duplex encoding the amino acids was made using an oligonucleotide 5'-CTACTACAAGGATCCTCCTCCT CCTCTGCAGCGAAAGACAGCA-3' and the extension primer, 5'-GATGCTGTCTTTCGCTGCAG-3'. The duplex was digested with *Pst*I and *Bam*HI and ligated into M13SK phage vector, and confirmed by DNA sequencing.

Virus templated Co_3O_4 nanowires synthesis

E4 virus was incubated with cobalt chloride aqueous solution for at least 30 minutes at room temperature to promote the binding of cobalt ions to the engineered virus. The concentration of E4 viruses was changed from 10^{11} phage / ml to 10^{13} phage / ml and cobalt ion concentration was changed from 1 mM to 10 mM. Depending on the relative concentration of M13 viruses and cobalt ions, different morphologies of cobalt oxide nanowires were observed. For the typical experimental condition, 100 μl of E4 viruses (10^{12} phage / ml) were incubated with 1 mL of 1 mM $CoCl_2 \cdot 6H_2O$ for 1hr. Then, 1 mL of 5 mM $NaBH_4$ was added and the solution was kept at room temperature for the further oxidation of nanowires. When the concentration of $NaBH_4$ was between 5 mM and 10 mM, similar results were obtained.

Transmission electron microscopy observation of virus templated nanowires

For the characterization of virus-templated nanowires by transmission electron microscopy, the nanowires were adsorbed on carbon coated copper grids. 20 μl of the sample solutions was dropped on a TEM grid for 20 minutes. After the incubation, in order to remove excess ions, the grids were put on water droplets of 50 μl for 2 minutes. These washing steps were repeated two times. The remained water was soaked using filter papers and the grid was dried in air for a few hours. The samples were observed by JEOL 200 CX or JEOL 2010. For the high-resolution images, JEOL2010 was used.

Electrochemical evaluation of virus templated nanowires

For electrochemical evaluation of the cobalt oxide nanowires, positive electrodes were prepared by mixing together the virus-based nanowires, Super P™ (MMM Carbon, Belgium) carbon black, and poly(vinylidene fluoride)-hexafluoropropylene (PVDF-HFP) binder in a mass ratio of 74: 15:11. Swagelok™ design cells using Li metal foil used as the negative electrode and a separator film of Celgard™ 2400 were assembled and saturated with the electrolyte, 1M $LiPF_6$ in ethylene carbonate and dimethyl carbonate (1:1 by volume). The assembled cells were galvanostically cycled between 3.0 V and 0.01 V using a MACCOR automated tester.

Virus assembly on the polyelectrolyte multilayer

LPEI (25,000 M_W and 250,000 M_W) (Polysciences) and PAA (90,000 M_W, 25% aqueous solution) (Polysciences), were used as received and prepared as 0.02 M solutions based on the repeat-unit molecular weight in Milli-Q water. The pH of the LPEI and PAA solutions of weakly charged polyelectolytes were adjusted to 5.0. LPEI/PAA

multilayer thin films were made by conventional LBL method by using a HMS programmable slide stainer (Zeiss). In a typical film assembly, 3.5–5.5 bilayers of LPEI/PAA were applied on the silicon substrate. In order to make a free standing film, 80.5–100.5 bilayers of LPEI/PAA were prepared on the Teflon-AF (DuPont) coated silicon substrate.

The viruses were dissolved in water to have a diluted concentration (10^{10} phages / ml) and the solution pH was adjusted by adding 0.01 M HCl or 0.01 M NaOH. Then, 1 ml of the virus solution was dropped on the prepared LBL films of LPEI/PAA (2 cm × 4 cm). After incubation for 30 minutes, virus assembled film was rinsed with Milli-Q water and dried by blowing with nitrogen.

The virus-ordered surface was characterized with AFM (Digital Instruments, Dimension 3100) in tapping mode at an amplitude set point of 0.8 V under dry condition. In order to obtain high-resolution images, supersharp silicon probe (Pacific Nanotechnolog, SSS-NCH) were used to capture the image. Height and phase images were taken at scanning rates of approximately 1.5 Hz.

Electrochemical measurement of virus nanowires monolayer

Cobalt oxide nanowires were grown on an assembled virus monolayer. The virus monolayer on the polyelectrolyte was dipped in cobalt chloride solution (1mM) and a solution of $NaBH_4$ whose volume is the same with cobalt chloride solution was added. When the concentration of $NaBH_4$ was 2 mM, uniform growth of cobalt oxide along the length of viruses was observed.

For the electrochemical measurement, 100 nm of Cu, which functions as a current collector, was deposited by E-beam evaporation on the assembled Co_3O_4 nanowires/polymer layer. This assembly was then tested in Swagelok^{TM} cells using a Li foil negative electrode separated from the multilayer by a liquid electrolyte dipped separator. . To prevent the oxidation of Cu after the deposition of Cu in vacuum, the sample was rapidly transferred to a glove box for the assembly of the battery. In fact, we could not observe the contribution of CuO in charging/discharging curve. The mass of cobalt oxide on the polymer is 22 $\mu g/cm^2$ measured by ICPMS.

Chapter 4.3 Results & Discussions

Virus-templated Co_3O_4 nanowires electrodes

Successful genetic engineering of E4 virus was confirmed by DNA sequencing. E4 virus is more negatively charged than wild type virus because it has more carboxylic acid group in its major coat p8 proteins. Zeta potential measurements confirmed that the E4 virus is more negatively charged. The titer curve shown in Figure 4.3 also supports that E4 virus has more carboxylic acid groups. For the titer curve, the pH of the virus solution was decreased by adding HCl. The pH was measured with the addition of droplets of 1M NaOH. In case of E4, more NaOH need to be added in order to reach the same pH value. After successful genetic engineering, cobalt oxide nanowires were synthesized using E4 viruses. To design the cobalt oxide nanowires electrodes, the E4 virus templates were incubated in aqueous cobalt chloride solution (1 mM) for at least 30 min at room temperature to promote cobalt ion binding[22]. As shown in Figure 4.4, the mass spectrum acquired by matrix assisted laser desorption/ionization (MALDI) confirmed that cobalt was bound with p8 proteins of E4 clones. MALDI spectrum data indicates that cobalt ions are bound to the engineered major coat proteins containing four carboxylic acid groups. Following reduction with $NaBH_4$ and spontaneous oxidation in water, monodisperse, crystalline cobalt oxide (Co_3O_4) nanowire were produced[23]. Figures 4.5A and 4.5B show transmission electron microscopy (TEM) images of the virus templated Co_3O_4 nanowires, where Co_3O_4 nanocrystals of 2~3 nm in diameter were uniformly mineralized along the length of the virus. The high resolution TEM electron diffraction pattern and lattice spacing (Fig. 4.5B) along with XRD confirms that the

crystal structure is Co_3O_4. The Figure 4.5B inset shows that the measured lattice spacing corresponds to the planes of Co_3O_4. The measured lattice spacing corresponds to the (311) and (400) planes of Co_3O_4. XRD data shown in Figure 4.6 also confirms that the crystal structure of the virus-templated nanowires is Co_3O_4. Because p8 proteins were genetically engineered with one hundred percent expression and cobalt ions have a strong binding affinity to the carboxyl groups of glutamate, homogeneous and high crystalline nanowires were synthesized. In order to study the detailed mechanism of nucleation and growth of cobalt oxide on a virus template, the kinetics was observed as shown in Figure 4.7. At two minutes after adding $NaBH_4$, the virus was not fully covered by nucleated cobalt particles. According to electron diffraction patterns, the crystal structure was not yet cobalt oxide. After 10 minutes, the nanowires became thicker and the morphology became smooth. Finally, after a few hours of incubation in water, the reduced cobalt particles were spontaneously oxidized resulting in the cobalt oxide nanowires. Furthermore, viral Co_3O_4 nanowires had a large surface area of 141.7 m^2/g as measured by the Brunauer-Emmett-Teller (BET) method as shown in Figure 4.8. Contrary to E4 viruses, solutions of wild type virus expressing no peptide insert or solutions without viruses formed irregular and large precipitates of Co/Co_3O_4 mixtures. Therefore, this biologically inspired, room-temperature, aqueous synthesis technique using the engineered viruses is both environmentally benign and has the potential for rapid synthesis.

Before evaluating the electrochemical properties of viral nanowires, the electrochemical property of viruses was tested. Samples of virus alone were deposited onto Cu foil current collectors, dried, and assembled into lithium half-cells. The sample

preparation and test procedure was precisely the same as with the Co_3O_4 nanowires. Cyclic voltammetry was conducted between the voltage range 0-3V, and the viruses exhibited no sign of decomposition, as seen in the data Figure 4.9. The only electrochemical activity detected was a trace signal associated with surface oxide on the Cu foil. Thus we conclude that the virus is remarkably stable over the electrochemical conditions of our tests, and by extension, in real-world lithium battery environments.

For electrochemical evaluation of the cobalt oxide nanowires, positive electrodes were prepared by mixing together the virus-based nanowires, Super P™ (MMM Carbon, Belgium) carbon black, and poly(vinylidene fluoride)-hexafluoropropylene (PVDF-HFP) binder in a mass ratio of 74: 15:11. Swagelok™ design cells using Li metal foil used as the negative electrode and a separator film of Celgard™ 2400 were assembled and saturated with the electrolyte, 1M $LiPF_6$ in ethylene carbonate and dimethyl carbonate (1:1 by volume). The experimental procedure are schematically described in Figure 4.10. The assembled cells were galvanostically cycled between 3.0 V and 0.01 V using a MACCOR automated tester. Voltage/capacity curves (Fig. 4.11 A) for the Co_3O_4/Li half cell showed similar behavior to Co_3O_4 nanoparticles produced by other methods. The larger first-insertion capacity compared to that in subsequent discharge is characteristic of this material, and is due to irreversible reactions occurring upon initial lithiation. Any biphasic nature[24] of Co_3O_4 and $Li_xCo_3O_4$ ($\sim Li_{1.47}Co_3O_4$) at the early stages of discharge was not clearly evident from the voltage traces (Fig. 4.11A). We observed reversible capacity (Fig. 4.11B) ranging from 600 to 750 mAh/g, which is about twice that of current carbon-based negative electrodes. The charge and discharge capacities stabilized at 600 mAh/g over 20 cycles. The reversible formation of Li_2O accompanying the redox

of cobalt nanoparticles and the reversible growth of a gel-like polymeric layer[25], resulting from electrolyte degradation, is believed to contribute to this reversible capacity. These two mechanisms require the electrodes to be composed of nanoscale material. At the nanometer scale, both the reversible formation of Li_2O, which is known to be electrochemically inactive in bulk, and the reversible formation of the gel-like layer catalyzed by cobalt nanoparticles, can occur[26]. The virus capsid-mediated growth of uniform sized cobalt oxide nanomaterials, in addition to the structural integrity and dense packing (Fig. 4.11A) imparted by the virus, provides electrochemical advantages. For instance, controlling all other experimental conditions, samples fabricated without the virus templates exhibited rapidly fading capacity (Fig 4.11B). This phenomenon, which is most likely attributable to incomplete oxidation of cobalt, inhomogeneous composition and large particle size, has also been observed for cobalt oxide prepared at low temperatures, in which high polarization is a contributing factor [24]. However, the cobalt oxide nanowires, templated by M13 virus and oxidized spontaneously at room temperature, demonstrate comparable properties to particles fabricated at temperatures above 500 °C.

An added advantage of this system is that the nano-texture of viral Co_3O_4 nanowires can be manipulated by controlling the interactions between the peptides and cobalt ions. For instance, a higher cobalt chloride concentration (5 mM) with 10 mM $NaBH_4$ produced branch-like nanowire structures (Fig. 4.12A); whereas, nucleation and growth of Co_3O_4 nanowires at 4 °C with 1mM cobalt ion and 5mM $NaBH_4$ resulted in the assembly of discrete nanoparticles (Fig. 4.12B). Furthermore, we have previously reported that biotemplating materials at reduced temperature can promote uniform

orientation of the peptide molecule during nucleation, which leads to the preferred crystallographic texture of nanocrystals[26]. All of this suggests the virus template can control the electrochemical behavior of a biomediated system, since the electrochemical properties of a material depend on its microstructure[27] and crystallographic orientation-dependent transport properties[28].

Hybrid Au-Co_3O_4 nanowires electrodes

To design new hybrid material electrodes with higher capacity, additional material specific peptide motifs were engineered into major coat p8 protein. This provides a general method for the systematic and controlled arrangement of two distinct nanomaterials, which can enhance the electrochemical properties through the cooperative contribution of each material. Increasingly, efforts to improve battery properties have focused on composite material design, such as surface coatings[29], in addition to engineered crystal chemistry[30]. However, significant challenges such as the achievement of uniform distributions of multiple phases are encountered when components are combined at the nanoscale. Here, we demonstrate a genetic based, virus-directed approach to place gold nanoparticles in Co_3O_4 nanowires. Gold nanoparticles were chosen based on their ability to provide high electronic conductivity where needed, the ability to maintain a thermodynamically stable interface with Co_3O_4, and the potential to act as a chemical catalyst for electrochemical reactions at the nanoscale. We designed a bifunctional virus template that simultaneously expressed two different peptide motifs. To accomplish this, a gold-binding peptide motif (LKAHLPPSRLPS) was isolated through gold substrate screening using a phage display library[31], which contains random

12mer peptide sequences. Then, bifunctional viruses were assembled into the p8 proteins using phagemid constructs[26], plasmids inserted into host bacterial cells, encoding for the gold-binding peptide motif[32]. Thus, upon infection of the plasmid-incorporating host cells with the E4 virus, a small percentage of subsequent E4 p8 proteins also displayed the gold-specific peptide. Therefore, two types of p8 proteins were produced: intact p8 proteins of E4 viruses and engineered p8 proteins containing the gold-binding peptide motif, randomly packaged onto the virus progeny (Fig. 4.13). This hybrid clone was named AuE4 virus. Incubation of the amplified AuE4 clones with a 5 nm gold colloid suspension (5×10^{13} particles / mL, Ted Pella) resulted in one dimensional arrays of Au nanoparticles bound to the gold-binding peptides distributed among p8 proteins (Fig. 4.14A). In contrast, wild type viruses and the E4 virus which do not have gold binding motifs, did not bind gold nanoparticles along the length of virus. After removing excess unbound gold nanoparticles by centrifugation, Co_3O_4 was nucleated and grown via the tetra-glutamate functionality, resulting in hybrid nanostructures of 5 nm Au nanoparticles spatially interspersed within the Co_3O_4 wires (Fig. 4.14B). The crystal structure of the Co_3O_4 was confirmed by electron diffraction. Inductively coupled plasma mass spectrometry (ICPMS) analysis indicated that Au nanoparticles were associated with Co_3O_4 in a mass ratio of 2.4 : 97.6.

The electrochemical properties of the hybrid Au-Co_3O_4 nanowires were evaluated using galvanostatic cycling and cyclic voltammetry. Interestingly, it was observed that the virus-mediated hybrid composite generated higher initial and reversible lithium storage capacity than the pure Co_3O_4 nanowires when tested at the same current rate (Fig. 4.15A). The higher lithium storage capacity may result from the formation of Au-Li

intermetallic compound or the conductive or catalytic effects of Au nanoparticles on the reaction of Li with Co_3O_4. The theoretical capacity of Au is approximately 90.7 mAh/g for the formation of Au_3Li_2 [33] and136.1 mAh/g for the formation of AuLi, which suggests a negligible contribution to the lithium storage capacity considering the Au:Co_3O_4 ratio. Indeed, cyclic voltammetry (Fig. 4.15B) shows no significant new redox peaks that could be associated with the lithiation of Au. It is more likely, considering the unique charging/discharging mechanism of Co_3O_4, wherein cobalt nanoparticles promote the reversible reaction of an organic layer that then contributes to the Li capacity, that Au nanoparticles play a role in this displacement reaction. This role may be one of improving electronic conductivity to the Co_3O_4 nanoparticles, or it may be catalytic in nature. Indeed, decreased cell polarization was observed in the galvanostatic voltage-capacity curves, which could result from either of these mechanisms. Furthermore, Au incorporation clearly increases the reaction rate upon reduction of Co_3O_4 as indicated by the enhanced reduction peak seen by cyclic voltammetry in Fig. 4.15B (measured on samples of similar mass at the same voltage sweep rate). While the exact electrochemical mechanism is still under investigation, our results show that a small amount of Au nanoparticles dispersed within Co_3O_4 to produce a hybrid materials markedly improves electrochemical performance. The specific capacity of the hybrid is estimated to be at least 30 % greater than that of our Co_3O_4 nanowires.

This scheme can be extended to test other combinations of electrochemically active materials within the construct of nanostructured Li ion batteries via material-specific peptide selection[31] or design[21]. This process of producing hybrid nanoarchitectures of spatially distributed inorganic materials by genetic engineering can

be harnessed for maximizing desired output performance in a concerted mechanism. In fact, the dispersion of metal nanoparticles in an oxide is a classic example where catalytic activity is enhanced by creating a bifunctional material[35]. A well known example is the Au/Co_3O_4 catalytic conversion of carbon monoxide to carbon dioxide[36]. Additionally, it was reported that gold is catalytically more active when dispersed in semiconductor metal oxides[37].

Virus based self assembly of a Li ion battery

The principles of self assembly and biotemplating can be further extended to control virus-virus interactions for organizing nanostructured electrodes over large length scales (Fig. 1C). Recently, we observed that negatively charged M13 viruses can form very ordered, two dimensional liquid crystalline layers on top of electrostatically cohesive films of linear poly(ethylene imine) (LPEI) / poly(acrylic acid) (PAA)[38]. The ordering of engineered viruses is driven by competitive electrostatic interactions, the interdiffusion of the polyelectrolyte, and the anisotropic shape of M13 viruses. By employing this technique to spontaneously order E4 viruses and subsequently grow Co_3O_4 on the virus coat proteins, two dimensional organized ensembles of nanowires were produced on a 10 cm length scale (Fig. 4.16A and B). The spatial distance and ordering behavior between viral nanowires can be manipulated by controlling both surface charge and fluidic forces. Furthermore, the thickness of the multilayered polymer can be varied from 10 nm to several micrometers independent of the substrate. This assembly process produces light weight, flexible, and transparent active material/substrate multilayers, constructed as free standing films by a simple dipping

method (Fig. 4. 16C). This process should be scalable using roll-to-roll processing. Moreover, the polymer electrolyte is believed to act as a solid electrolyte because of the relatively fast ionic conductivity of LPEI and PAA pairs[39, 40]. Thus the assembled layers comprise a negative electrode material grown upon a solid electrolyte or separator membrane. For electrochemical evaluation, 100 nm of Cu, which functions as a current collector, was deposited by E-beam evaporation on the assembled Co_3O_4 nanowires/polymer layer. This assembly was then tested in Swagelok™ cells using a Li foil negative electrode separated from the multilayer by a liquid electrolyte dipped separator[41]. Figure 4.16D shows the capacity for the assembled monolayer of Co_3O_4 nanowires/Li cell at two different charging rates. The cell was found to sustain and deliver 94 % of its theoretical capacity at a rate of 1.12 C and 65% at a rate of 5.19 C, demonstrating the capability for high cycling rate. We believe that the power of the cell can be further increased by alternating stacks of nanowire monolayers and polymer layers of LPEI and PAA or other polyions. In addition, the Au-Co_3O_4 hybrid nanowires should also increase the total capacity.

The genetic approach presented for exploiting biomolecular interactions and self assembly at various length scales has technological potential in the development of electrodes for Li ion batteries. Our results demonstrate that these traditionally biological principles can be utilized for the rational design and assembly of nanoscale battery components, exhibiting improved performance in properties such as specific capacity and rate capability. The genetic control in the viral synthesis of monodisperse oxide nanowires and the nanoarchitecture of hybrid nanowires can be advanced through further modification of other proteins. Heterostructured nanowires, comprising anode and solid

electrolyte, and bio-energy transducing nanowires, coupled with biomolecules, are currently being investigated. Moreover, we anticipate that self-organized virus monolayers for the generation of anodic as well as cathodic materials on ionically conducting polyelectrolyte films may present potential architectures for interdigitated batteries [42].

Chapter 4. 4 Conclusion

In this chapter, biotemplating was studied and applied to grow electrochemically useful materials on an M13 virus template. The biologically inspired method to grow nanomaterials with specific peptides resulted in homogenous and uniform nanowires. Because the entire process is at room temperature in aqueous solution, this method is also environmentally benign. As an application to show the advantage of our methods, virus based cobalt oxide nanowires were demonstrated as materials for Li ion battery electrodes. In order to improve the electrochemical property further, we turned to genetic engineering and inserted a gold binding peptide sequence. Therefore, two types of protein were fused around the virus. The viruses then assembled as nanowires composed of both cobalt oxide and gold particles. The resulting electrodes stored 30 percent more energy than the pure cobalt oxide version.

The principles of biological self assembly and biotemplating were further extended to control virus-virus interactions for organizing nanostructured electrodes over large length scale. By harnessing the electrostatic nature of the assembly process with the functional properties of the virus, we can create highly ordered composite thin films combining the function of the virus and polymer systems. We studied the method by which genetically engineered virus can spontaneously assemble into a two-dimensional liquid crystalline layer on top of electrostatically cohesive polymer film.

In our approach, once the DNA gene is programmed for a functional device (i.e., a battery), very little post-synthesis processing is necessary. As with biological organisms, the encoded DNA sequence lead to the production of biomolecules that are assembled into the functional organism. In our scheme, most of our battery fabrication

was done through genetic manipulation -- giving an organism that wouldn't normally make battery electrodes the information to make a battery electrode, and to assemble it into a device. A genetically engineered organism has a DNA sequence that codes for the synthesis and assembly of materials, which allows one to literally pull a device straight out of a beaker. None of this has been accomplished with traditional approaches of battery formation. It is a new paradigm for synthesizing and assembling materials.

Chapter 4.5 References

1. A. S. Claye, J. E. Fischer, C. B. Huffman, A. G. Rinzler, R. E. Smalley, *J. Elecrochem. Soc.* **147**, 2845 (2000).

2. J. S. Sakamoto, B. Dunn, *J. Electrochem. Soc.* **149**, A26 (2002).

3. A. R. Armstrong, G. Armstrong, J. Canales, R. Garcia, P. G. Bruce, *Adv. Mater.* **17**, 862 (2005).

4. S. C. Mui et al., *J. Electrochem. Soc.* **149**, A1610 (2002).

5. T. Cassagneau, J. H. Fendler, *Adv. Mater.* **10**, 877 (1998).

6. A. S. Aricò, P. Bruce, B. Scrosati, J-M. Tarascon, W. V. Schalkwijk, *Nat. Mater.* **4**, 366 (2005).

7. S. Mann, *Biomineralization: principles and concepts in bioinorganic materials chemistry* (Oxford University Press, New York, 2001).

8. A. M. Belcher et al., *Nature* **381**, 56 (1996).

9. M. M. Murr, D. E. Morse, *Proc. Nat. Acad. Sci. USA* **102**, 11657 (2005).

10. N. C. Seeman, *Nature* **421**, 427 (2003).

11. S. Brown, Nat. *Biotechnol* **15**, 269 (1997).

12. T. Douglas, M. Young, *Nature* **393**, 152 (1998).

13. S. Zhang, *Nat. Biotechnol.* **21**, 1171 (2003).

14. Y. Huang et al., *Nano Lett.* **5**, 1429 (2005).

15. K. T. Nam, B. R. Peelle, S.-W. Lee, A. M. Belcher, *Nano Lett.* **4**, 23 (2004).

16. C. Mao and D. J. Solis et al., *Science* **303**, 213 (2004).

17. S. W. Lee, C. Mao, C. Flynn, A. M. Belcher, *Science* **296**, 892 (2002).

18. Z. Dogic, S. Fraden, *Phys. Rev. Lett.* **78**, 2417–2420 (1997).

19. P. Poizot, S. Laruelle, G. Grugeon, L. Dupont, J-M. Tarascon, *Nature* **407**, 496 (2000).

20. S. Joy et al., *Langmuir* **16**, 1354 (2000).

21. B. R. Peelle, E. M. Krauland, K. D. Wittrup, A. M. Belcher, *Langmuir* **21**, 6929 (2005).

22. The mass spectrum acquired by matrix assisted laser desorption/ionization (MALDI) confirmed that cobalt was bound with p8 proteins of E4 clones.

23. 100 μl of E4 viruses (10^{12} phage / ml) were incubated with 1 mL of 1 mM $CoCl_2 \cdot 6H_2O$ for 1hr. Then, 1 mL of 5 mM $NaBH_4$ was added and the solution was kept at room temperature for the further oxidation of nanowires.

24. D. Larcher, G. Sudant, J-B. Leriche, Y. Chabre, J-M. Tarascon, *J. Electrochem. Soc.* **149**, A234 (2002).

25. J.-M. Tarascon et al., *C. R. Chimie* **8**, 9 (2004).

26. C. Mao et al., *Proc. Natl. Acad. Sci. U. S. A* **100**, 6946 (2003).

27. N. Pereira et al., *J. Electrochem. Soc.* **152**, A114 (2005).

28. J. B. Bates, *J. Electrochem. Soc.* **147**, 59 (2000).

29. J. Kim, M. Noh, J. Cho, H. M. Kim, K.-B. Kim, *J. Electrochem. Soc.* **152**, A1142 (2005).

30. G. Ceder et al., *Nature* **392**, 694 (1998).

31. S. R. Whaley, D. S. English, E. L. Hu, P. F. Barbara, A. M. Belcher, *Nature* **405**, 665 (2000).

32. Bacteria containing the engineered phagemids are inoculated into 20 ml of Terrific Broth (TB) with Ampiclin (100 ug / ml). The culture was maintained at 37 °C until mid-log phage ($OD_{600} \sim 0.5$). 10 ul E4 bacteriophage and 20 ul IPTG (100 mg / ml) were added into the bacteria culture. After 4.5~5 hours incubation at 37 °C, phages were purified using regular purification procedure.

33. G. Kienast, J. Verma, Z. *Anorg, Allg. Chem.* **310**, 143 (1961).

34. Although we have only demonstrated virus based Co_3O_4 nanowires for Li ion battery application, our group has already selected or is identifying peptides with the

ability to recognize and nucleate the electrochemically useful materials including TiO_2 and $LiCoO_2$.

35. D. R. Rolison, *Science* **299**, 1698 (2003).

36. M. Matsumiya et al., *J. Electrochem. Soc.* **151**, H7 (2004).

37. M. Haruta, T. Kobayashi, H. Sano, N. Yamada, *Chem. Lett.*, 405 (1987).

38. P. J. Yoo, K. T. Nam et al., unpublished data.

39. D. M. DeLongchamp, P. T. Hammond, *Chem. Mater.* **15**, 1165 (2003).

40. P. T. Hammond, Adv. Mater. **16**, 1271–1293 (2004).

41. To prevent the oxidation of Cu after the deposition of Cu in vacuum, the sample was rapidly transferred to a glove box for the assembly of the battery. In fact, we could not observe the contribution of CuO in charging/discharging curve. The mass of cobalt oxide on the polymer is 22 $\mu g/cm^2$ measured by ICPMS.

42. J. W. Long, B. Dunn, D. R. Rolison, H. S. White, *Chem. Rev.* **104**, 4463 (2004).

Figure 4.1 The schematic diagram of our idea.

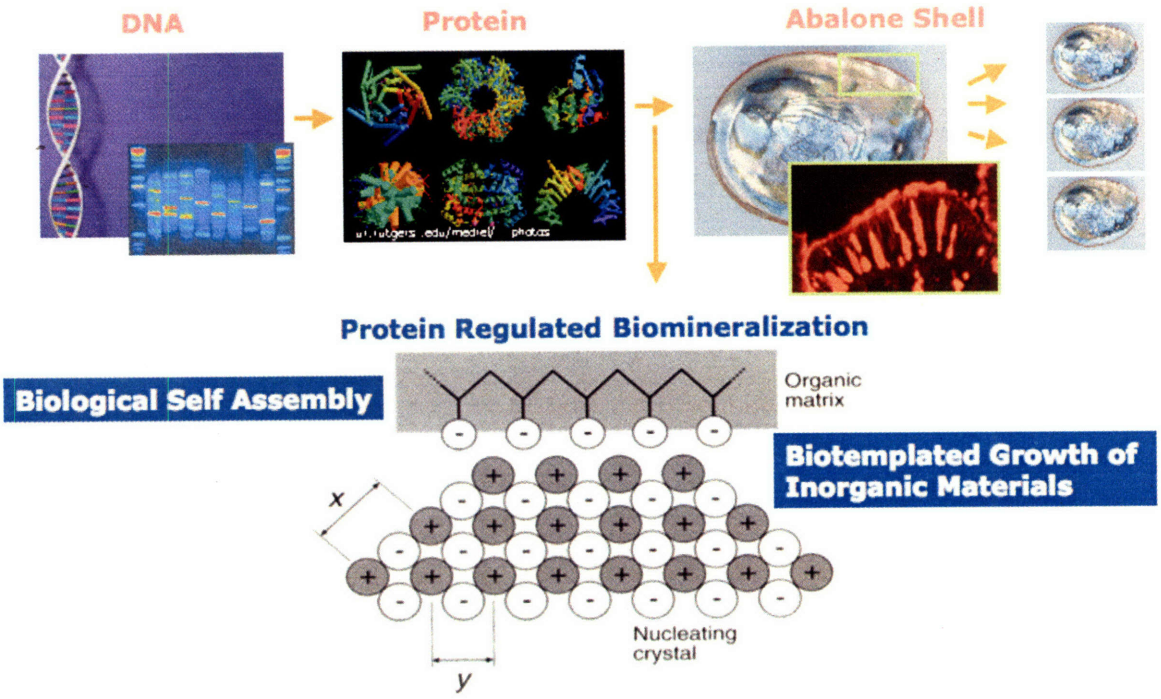

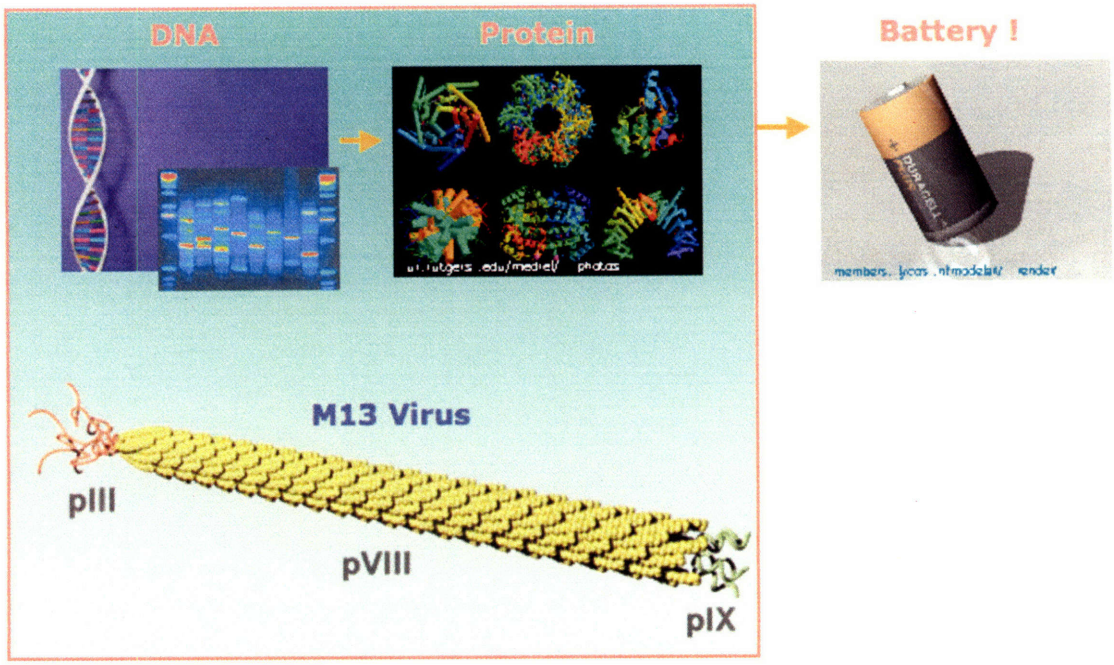

Figure 4.2. Schematic diagram of the virus enabled synthesis and assembly of nanowires as negative electrode materials for lithium ion batteries. Rationally designed peptide or/and materials specific peptide identified by biopanning was expressed on the major coat p8 proteins of M13 bacteriophage viruses to grow Co_3O_4 and Au/ Co_3O_4 nanowires. The macroscopic ordering of the engineered viruses was utilized for fabricating the assembled monolayer of Co_3O_4 nanowires for the flexible, light weight Li ion batteries.

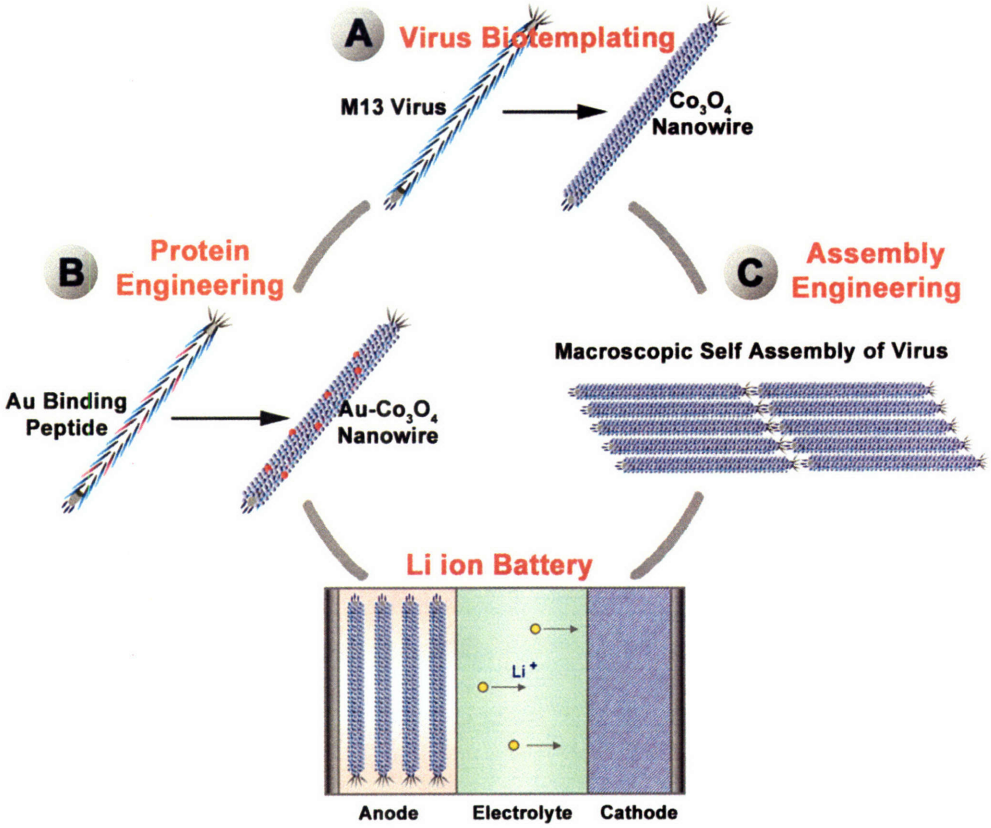

Figure 4.3. Titer curve of E4 virus and wild type virus. After dropping pH of virus solution with the addition of HCl, the droplets of 1M NaOH were added and pH was measured.

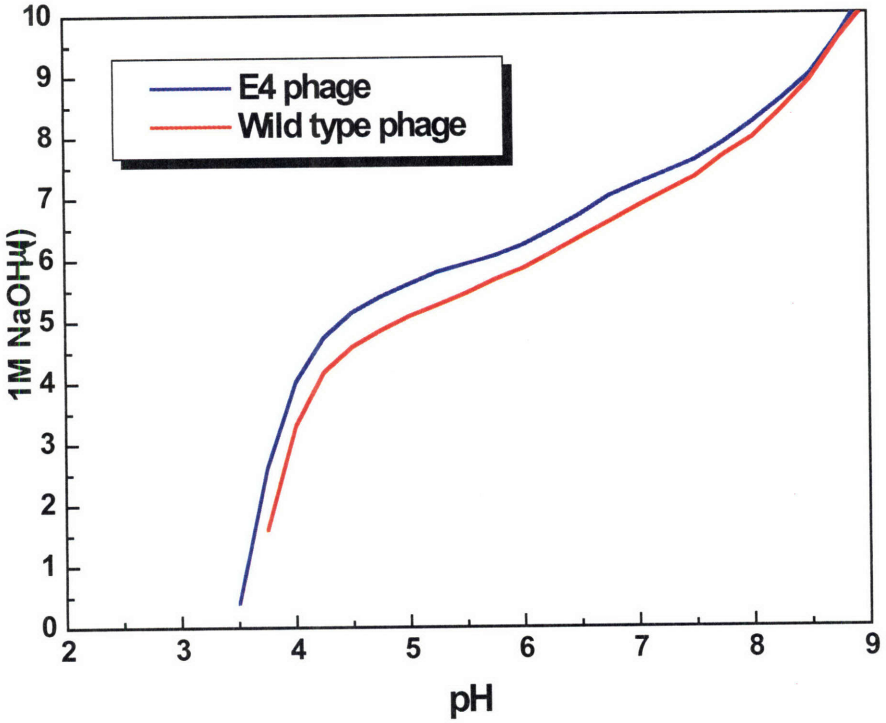

Figure 4. 4. Mass spectrum of matrix assisted laser desorption/ionization (MALDI). Cobalt ions are bound with p8 proteins of E4 viruses.

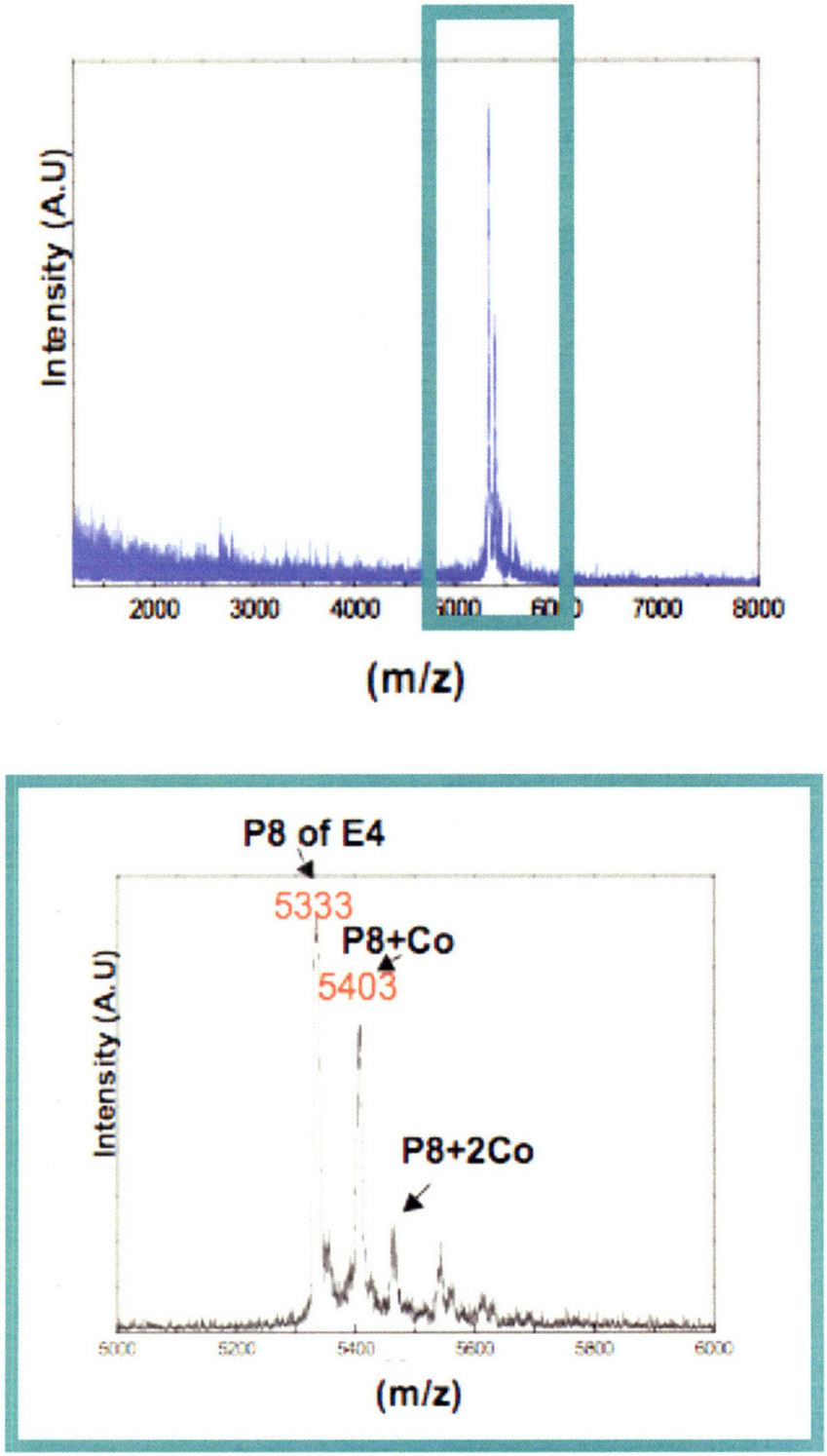

Figure 4. 5 Characterization of the M13 virus templated Co_3O_4 nanowires. (a) TEM image of virus templated Co_3O_4 nanowires. (b) High resolution TEM image of a Co_3O_4 viral nanowire. Electron diffraction pattern (Inset, upper right) confirmed that the crystal structure is Co_3O_4. Magnified image (Inset, lower right) shows the lattice fringe of Co_3O_4 nanocrystals along the major coat p8 proteins of a virus.

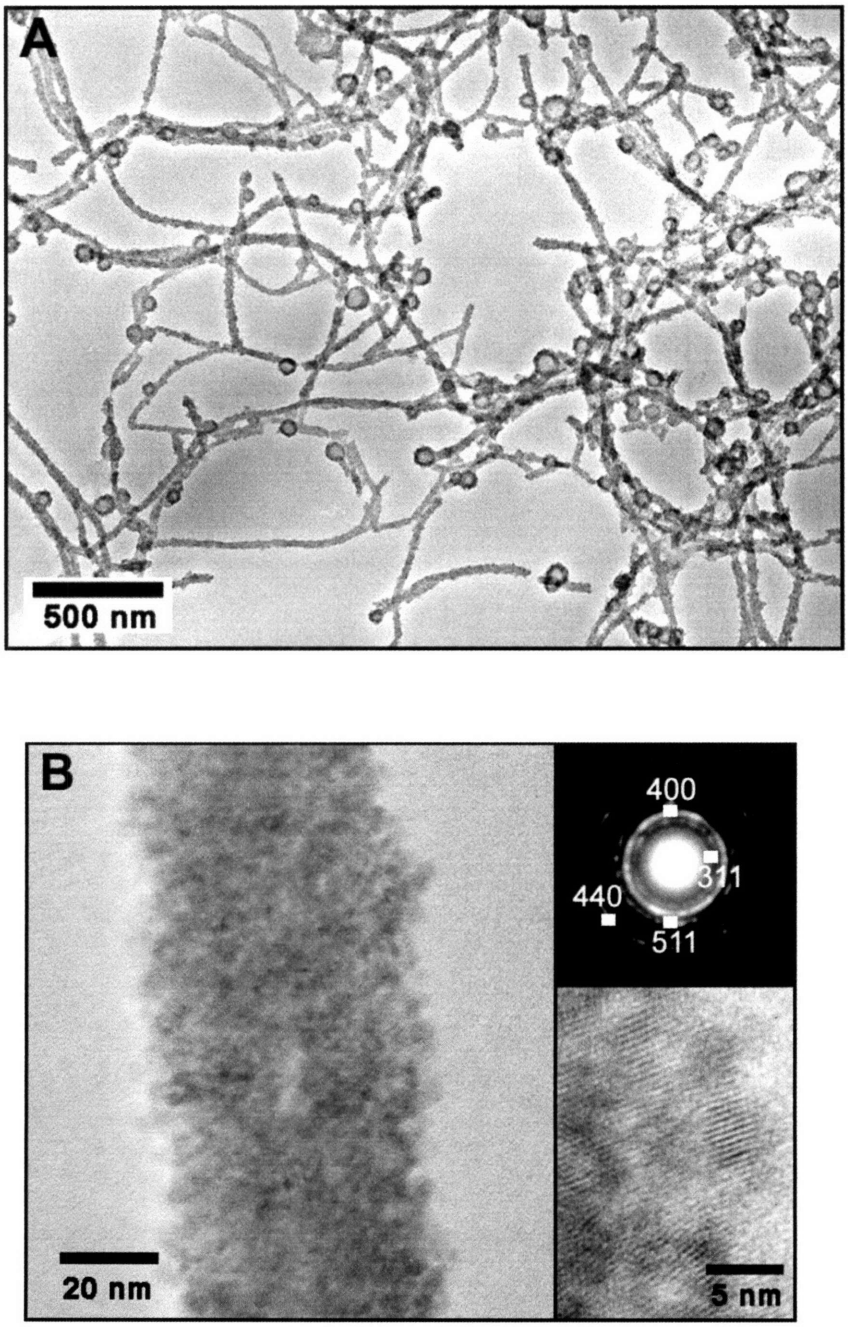

Figure 4.6 XRD data of virus templated cobalt oxide nanowires. This data confirms that the crystal structure of virus tempalated nanowires is cobalt oxide.

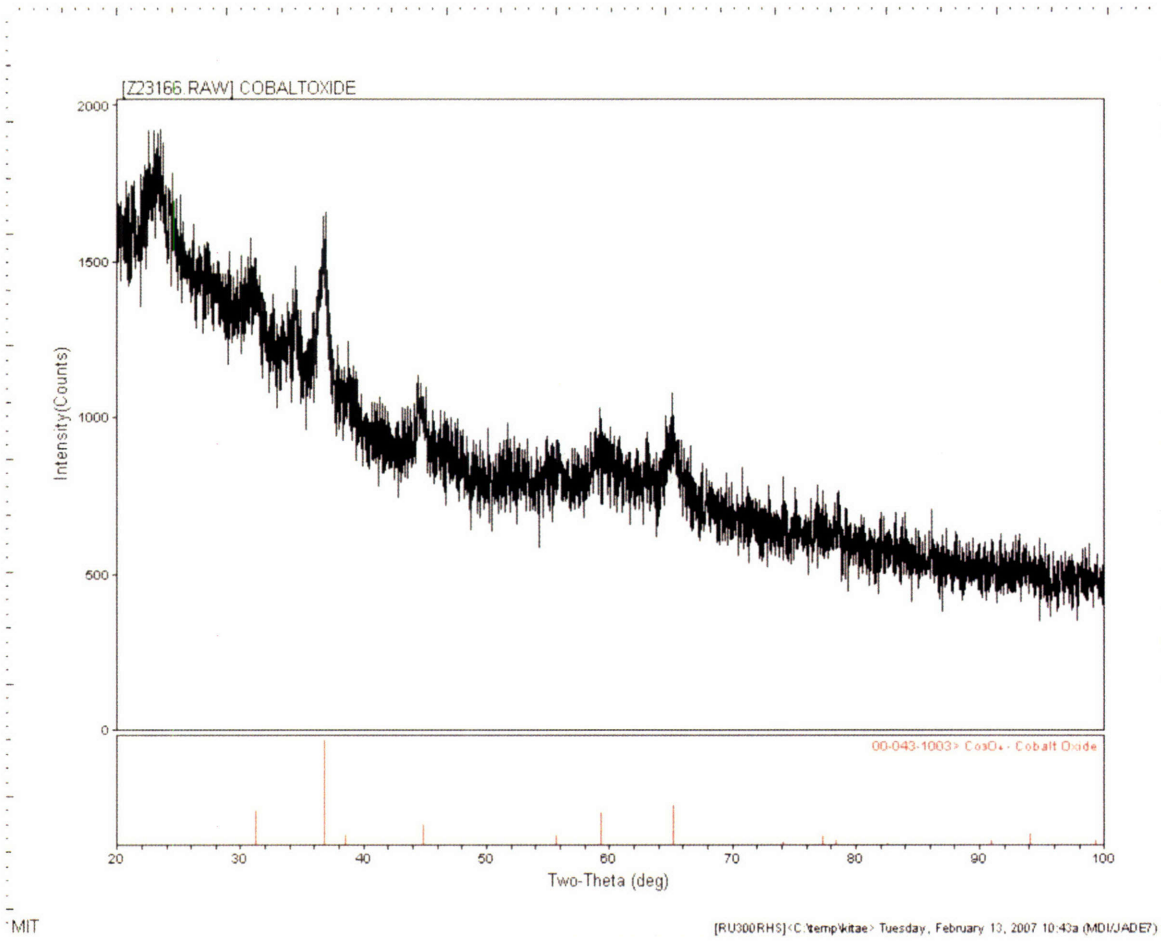

Figure 4.7 The growth kinetics of cobalt oxide nanowires templated by engineered viruses

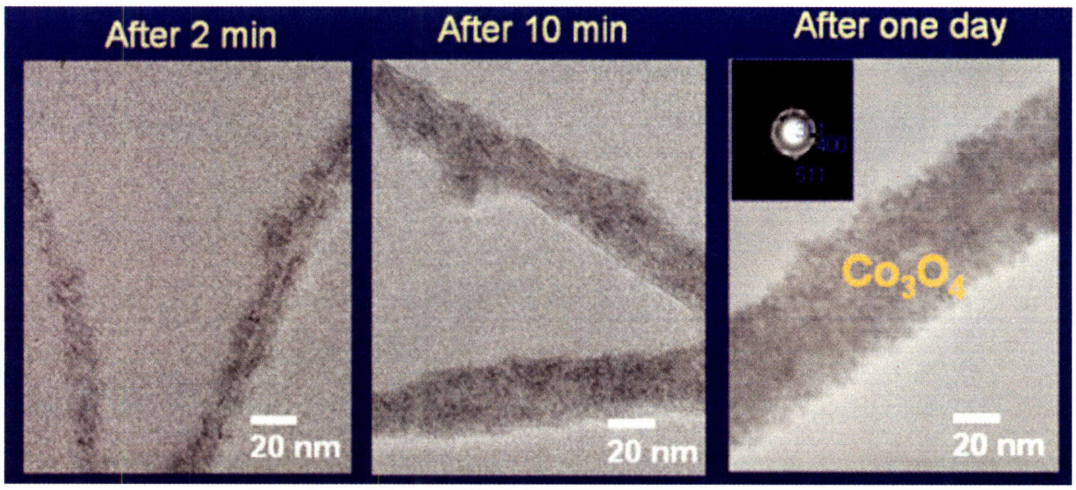

Figure 4.8. Surface area measured by Brunauer-Emmett-Teller (BET) method

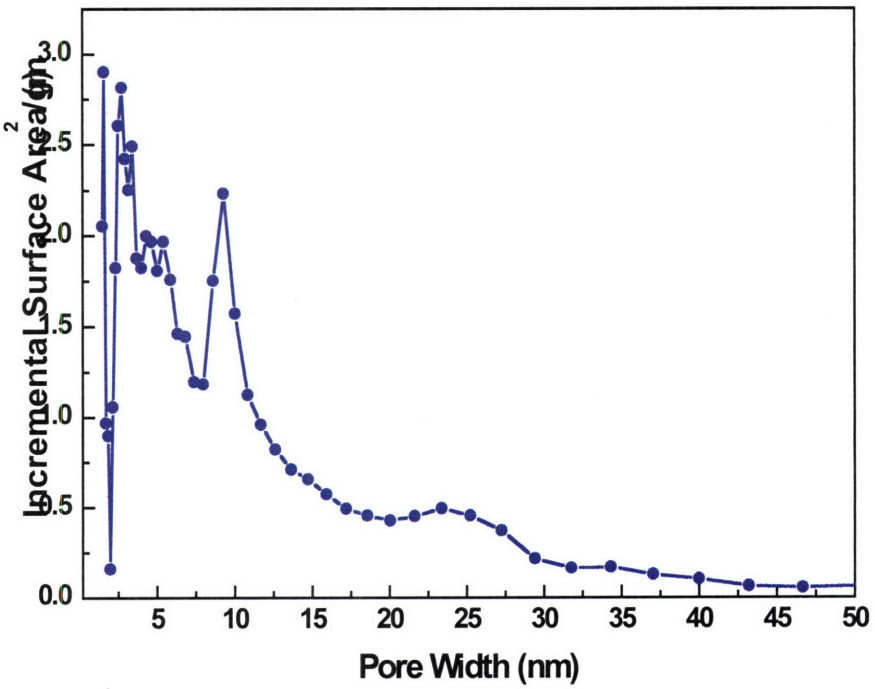

Figure 4. 9. Cyclic voltammograms of the viruses at a scanning rate of 0.3 mV/sec.

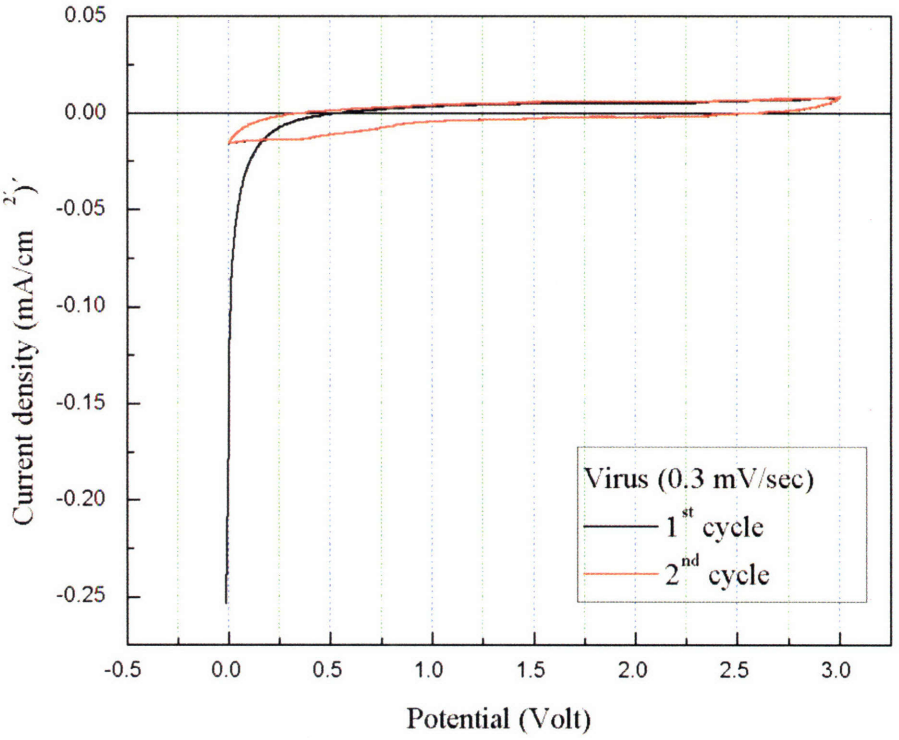

Figure 4.10. The experimental procedure to measure the electrochemical property of virus based battery.

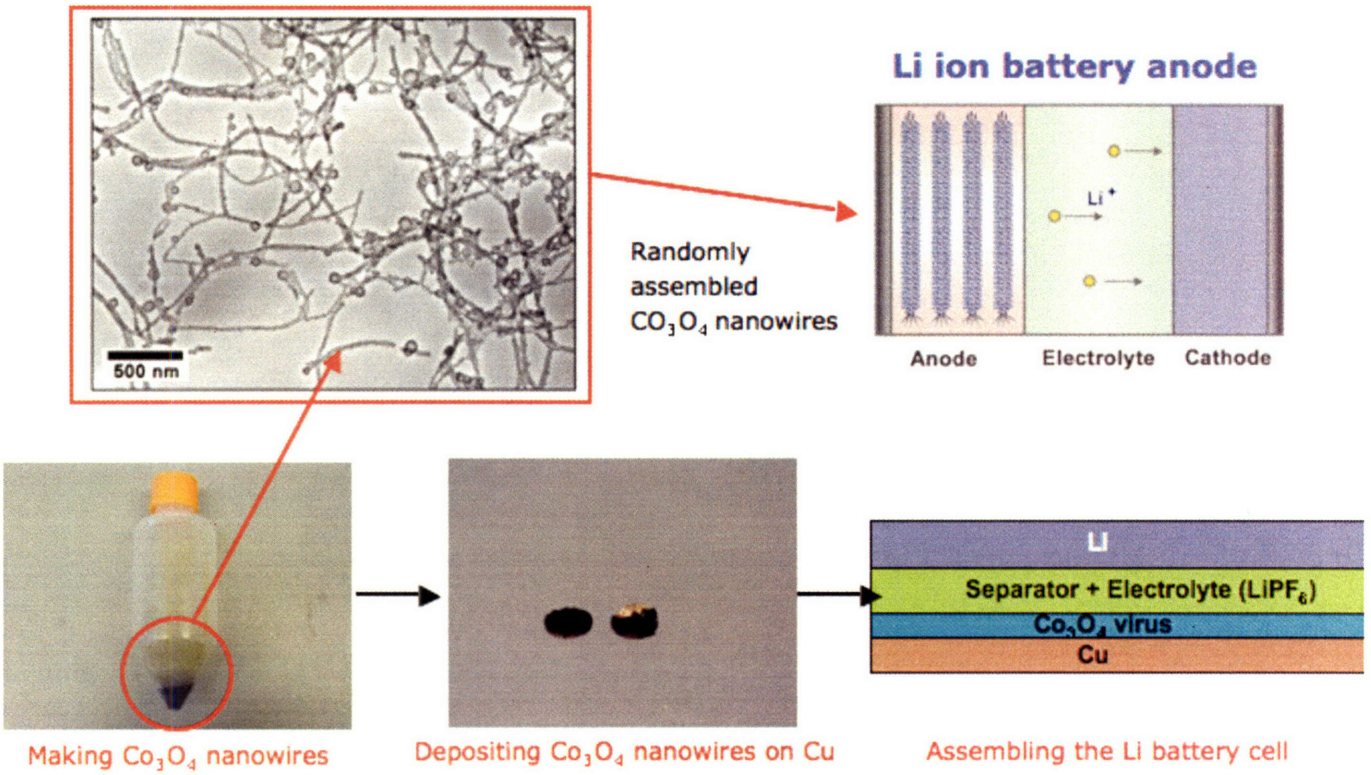

Figure 4.11 The electrochemical property of virus based cobalt oxide nanowires (a) Charging-discharging curves for a virus meditated Co_3O_4 /Li half cell cycled between 3 V and 0.01V at a rate of C/26.5. C was defined as one Li per hour. (b) Specific capacity vs. cycle number for the same cell. The mass of just Co_3O_4 was considered. For comparison, the data for the powder which was fabricated without viruses at the same condition are shown.

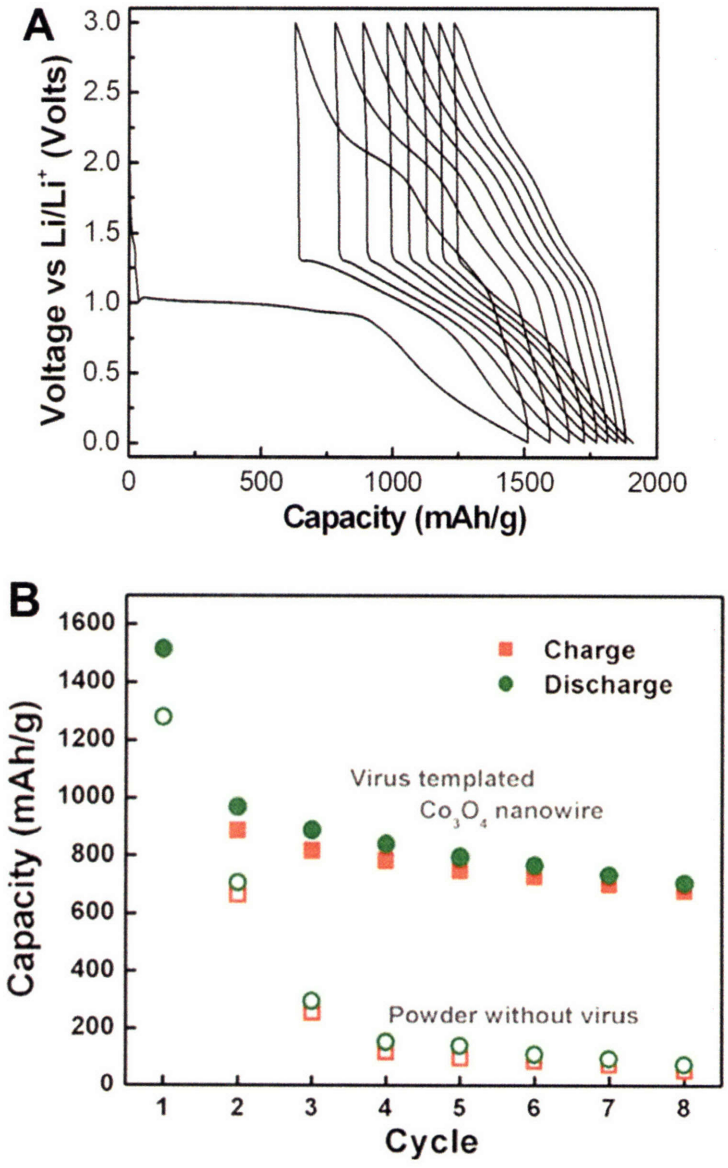

Figure 4.12 (a) TEM images of differently nanostructured Co_3O_4 viral nanowires which were fabricated at higher cobalt ion concentration. (b) TEM images of the assembly of the discrete Co_3O_4 nanocrystals (on the p8 proteins) which were synthesized at 4 ^{o}C.

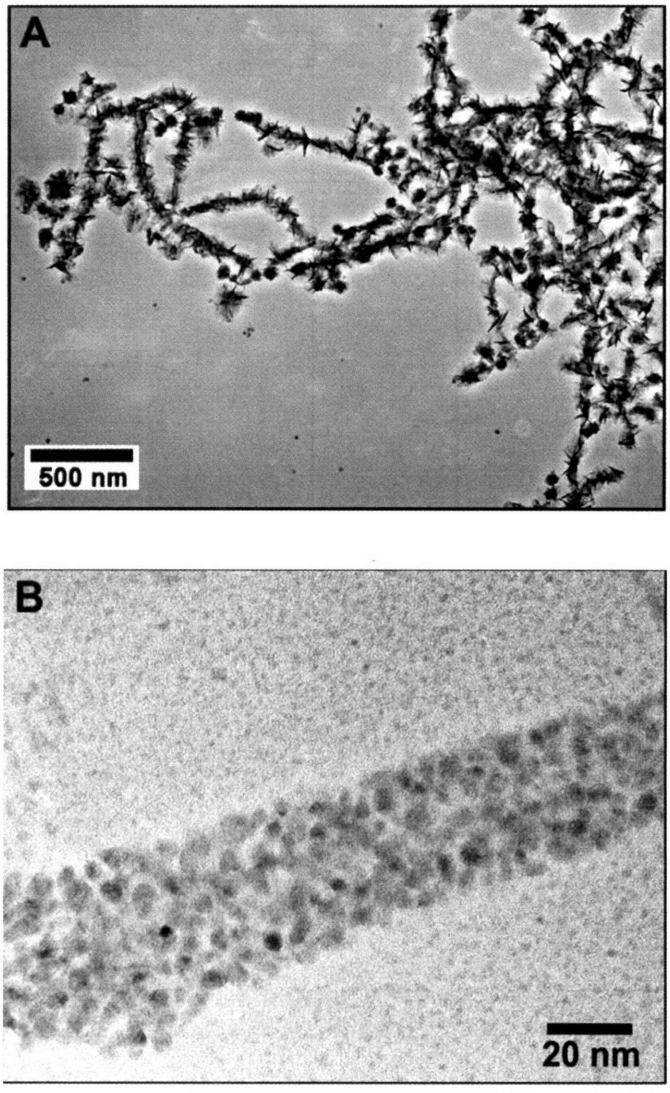

Figure 4.13 Visualization of the genetically engineered M13 bacteriophage viruses. P8 proteins containing gold binding motif (yellow) was doped by the phagemid method in E4 clones which can grow Co_3O_4.

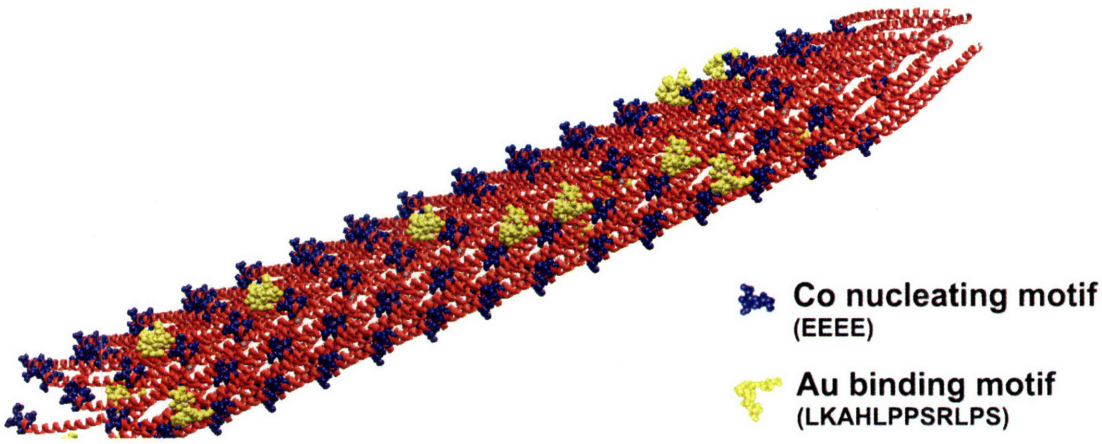

Figure 4.14. (a) TEM images of the assembled gold nanoparticles on the virus. Control experiments proved that gold nanoparticles were bound by the gold specific peptides. (b) TEM image of hybrid nanowires of Au nanoparticles/Co_3O_4.

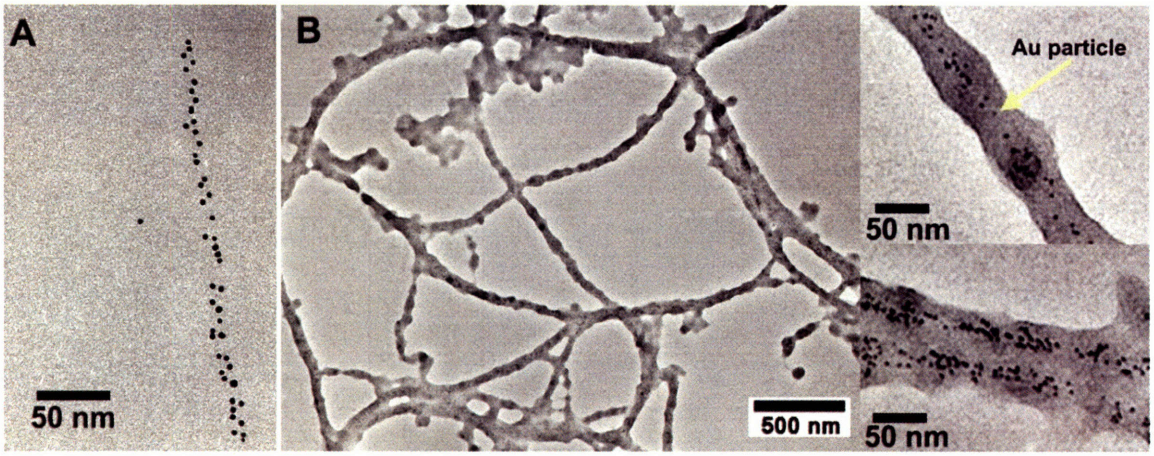

Figure 4.15 (a) Specific capacity of hybrid Au-Co_3O_4 nanowires. Half cell with Li electrode was cycle with a rate of C/26.5. Virus mass was subtracted and the mass of active materials such as Co_3O_4 and Au was counted. The capacity of virus directing Co_3O_4 nanowires without Au nanoparticles was also compared. (b) Cyclic voltammograms of hybrid Au-Co_3O_4 and Co_3O_4 nanowires at a scanning rate of 0.3 mV/sec.

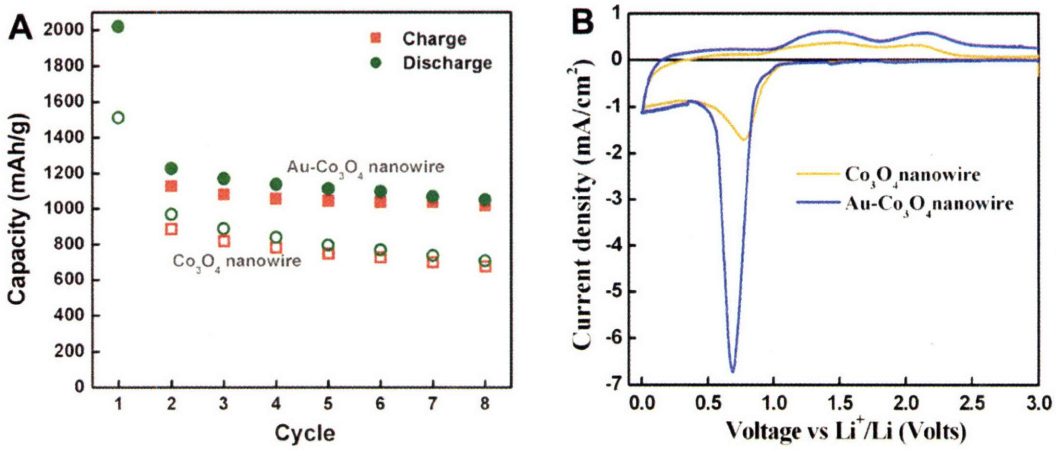

Figure 4. 16. Two dimensional assembly of Co_3O_4 nanowires driven by liquid crystalline ordering of the engineered M13 bacteriophage viruses. (a) and (b) Phase mode AFM image of macroscopically ordered monolayer of Co_3O_4 coated viruses. *Z*-range is 30 ° (c) Digital camera image of a flexible and transparent free standing film of $(LPEI/PAA)_{100.5}$ on which Co_3O_4 viral nanowires are assembled into nanostructured monolayer with dimension of 10 cm X 4 cm. (d) Capacity for the assembled monolayer of Co_3O_4 nanowires/Li cell at two different charging rate.

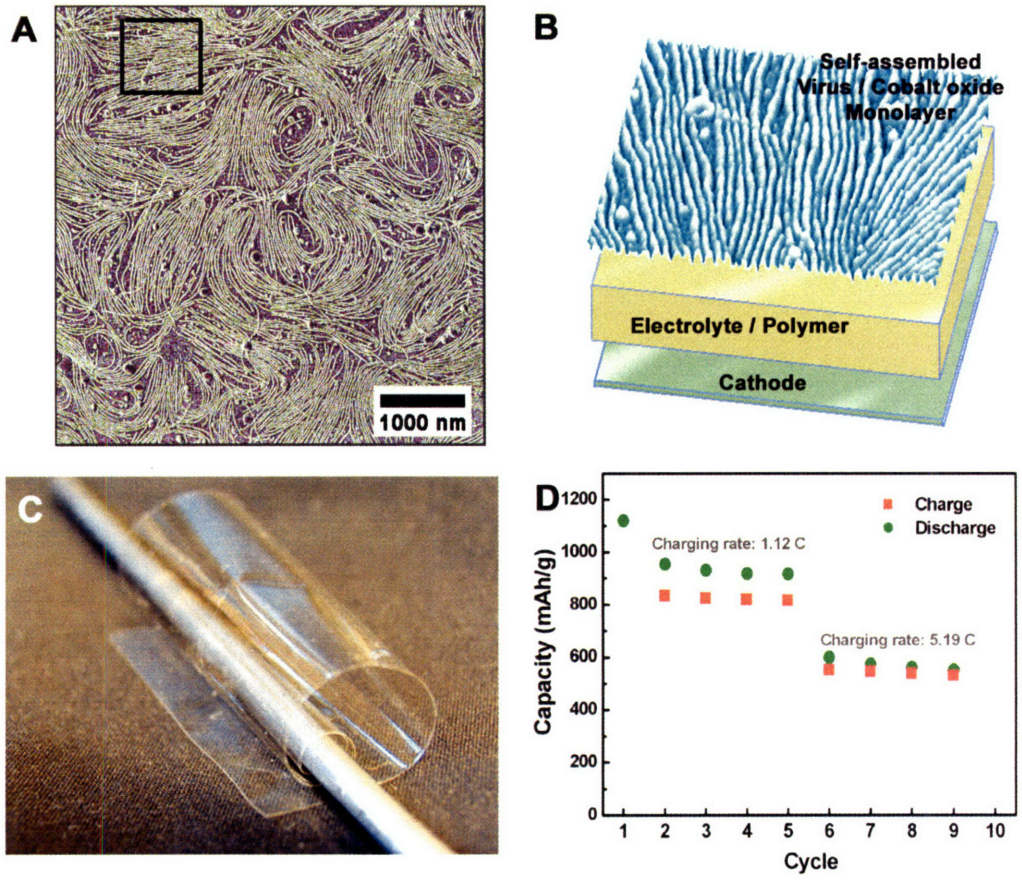

Chapter 5. Peptide-mediated reduction of silver ions on engineered biological scaffolds

Chapter 5. Summary

We report the spontaneous reduction of silver ions into nanostructures by yeast displaying glutamic acid (E_6) and aspartic acid (D_6) peptides on their surface. The increase in reduction capability of E_6 expressing yeast over D_6 yeast was examined by Monte Carlo simulations of the peptides. On average, E_6 peptides assumed a bent-like structure while D_6 peptides were more extended. Taken together, these results let us hypothesize that reduction of silver ions was facilitated by the coordination to carboxylic acid groups, and a local increase in silver concentration around the peptides. In addition, the importance of tethering peptides to a biological scaffold was demonstrated by the decreased reduction ability of soluble peptides. This principle was further extended to the M13 virus for fabricating crystalline silver nanowires. These insights into the spontaneous reduction of metal ions on biological scaffolds should help further the formation of novel nanomaterials in biological systems.

Chapter 5.1 Introduction

Biological systems have developed biomineralization processes to nucleate, grow, and assemble inorganic materials[1]. Examples of biomineralized products include pearls, bone, keratin, shell, calcite, siliceous materials synthesized by diatoms[2] and sponges[3], and magnetite in magnetostatic bacteria[4]. An important component of biomineralization is the protein or peptide template that controls the shape and crystal structure of biominerals as well as the assembly behavior. The extraction of nucleating biomolecules from the biominerals and the identification of materials specific peptides through combinatorial approaches[5, 6] have broadened the possible application of biominearlization in nanoelectronics and nanobiotechnology. We hope to apply the underlying mechanism to synthesize technologically important materials beyond those few existing biominerals in nature. Peptides have been engineered[7] to grow and assemble[8] semiconductor, magnetic[9], metal oxide nanomaterials[10], and we extend this approach to the spontaneous reduction of silver by introducing peptide sequences on yeast and M13 viruses to facilitate the growth of templated silver nanostructures. Previously, in our studies, we used reducing agents or established chemical reactions for biologically-templated growth; but for this study, we harnessed the reducing capability of engineered organisms instead.

Organisms such as bacteria[11] and fungi[12] are reported to synthesize silver particles intra- or extracelluarly when they are exposed to silver salts. Although there is growing interest in the bioinspired synthesis of silver nanoparticles, a general understanding of growth is not yet known. Recently, the role of specific peptide motifs has been explored through identification of dodecamer peptides that are reported to generate silver nanoparticles of various morphology[13]. The importance of peptides was demonstrated as

studies with single amino acid solutions of lysine, proline, serine, and arginine showed them to be incapable of silver reduction[13]. Additionally, tryptophan and aspartate, which can be used as reducing agents in the synthesis of gold nanoparticles at the elevated temperature, did not show the ability to reduce silver ions[14]. In peptides, the conformation, overall charge, and functional groups may all contribute to biological reduction in conjunction with solution pH, light, temperature, and other ions in solution. Although it has been experimentally demonstrated that biological systems such as cells, enzymes and peptides can reduce metal ions, the detailed mechanisms have not been revealed. The conformation, overall charge, and functional groups of biomolecules may all contribute to biological reduction in conjunction with other factors such as solution pH, light, temperature, and other ions in solution. Cooperative mechanisms may be involved in the natural biomineralization process. As an effort to contribute the understanding of spontaneous reduction, we investigated the effects of carboxyl groups among the possible reducing mechanisms, Different from the previous studies by other groups where polypeptide or single amino acid was studied, this work utilized the hexamer peptides which were short enough to see the molecular effects and long enough to have the needed conformations. Additionally, prior work using organisms such as yeast, bacteria and fungi have demonstrated the formation of silver particles in solution but have not controlled the spatial distribution of the grown nanoparticles. The present works represents the first demonstration of templated reduction of silver ions on engineered biological scaffolds resulting in the controlled arrangement of the silver nanoparticles.

In this work, we investigate the spontaneous reduction of silver ions by carboxylic acid containing peptides. Carboxylic acid groups are known to coordinate metal ions that may act as a nucleation site for nanoparticle formation[15-17]. We anticipated that the populated aggregations of silver ions resulting from their affinity with linked carboxylic acid groups might cause reduction. We displayed hexa-glutamic acid and aspartic acid peptides on the surface of yeast and evaluated its silver ion reduction capability. Yeast surface display provides a convenient model system for the study of genetically engineered biomolecules with inorganic materials[18]. Our findings demonstrate 1) spontaneous reduction of silver facilitated by carboxylic acid groups in the presence of ambient light, 2) the importance of peptide conformation on reduction capability, and 3) the increased reduction capability of the peptides when anchored on a biological scaffold. The principle of the peptide-mediated reduction elucidated by the engineered yeast was further extended to a filamentous M13 virus scaffold for fabricating crystalline silver nanowires.

Chapter 5.2 Experimental

Genetic Engineering of Yeast Displayed Peptides

Hexamer peptides were engineered onto the surface of yeast as previously described. Briefly, peptides were displayed as fusions to the C-terminus of Aga2, which is encoded on a 2-micron plasmid downstream of a Gal-based promoter. The expression vectors were maintained in *S. cerevisiae* strain EBY100, which has Aga1 under control of a Gal-based promoter integrated in its genome, as previously described[18]. Peptide expression vectors (X_6) were generated from annealed oligonucleotides (i.e. G_6 peptide oligos: 5'GTGGCggtggtg-gtggtggcggaTAGCCAGTAGC and 5'CTGGCTAtccgccaccaccaccaccGCCACCGCC) with BstXI compatible sticky ends ligated into BstXI sites of expression vector pBPZ. The complete list of oligonucleotides used is available upon request. All vectors were amplified, sequenced, and then transformed into EBY100. Peptide expression was induced by growing cells at mid-log phase in Select-Galactose media at 30 °C for 18-24 hours.

Silver Reduction by Yeast

Among various silver salt precursors, silver acetate ($AgOOCCH_3$) salt was chosen because metal ions from acetate salt were found to load faster and to a greater extent within block copolymer containing carboxylic acid group than metal ions from chlorides, nitrates and sulfates[15]. In addition, the silver ion reduction rate constant from silver formate (AgOOCH), which has almost the same structure as $AgOOCCH_3$, was reported as higher than that of Ag_2SO_4 and $AgNO_3$[16]. Silver acetate salt (99% pure) was obtained

from Alfa Aesar. In a typical experiment, engineered 1 O.D. (O.D. is equivalent to absorbance units at 600 nm) yeast cells (10^6-10^7 cells) were washed 3 times in 1mL of Millipore water and incubated in 1mM aqueous solution of $AgOOCCH_3$ for 24-90 hours at room temperature under ambient light. The sample was agitated via rocking to avoid yeast cell sedimentation. For control experiments in which the mixtures were kept in the dark, the vials were wrapped with aluminum foils and placed in the dark room. These samples were analyzed by UV-Vis absorption spectroscopy, Transmission Electron Microscopy (JEOL 200CX TEM and JEOL 2010 TEM) and Environmental Scanning Electron Microscopy (FEI/Philips XL 30 FEG-ESEM). For TEM analysis, solutions were dropped on the copper grid, washed with distilled water several times and dried. For SEM specimen preparation, yeast cells were first settled on a silicon substrate. After four hours fixation with 2 % (v/v) glutaraldehyde, 2 % (v/v) paraformaldehyde, 5 % sucrose in 0.1 M sodium cacodylate buffer, the specimen was rinsed in distilled water, dehydrated in 100 % dry ethanol and critical point dried in CO_2. Specimens were examined in FEI/Philips XL 30 FEG-ESEM with and without surface carbon coating layers.

Genetic Engineering of M13 Virus and Silver Reduction by the Engineered Virus

To display tetraglutamic acid (-EEEE) on the n-terminus of the p8 protein on M13 bacteriophage (producing so-called E4 phage), a small DNA duplex encoding the amino acids was made using an oligonucleotide 5'-CTACTACAAGGATCCTCCTCCT CCTCTGCAGCGAAAGACAGCA-3' and the extension primer, 5'-GATGCTGTCTTTCGCTGCAG-3'. The duplex was digested with *Pst*I and *Bam*HI and ligated into M13SK phage vector[39], and confirmed by DNA sequencing. The E4 phage

was incubated in an aqueous solution of 1 mM silver acetate for two hours at room temperature under ambient light. These samples were analyzed by UV-Vis absorption spectroscopy and Transmission Electron Microscopy (JEOL 200CX TEM and JEOL 2010 TEM). For TEM analysis, solutions were dropped on the copper grid, washed with distilled water several times and dried.

Molecular Simulation of the Hexamer Peptides

Monte Carlo (MC) simulations of the hexamer peptides were performed using the OPLS-AA force-field (Jorgensen, W.L., MCPRO, Version 1.68, Yale University, New Haven, CT, 2002) with an implicitly included solvent environment through the Poisson-Boltzmann equation. The peptides were equilibrated for 100 k MC steps prior to averaging over 1 M MC steps.

Chapter 5.3 Results & Discussions

When the hexa-glutamic acid expressed (clone named as E_6) or hexa-aspartic acid expressed (clone named as D_6) engineered yeasts were incubated in an aqueous solution of $AgOOCCH_3$ for 24 hours at room temperature, the solution turned an orange color as shown in Fig. 5.1a. Reduction of the silver ions was evident by a gradual and steady increase of the reddish color. The characteristic reddish color of the solution and absorption peak at ~400 nm are due to surface plasmon resonance of silver nanoparticles and are dependent on the size and shape of the particles. Interestingly, without any known reducing agent in solution, silver ions were bio-reduced by the genetically engineered yeast. Contrary to E_6 or D_6 yeasts, little color change was seen for yeast expressing hexa-glycine (clone named as G_6) (Fig. 5.1b), and solutions without yeast did not show any color change. These control experiments indicate that the carboxylic acid groups of glutamic acid or aspartic acid are involved in the reduction of silver ions. Typically, the carboxylic acid groups in block copolymer systems have been utilized for silver deposition because of their binding affinity to positive silver ions. However, in all the cases, the post treatment with a reducing agent, such as H_2[17] and $NaBH_4$[19], or UV[16] and γ-radiation[20], was necessary. To our knowledge, there is no prior report of carboxylic acid mediated silver reduction in water at ambient conditions. To understand the reduction mechanism, we conducted control experiments in which the mixtures were kept in the dark. Interestingly, even after a few days, no reduction was evident in these samples (Fig. 5.1). Conversely, mixtures kept under ambient light but with UV energy blocked by polymer coatings, exhibited significant silver reduction (Fig. 5.2). This result suggests

that the reduction of silver ions is the cooperative result of the carboxylic acid and visible light. Even though the un-induced cells, named UI, expressed no surface peptides, the yeast solution changed colors with absorption peak comparable to D_6. In this case, the reduction of silver ion is possibly due to negative charge and the presence of polysaccharide on the yeast surface. Using UV light as a reducing agent, polysaccharides and its derivatives are shown to photo-chemically synthesize metal nanoparticles such as gold and silver[21-23]. However, the growth of silver particles with un-induced cells was less controlled than peptide-assisted nucleation, as witnessed by further electron microscopy analysis.

Transmission electron microscopy (TEM) analysis (Fig.5.3c~3g) showed homogeneous silver nanoparticles with sizes of approximately 10-20 nm coated on the cell wall of yeast expressing peptides. The large cell walls observed were likely a drying artifact from sample preparation on non-fixed yeast cells. Consistent with the color change and UV-Vis absorption spectroscopy trends, the average particle size was larger and the density distribution greater for the E_6 than for the D_6 solution. An electron diffraction pattern (Fig. 5.3h) and a high resolution TEM (HRTEM) image (Fig. 5.3i) confirmed that the particles coating the yeast were crystalline silver nanoparticles. The silver nanoparticles were not aggregated but stabilized by the expressed peptides. For the un-induced yeast (Fig. 5.3a-3b), the morphological features were quite different from that of induced ones. No obvious coating layer was observed and silver nanoparticles were not bound to the surface of the yeast and aggregated to large irregular particles (Fig. 5.4).

As mentioned above, the silver ion reduction in this case could have been mediated by the negative charge or polysaccharide of the yeast surface. It is highly likely that the

silver nanoparticles formed by polysaccharides were not strongly bound to the yeast surface due to the weak interaction between the silver particles and the polysaccharides[23]. This could also explain why the number of silver nanoparticles near the yeast surface was much less than that of D_6 even though UV-Vis absorption and color change were similar. Scanning Electron Microscopy (SEM) analysis (Fig. 5.5a-c, e-g) also demonstrates that engineered yeast provided a template for silver nanoparticle growth and the density of nanoparticles could be controlled by means of genetic engineering of expressed peptides. Silver nanoparticles appeared as bright dots due to their electron dense metallic character. Conversely, a lack of nanoparticles was noticed in E_6 yeast not exposed to silver solution (Fig. 5.5d and 5h).

These results suggest that carboxylic acid containing peptides facilitate the reduction of silver. We believe that the energy barrier for silver reduction is lowered when silver atoms are bound to peptides containing carboxylic groups. The lowered energy barrier of reduction is overcome by the energy of ambient light, initiating the nucleation. Carboxylic groups are nucleophilic such that their binding with silver ions induces partial electron transfer displacing the Fermi level of silver cluster toward the more negative potentials, which makes photo-reduction of silver ion more facile[24]. In this regard, silver ion binding to carboxyl groups catalyzes the reduction of silver ions, as in the case of silver ion-catalyzed amine oxidation[25] and silver ion-catalyzed amino acid oxidation[26].

Surprisingly, silver ions exposed to E_6 yeast result in greater nanoparticle formation than those exposed to D_6 yeast. Assuming a similar binding affinity to Ag^+ through the carboxylic acid complex, the different reduction kinetics appears counterintuitive. In order to understand differential reduction between E_6 and D_6 yeast, we explored the local

conformation of these peptides. When present as an individual neutral amino acid, silver ion affinity of glutamate was calculated to be slightly higher than aspartic acid using hybrid density functional theory[27]. In addition to this aggregate difference over six residues, Monte Carlo simulations show a structural difference between the peptides. The additional alkyl link in glutamic acid allows for slight increases in conformational freedom and non-polar surface area, resulting in a more folded backbone conformation. This gives rise to a pocket-like structure in hexa-glutamic acid (Fig. 5.6), while hexa-aspartic acid on average assumes a more linear conformation. The pocket-like structure of E_6 peptides would contain a greater local concentration of carboxylic acid residues and therefore, a greater level of silver ions. This may increase particle formation as the silver redox potential depends on the number of Ag in the cluster. The redox potential of a single silver ion is -1.8 V and increases as the atom number in a cluster increases up to 0.799 V for bulk silver[28]. Taken together, silver ions bound to carboxyl groups reduce more easily while simultaneously increasing the local concentration of silver ions, which may further reduce the energy barriers to reduction. As a result of these cooperative mechanisms, silver ions can be photo-reduced by the carboxylic acid group even under ambient light.

The importance of fixing peptides to a biological template was demonstrated by observing the nanoparticle growth of soluble peptides. We tested the reduction ability of various concentrations of soluble hexa-glutamic acid peptide in silver solution (1 nM - 1 mM peptide solution, 1 mM - 8 mM $AgOOCCH_3$ solution). According to the absorption data, reduction was only observed at 1 mM peptide and 8 mM $AgOOCCH_3$ solution (Fig . 5.7). Considering the approximate number of hexa-glutamate peptides on the yeast ($5x10^4$

peptides/cell) and the yeast concentration (1 O.D. ~$2x10^7$ cells/mL), the total concentration of the peptides expressed on all the yeasts in solution is ~10^{12} peptides/mL. Conversely, the soluble peptide experiments at 1 mM contained $6x10^{17}$ peptides/mL. Indeed, there are no prior reports on the silver ion reduction mediated by soluble glutamic or aspartic acid peptides. Therefore, the fixing of the peptides in a biological scaffold on the yeast surface may be an additional factor in the reduction mechanism. Enhanced reaction rate has been observed before in other constrained systems including "membrane catalysis" [29, 30] and "micelle catalysis"[31] when one of two reactants remains fixed on a two-dimensional surface. This may be explained by the increased collision probability of reactants towards a fixed target[32-34]. The yeast biological templates inherently provide a two-dimensional tethering effect, so we can expect more efficient reactions on our biological scaffolds. To further investigate peptide-mediated reduction, we expanded this rationale to template silver nanowires on an M13 bacteriophage surface that has increased surface peptide density.

In order to template silver nanowires, we engineered a tetraglutamic acid peptide (-EEEE, called E4) onto the n-terminus of p8, the major coat protein of M13 bacteriophage. Roughly 2700 copies of the p8 major coat protein self-assemble into the capsid of the wild type virus, resulting in 5 fold rotation symmetry along the length of virus. Previously, the E4 virus was utilized as a biological template to grow and assemble cobalt oxide nanowires for nanostructured Li ion battery electrodes[10]. We anticipate that the higher density of glutamate expressed on peptides of the engineered M13 bacteriophage (as compared to that of the yeast) can lead to the formation of nanowires. Indeed, computational simulation of p8 protein assembly shows that the distance between

the helically arranged nearest neighbors of the tetraglutamate is around 3 nm at 100% incorporation.

When E4 virus was incubated in an aqueous solution of 1 mM silver acetate for two hours at room temperature, the solution turned red as shown in Fig. 5.8 a. The appearance of a red color clearly indicated the reduction of silver ions. Alternatively, a silver solution incubated with wild type phage (M13KE) exhibited a turbid yellow color, and revealed that large and irregular precipitates were formed. UV-Vis spectra showed no absorption peak between 200 nm and 800 nm. The reduction of silver ions by wild type viruses was presumably due to the negatively charged surface of the virus[35] as with the yeast surface.

TEM analysis shows the detailed structured of nucleated silver on the virus particles. Wire-like structures were observed along the length the E4 (Fig. 5.8b). Conversely, wild-type virus produced large and irregular silver particles (Fig. 5.9). The length of silver wires on the E4 virus corresponds to the length of the virus particles, and the thickness is approximately 30 nm. The high resolution TEM image in Fig. 5.8d shows the silver wire formed on the E4 virus. The crystallographic structure of silver wires made by the E4 virus was determined by SAED in combination with HRTEM.

A diffraction image (Fig. 5.8d) shows the single crystal patterns of <100> and <112> are superimposed. Diffraction spots from (200), (020), and (220) planes of square symmetry correspond to the [001] zone while the (111), (220) and (311) diffraction spots of rectangular symmetry correspond to the [112] zone. The additional spots can be explained by double diffraction. This analysis suggests that five {111} twin boundaries are located cyclically with D5h symmetry along the longitudinal axis of Ag wire[36]. The formation of the crystals may be associated with the highly oriented p8 proteins and the

five fold symmetry of the arrangement of p8 proteins. The nucleation and growth process seem to have an analogy to the molecular epitaxy in biomineralization[37] and epitaxial growth in vacuum technology. In contrast, we previously reported the regulation of the crystal orientation on the viruses where the textured assembly of nanoparticles was transformed into single crystal nanowires via heat-annealing based on the mechanism of orientated aggregation-based crystal growth[9]. Here, the higher density of incorporated peptides combined with the slow kinetics of the silver reduction allow the nucleated silver to grow in the thermodynamically most favorable single crystalline form without post annealing.

The genetically engineered scaffolds not only mediate the reduction of silver ions but also act as templates for the synthesis of nanostructures. Our results demonstrate that short peptides containing carboxylic acid functional groups facilitate reduction under ambient light and the reduction ability is dependent on the local concentration of silver ions associated with the conformation of peptide. Additionally, this study suggests that tethering peptides to a biological scaffold enhances the reduction ability, and the surface density of the peptides on the scaffold determine the final nanostructure of silver. We anticipate that this study will contribute to the understanding of the spontaneous reduction of metal ions in biological systems and facilitate the implementation of environmentally benign biological methods for fabricating technologically important nanomaterials.

Chapter 5.4 Conclusion

The spontaneous reduction of silver ions by the carboxyl group expressing peptides on the biological scaffolds was demonstrated. Our findings demonstrate 1) spontaneous reduction of silver facilitated by carboxylic acid groups in the presence of ambient light, 2) the importance of peptide conformation on reduction capability, and 3) the increased reduction capability of the peptides when anchored on a biological scaffold. The principle of the peptide-mediated reduction elucidated by the engineered yeast was further extended to a filamentous M13 virus scaffold for fabricating crystalline silver nanowires. The genetically engineered scaffolds not only mediate the reduction of silver ions but also act as templates for the synthesis of nanostructures. This study is anticipated to contribute to the understanding of the spontaneous reduction of metal ions in biological systems and facilitate the implementation of environmentally benign biological methods for fabricating technologically important nanomaterials.

Chapter 5.5 References

1. Stephen Mann, *Biomimetic materials chemistry*. (VCH, New York, 1996)

2. N. Poulsen, M. Sumper, and N. Kroger, *Proceedings of the National Academy of Sciences of the United States of America* **100** (21), 12075 (2003).

3. J. N. Cha, K. Shimizu, Y. Zhou et al., *Proceedings of the National Academy of Sciences of the United States of America* **96** (2), 361 (1999).

4. A. Scheffel, M. Gruska, D. Faivre et al., *Nature* **440** (7080), 110 (2006).

5. S. Brown, *Nature Biotechnology* **15** (3), 269 (1997)

6. S. R. Whaley, D. S. English, E. L. Hu et al., *Nature* **405** (6787), 665 (2000)

7. M. Sarikaya, C. Tamerler, A. K. Y. Jen et al., *Nature Materials* **2** (9), 577 (2003).

8. P. J. Yoo, K. T. Nam, J. F. Qi et al., *Nature Materials* **5** (3), 234 (2006).

9. C. B. Mao, D. J. Solis, B. D. Reiss et al., *Science* **303** (5655), 213 (2004).

10. K. T. Nam, D. W. Kim, P. J. Yoo et al., *Science* **312** (5775), 885 (2006).

11. T. Klaus, R. Joerger, E. Olsson et al., *Proceedings of the National Academy of Sciences of the United States of America* **96** (24), 13611 (1999).

12. P. Mukherjee, A. Ahmad, D. Mandal et al., *Nano Letters* **1** (10), 515 (2001).

13. R. R. Naik, S. J. Stringer, G. Agarwal et al., *Nature Materials* **1** (3), 169 (2002).

14. P. R. Selvakannan, A. Swami, D. Srisathiyanarayanan et al., *Langmuir* **20** (18), 7825 (2004).

15. B. R. Peelle, E. M. Krauland, K. D. Wittrup et al., *Langmuir* **21** (15), 6929 (2005).

16. R. T. Clay and R. E. Cohen, *Supramolecular Science* **5** (1-2), 41 (1998).

17. S. K. Ghosh, S. Kundu, M. Mandal et al., *Journal of Nanoparticle Research* **5** (5-6), 577 (2003).

18. S. Joly, R. Kane, L. Radzilowski et al., *Langmuir* **16** (3), 1354 (2000).

19. K. Esumi, A. Suzuki, A. Yamahira et al., *Langmuir* **16** (6), 2604 (2000).

20. A. Henglein, *Langmuir* **17** (8), 2329 (2001).

21. K. Esumi, T. Hosoya, A. Suzuki et al., *Journal of Colloid and Interface Science* **226** (2), 346 (2000).

22. H. Z. Huang and X. R. Yang, *Carbohydr. Res.* **339**, 2627 (2004)

23. Y. Yonezawa, A. Takami, T. Sato et al., *Journal of Applied Physics* **68** (3), 1297 (1990).

24. M. Maillard, P. R. Huang, and L. Brus, *Nano Letters* **3** (11), 1611 (2003).

25. B. M. Rybak, M. Ornatska, K. N. Bergman et al., *Langmuir* **22** (3), 1027 (2006).

26. H. Iloukhani and H. Bahrami, *International Journal of Chemical Kinetics* **31** (2), 95 (1999).

27. T. Shoeib, K. W. M. Siu, and A. C. Hopkinson, *Journal of Physical Chemistry A* **106** (25), 6121 (2002).

28. A. Henglein, *Chem. Rev.* **89**, 1861 (1989).

29. J. Keizer, *Accounts of Chemical Research* **18** (8), 235 (1985).

30. M. A. R. B. Castanho and M. X. Fernandes, *Eur. Biophys. J.* **35**, 92 (2006).

31. K. Mallick, S. Jewrajka, N. Pradhan et al., *Current Science* **80** (11), 1408 (2001).

32. S. K. Ghosh, S. Kundu, M. Mandal et al., *Langmuir* **18** (23), 8756 (2002)

33. S. L. Hardt, *Biophys. Chem.* **10**, 239 (1070)

34. P. Laszlo, *Accounts of Chemical Research* **19** (4), 121 (1986).

35. Carlos F. Barbas, *Phage display : a laboratory manual.* (Cold Spring Harbor Laboratory Press, Cold Spring Harbor, NY, 2001).

36. A. Graff, D. Wagner, H. Ditlbacher et al., *European Physical Journal D* **34** (1-3), 263 (2005).

37. P. U. P. A. Gilbert, M. Abrecht, and B. H. Frazer, *Molecular Geomicrobiology* **59**, 157 (2005).

Figure 5.1. Characterization of yeast solutions incubated in 1 mM $AgCOOCH_3$ solution. Yeast cell concentration is 1 O.D. Yeast solutions are named for corresponding clones. Expressed peptides are: E_6 - hexa-glutamic acids, D_6 – hexa-aspartic acids, G_6 – hexa-glycine acidis, UI- uninduced clone with no surface expressed peptides, E6 dark - hexa-glutamic acids, incubated in the dark. (a) Photograph of the yeast solutions shows color change resulting from silver nanoparticles formation. (b) UV-Vis absorption spectra of the same solutions. Peak at 260 nm comes from DNA of yeast cells.

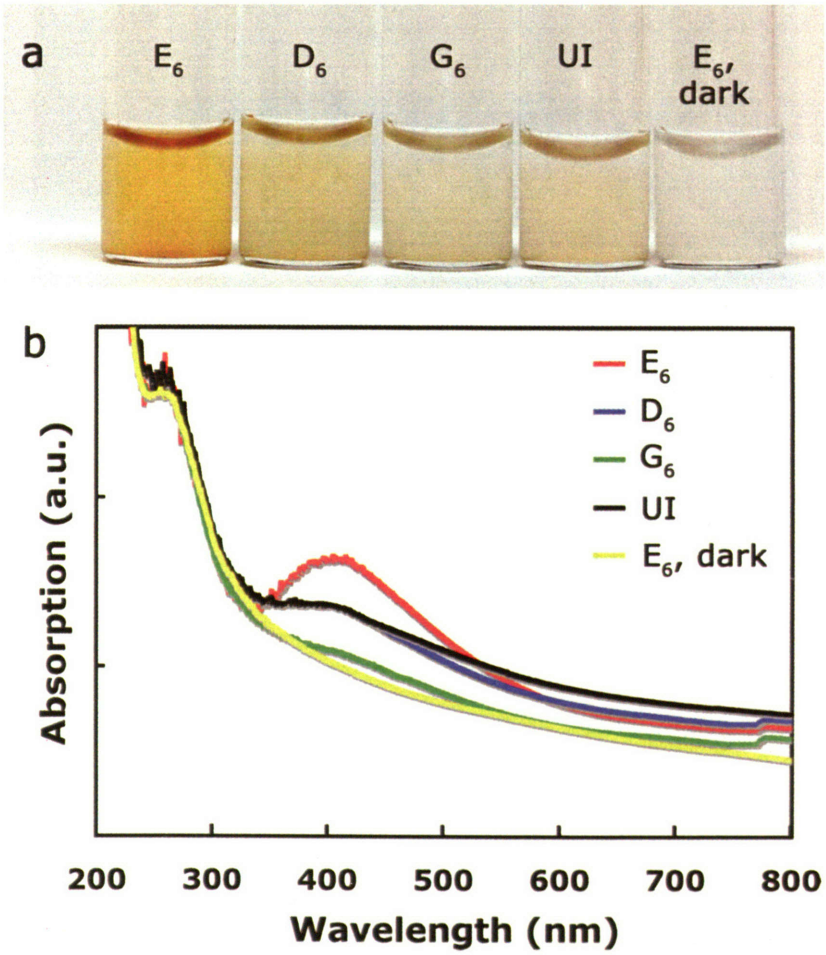

Figure 5.2 UV-Vis absorption spectra of the E_6 yeast with and without UV-light blocking polymer coatings. Yeast solutions are incubated in 1 mM $AgCOOCH_3$ solution.

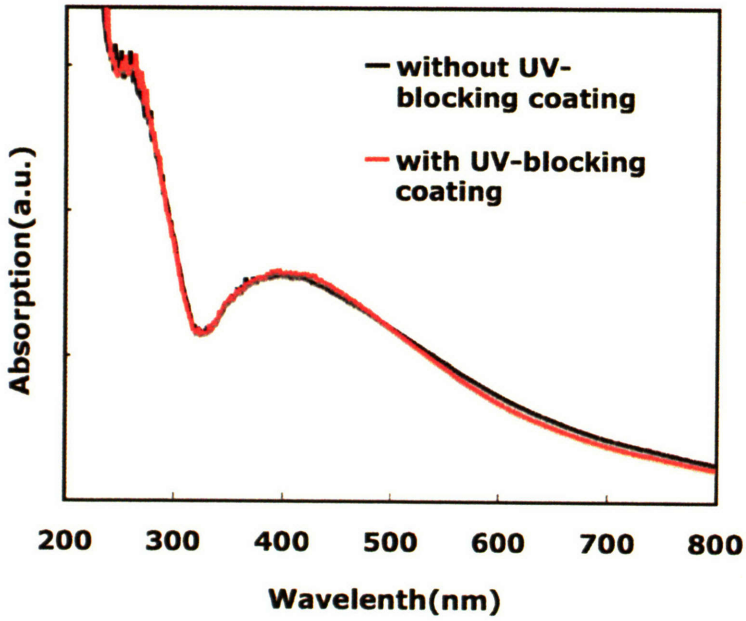

Figure 5.3 TEM analysis of silver reduction by engineered yeast. (a) Un-induced(UI). (b) Un-induced(UI) high magnification. (c) D_6. (d) D_6 high magnification. (e) E_6. (f) E_6 high magnification. (g) Low magnification image of E_6 showing several cells coated with silver nanoparticles layer. (h) Electron diffraction pattern confirms the crystalline nature of the silver nanoparticles. (i) High Resolution TEM image of silver nanoparticles.

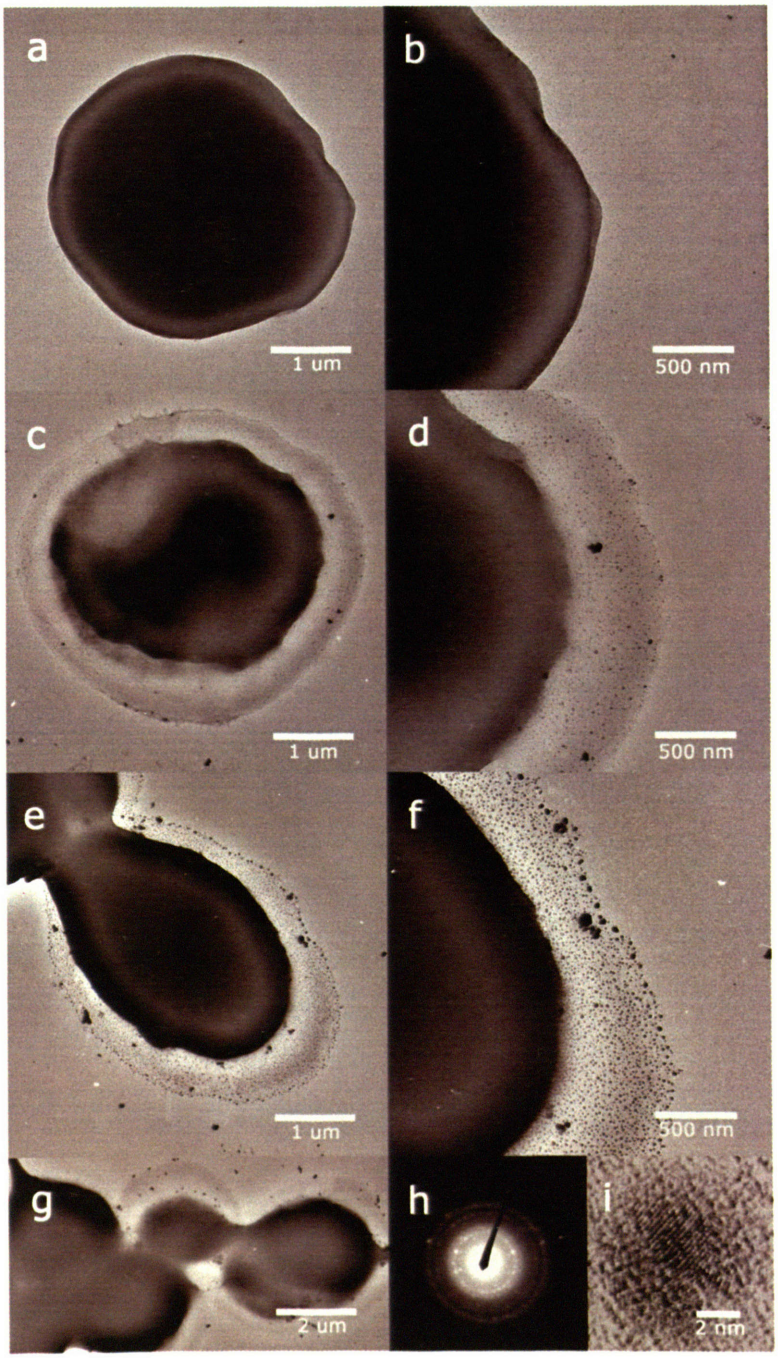

Figure 5.4 Silver nanoparticles synthesized by un-induced yeast solution. Particles are aggregated and not bound to yeast surface peptides.

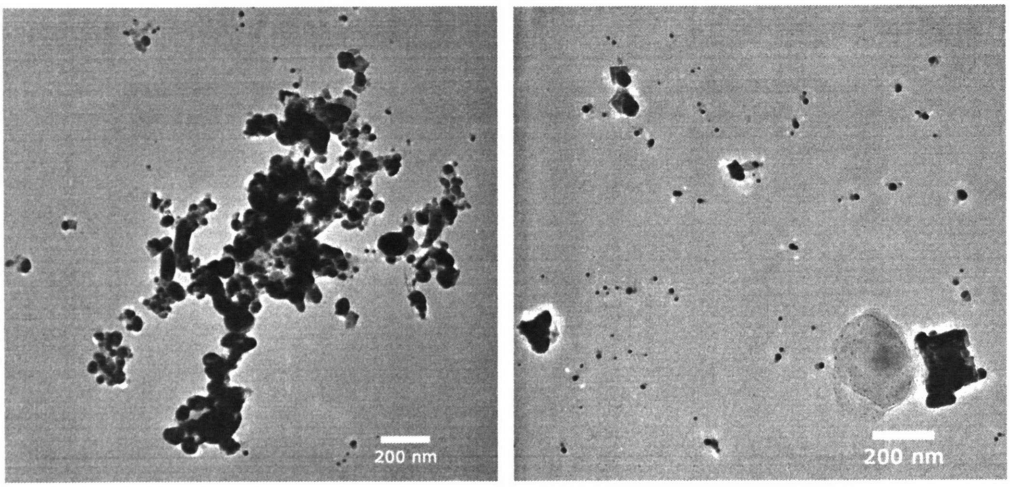

Figure 5.5 Scanning electron micrographs of yeast cells. The yeast solutions are prepared as those in Fig. 2, except control sample. Control sample is pristine E_6 yeast not exposed to silver solution. (a)-(d) Low magnification images (5000-30000X) of yeast cells with carbon 10nm coating layer: (a)-(c) E_6, (d) control sample. (e)-(h) High magnification images (80000X) without coating layer: (e) E_6, (f) D_6, (g) Un-induced (UI), (h) control sample. Yeast cells were not coated with conducting materials to visualize small particle features.

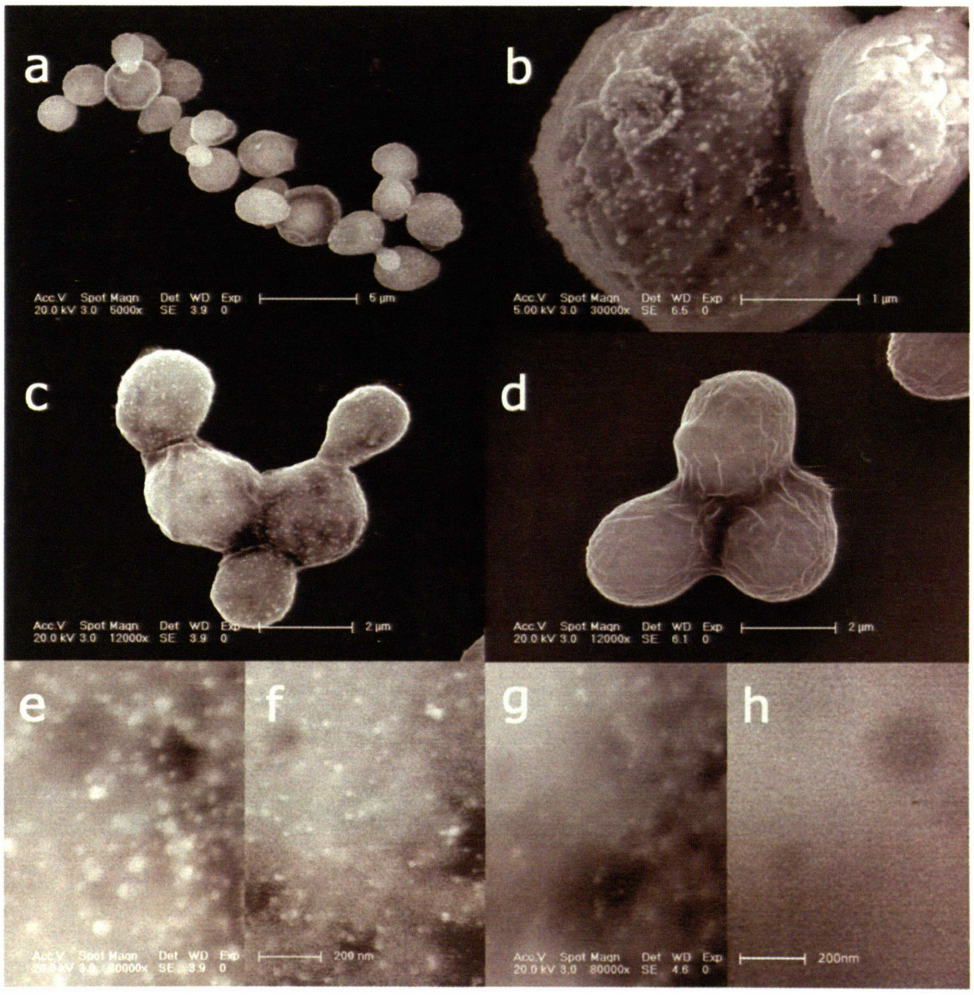

Figure 5.6 Average conformations of (a) hexa-aspartic acids(D_6) and (b) hexa-glutamic acids(E_6) from Monte Carlo simulations. Atom colors are: grey – carbon, white – hydrogen, red – oxygen, blue – nitrogen. Blue spheres indicate counter ions (Z = +1) placed in simulation to balance charge during the simulation.

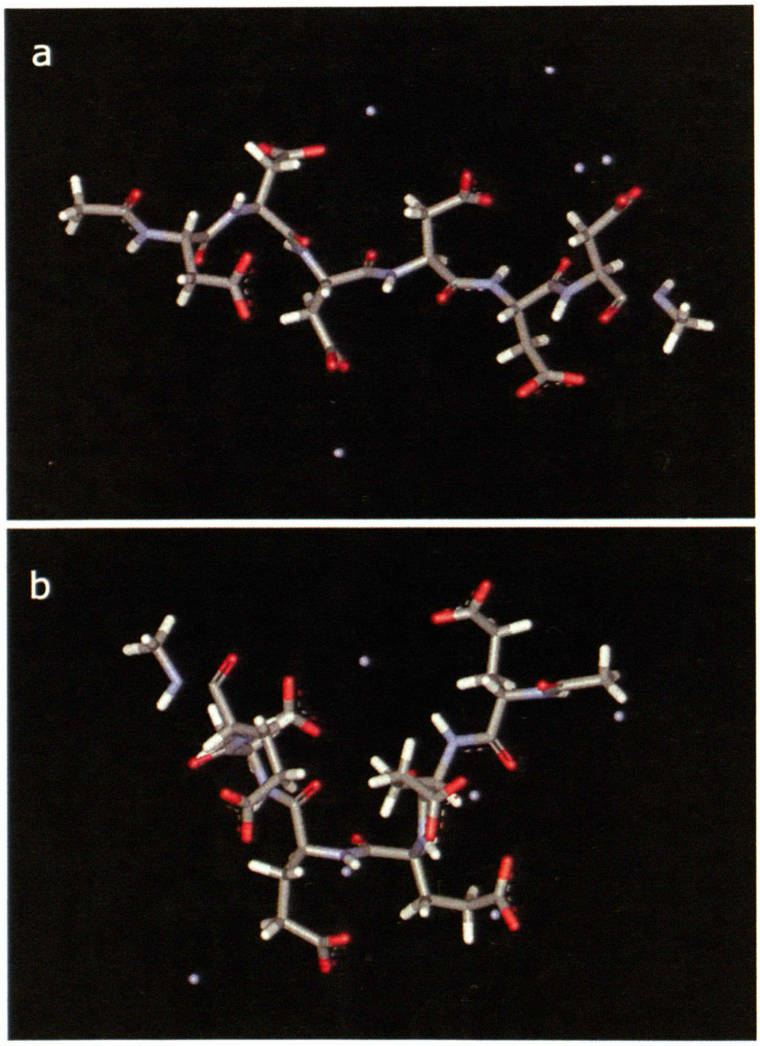

Figure 5.7 UV-Vis absorption analysis of the silver reduction by soluble hexa-glutamic acid peptide. (a) Various peptide concentrations. Concentration of $AgOOCCH_3$ is 8 mM. (b) Various $AgOOCCH_3$ solution concentrations. Concentration of hexa-glutamic acid solution is 1 mM.

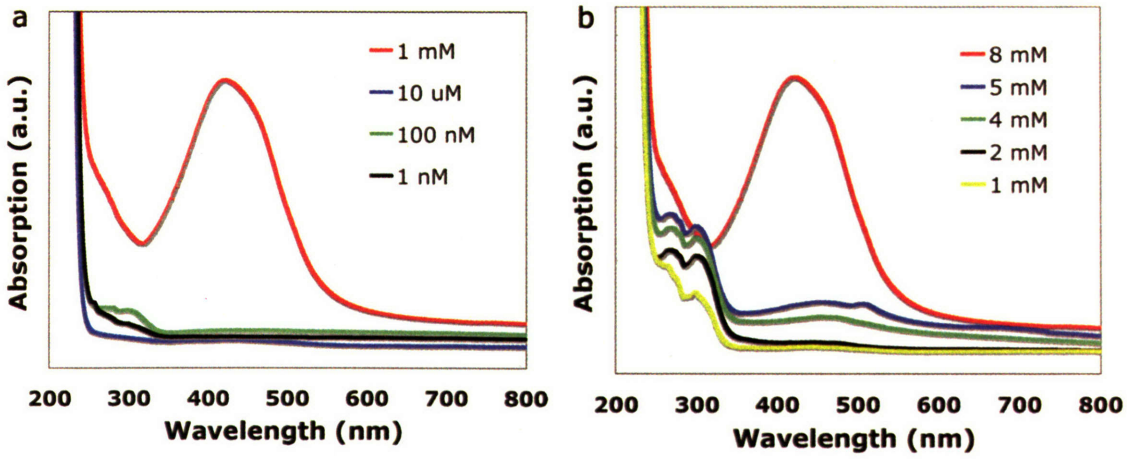

Figure 5.8 Silver reduction by engineered virus (a) photographs of the silver solution reduced by E4 virus (left) and wild type virus (b) TEM image of the virus based silver wires (c) High resolution TEM image of the virus based silver wire (d) High resolution TEM image of the virus based silver were and diffraction pattern (inset).

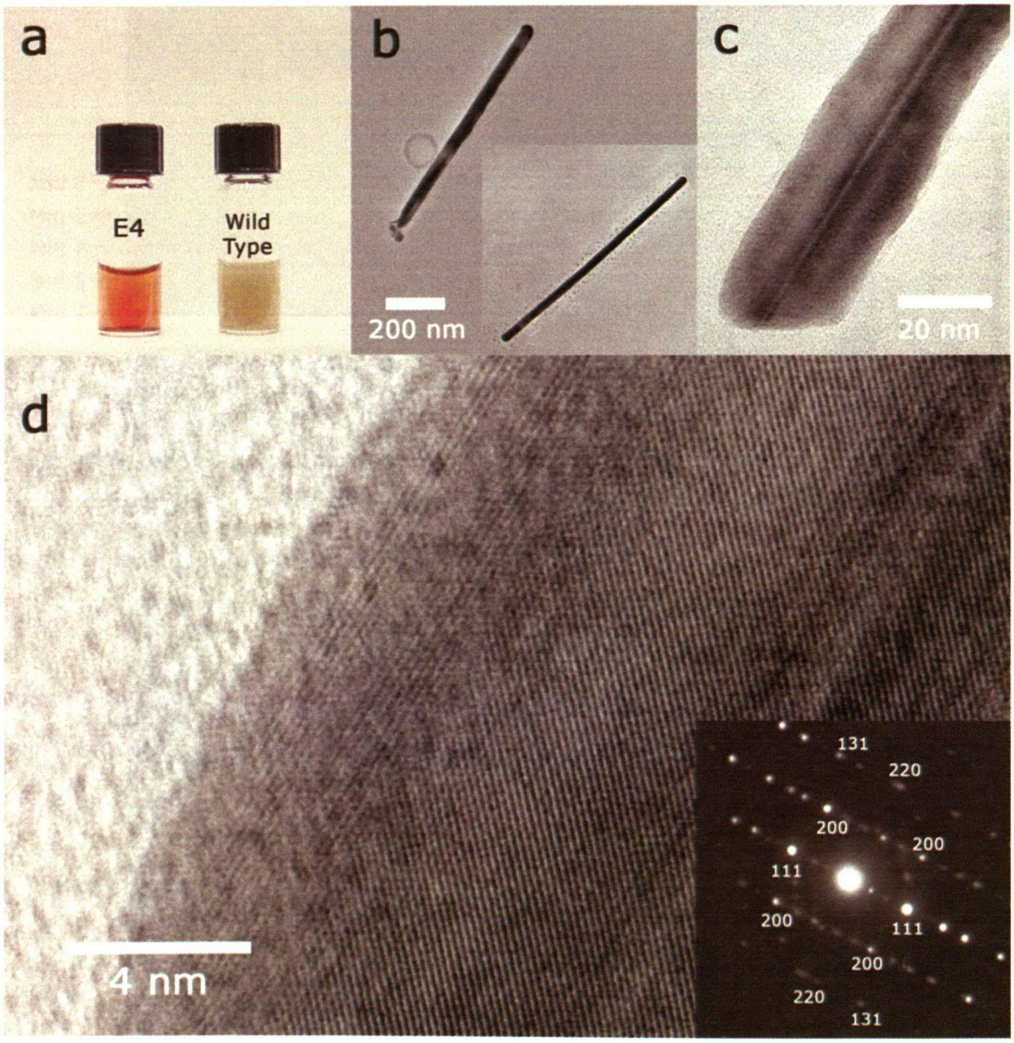

Figure 5.9 Silver nanoparticles produced by wild-type M13 viruses. Large and irregular silver particles are generated.

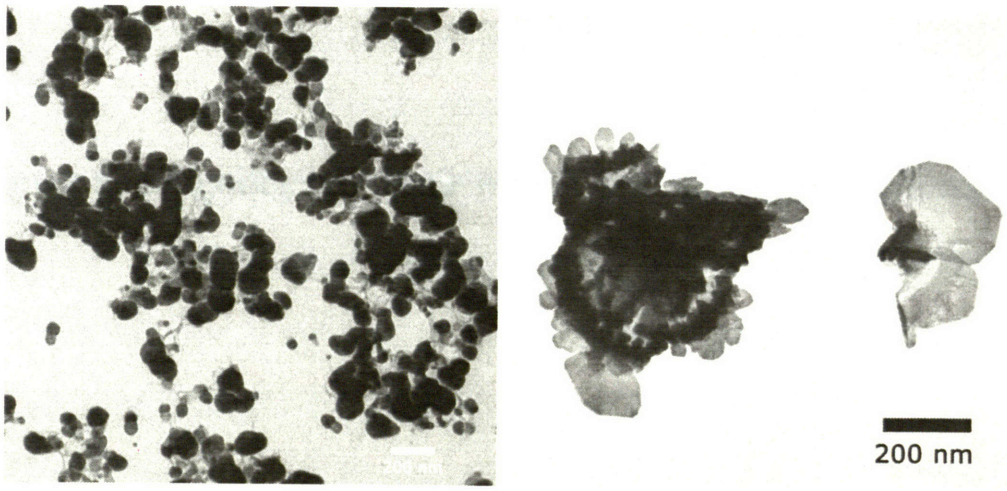

Figure 5.10 Silver nanowires by E4 M13 viruses. Aggregations are observed.

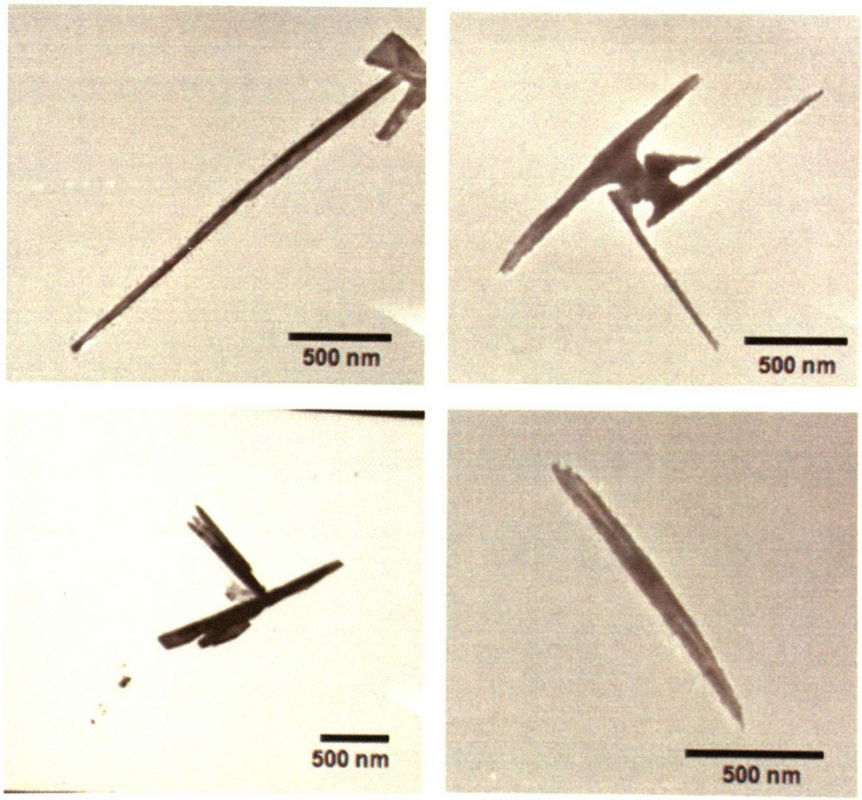

Chapter 6. Ongoing research works and future directions

Chapter 6. Summary

The principle of biological self-assembly and biotemplating which were investigated in the previous chapter of this thesis can be extended into a variety of the technologically important issues. In this chapter, the ongoing studies which are not yet completed and need further investigation are described briefly, suggesting the future direction of the work. The understanding of biotemplating through the study in the previous chapters can provide the foundation for synthesizing virus-based nanowires of different materials. Different strategies to grow nanowires are discussed in this chapter. Additionally, it is demonstrated that biological self-assembly and selective binding can be applied to fabricate flexible, electrochemically active fibers.

Chapter 6.1 Searching for magnetic responsive peptide

Living creatures utilize the strong mechanical property of biominerals, which is mainly due to the hybrid nanostructuring of proteins and inorganic materials. Examples include pearl, bone, keratin, shell and calcite. In addition to the mechanical property of biominerals, creatures use inorganic materials for several other functions. Another interesting biomineral within an organism is the magnetic particle of the ferric/ferrous oxide, magnetite, which gives the organism the ability to orient itself in relation to an ambient magnetic field. Magnetite has been discovered in bees, homing pigeons, dolphins and various other organisms, including man. An important example is found in magnetotactic bacteria, which produce aligned magnetic nanoparticles. This magnetite particle is bounded by a membrane called a magnetosome. The magnetosome is believed to play an important role in producing and aligning the magnetite particles. Individual particles align their magnetic field so that the magnetic field of the bacteria ($6x\ 10^{-17}$ J/T per crystal) can be used to orient and navigate the bacteria along geomagnetic field line. Recently, in addition to this explanation, scientist started to realize that the compass sense (the ability to identify magnetic north) in more highly evolved creature is more likely to rely on a chemical reaction involving radicals. In order to explain how a homing pigeon can return to its loft, Mora et al[1], suggests that magnetoreception (probably magnetite based) associated with chemical reaction occurs in the bird's upper beak, which help them remembering variation in the strength of the earth's magnetic field. There is also growing evidence that magnetism can have a biological effect. Hore's team[2] has demonstrated that a weak magnetic field can affect the production of a certain molecule found in a photosynthetic bacterium, suggesting that the bacteria would grow better in a

magnetic field. The experimental evidence of magnetic effects on biological systems leads several questions: Can biomolecules, especially peptides, recognize the magnetization status of magnetic materials? Can the interaction between peptides and magnetic materials be regulated by a magnetic field? To answer these questions, we are searching for magnetically responsive peptides.

We are trying to find the specific peptide sequences that can bind magnetic materials with response to magnetic fields. In other words, we hope to find the specific peptide which adheres to magnetic materials under a magnetic field but detach from it without the magnetic field and vice versa. This study is expected to provide the scientific foundation of understanding the function of magnetic particle in organisms as well as introducing a new concept in bio-nano application. Potentially, this reversible interaction between peptides and magnetic materials depending on magnetic field may function as a switch, which is similar in concept to a supramolecular switch.

In order to identify the peptide sequence which has the affinity against magnetic materials, we have chosen single crystal (111) and (100) Fe_3O_4 as a target substrate. Fe_3O_4 is ferromagnetic materials and depending on the crystal orientations, it represents different magnetic behavior. Figure 6.2 shows the peptide sequences that were identified after 5 rounds against (111) and (100) Fe_3O_4 single crystal substrate. As shown in Figure 6.2, peptide sequences have the similarity. In order to see the effect of magnetic field on the binding affinity of peptides, we did the biopanning against (111) Fe_3O_4 substrate under magnetic field. The strength of the applied magnetic field is strong enough to induce the saturated magnetization. In this experiment, magnetic field was applied by using hard ferromagnets. Figure 6.3 shows the peptide sequences that were identified

after third round biopanning. At this point, it is not certain that the identified peptides under the magnetic field represent the magnetic responsive binding behavior against Fe_3O_4 substrate. Hence, more investigations are needed.

Chapter 6.2 Virus templated TiO_2 nanowires

- This project collaborated with Forrest Liau-

In my Ph.D work, cobalt oxide nanowires were successfully grown on the engineered viruses. In this case, carboxylic acid functionality was expressed on the surface of viruses and was utilized as nucleation sites. A similar strategy can be applied to synthesize the metal compound nanowires because most metal salts form negatively charged ions in aqueous solution and thus the ions can bind with the carboxylic acid group. However, there are still remaining challenges to synthesize the good quality metal oxides at room temperature without any further heating process and furthermore some useful metal complexes in water is negatively charged. Therefore, in order to suggest the solution about the potential challenge and thus extend our biological approach into other technological issues, the new strategy to grow the metal oxide nanowires at room temperature was developed. Herein, amine functionality was utilized to grab negatively charged metal ions for subsequent nucleation.

As a proof of concept, TiO_2 nanowires were grown on the engineered virus template. Titanium oxide has attracted much industry attention for its useful electrical and optical properties. For example, TiO_2 can be used as anode materials for Li ion battery technology and as photocatalyst in many chemical applications. The morphology and nanostructure affect its properties significantly. New methods for synthesizing specific forms of titanium oxide could be of commercial importance.

The process involves a hydrolysis equilibrium reaction of ammonium hexafluorotitanate and a flourine ion consumption reaction with boric acid.[3] A primary advantage to this approach is the ability to synthesize titanium oxide near ambient

conditions via a simple procedure in solution. In order to attach negatively charged hexafluorotitanate on viruses, the pH of the virus solution was decreased so that overall charge of virus became positive. After attaching hexafluorotitanate, H_3BO_3 was added to obtain TiO_2 nanowires. The ligand exchange equilibrium reaction that results in TiO2 synthesis is shown below.

$$TiF_6^{2-} + 2H_2O \rightarrow TiO_2 + 6F^- + 4H^+$$

$$H_3BO_3 + 4HF \rightarrow BF^{4-} + H_3O+ + 2H_2O$$

Figure 6.4 shows XRD data of the virus templated nanowires. It confirms that the crystal structure is anatase, which is the useful phase for many applications such as photocatalysts. Interestingly, without a further annealing step, at room temperature, we could successfully synthesize titanium oxide nanowires that have the good crystal quality. Figure 6.5 shows a TEM image of the virus templated nanowires. As shown in Figures, viruses could act as scaffolds to grow nanowires. Titanium nanoparticles were selectively grown along the length of the viruses. Crystal structure was also confirmed by the electron diffraction pattern. However, because we utilized one amine functionality at the end of the p8 protein, homogeneous morphology could not be obtained. Further studies to insert more amine functionalities by genetic engineering are needed.

It is believed that the virus based titanium nanowires can be useful for photocatalysts or supercapacitors. When coupled with the biological self-assembly of two-dimensional virus monolayers on the polyelectrolytes, the developed nanowire synthesis technology could be the foundation for the self-assembled, functional devices.

Chapter 6.3 Virus templated Pt nanowires

When metal salt in aqueous solution forms a positive complex, the utilization of negative charged carboxylic acid can be a good method to induce the selective nucleation and growth of metal on virus coat proteins. While transition metals such as Co, Ti, Ni and Fe normally exist as positive ions, some of noble metal salts are more general as negative ion complexes. For example, when $HAuCl_4$ dissolves in water, negative ion complexes of $[AuCl_4]^-$ are stable. It is the same case for Pt.

In order to extend our strategy by the application of carboxylic functionality, relatively new salts of noble metal Pt were found and utilized for growing Pt nanowires on our engineered virus template. Tetrammineplatinum(II)chloride, $Pt(NH_3)_4Cl_2$ was newly used as a salt. When it was dissolved in water, tetrammineplatinum(II)chloride, $Pt(NH_3)_4Cl_2$ could be dissociated into $Pt(NH_3)_4^{2+}$ and Cl^-. Therefore, $Pt(NH_3)_4^{2+}$ can interact with the carboxylic group of p8 proteins of viruses, resulting in the selective nucleation and growth.

Figure 6.6 shows TEM images of virus-based Pt nanowires. At lower concentration (0.1mM) of Pt ions (left image), Pt nanoparticles cannot cover the entire body of the virus, resulting in the growth of discrete nanoparticles. The same morphology can be observed when the virus concentration is higher than the optimum condition. In fact, the relative concentration between the viruses and Pt ions are important to determine the final morphology. When the concentration of Pt ions is 0.5mM (right image), the major coat proteins could be covered fully with the grown Pt nanoparticles. The nanosize Pt nanoparticles were homogeneously nucleated and grown along the length of M13 viruses. The concentration of $NaBH_4$ that was used for the reduction was 5 mM. After

incubating the viruses in Pt ion solution for 1 hour, the same volume of $NaBH_4$ with Pt ion solution was added. After at least 30 minutes, a color change in the solution was observed.

Pt nanostructures have attracted a lot of attention for their catalyst and electronic conductor applications. Especially, because it has relatively stronger resistance against oxidation compared to other metals, Pt could be used as an electrode that is functional at high temperatures. Examples are the electrode for fuel cells and memory devices. Additionally, when Pt exists as a nanostructure, it exhibits catalytic property for a variety of chemical reactions. The homogeneous alignment of Pt nanoparticles forming one-dimensional nanostructures is also expected to show unique catalytic properties.

Chapter 6.4 Virus Based Fiber Electrode for Li Ion Battery

Naturally, silk spiders and silk worms can spin the liquid crystalline protein fiber (fibroin) by passing aqueous solution through their spinnerat. When the extracted fibers are exposed to air, they harden into a flexible and highly oriented semicrystalline fiber whose properties are superior to artificial polymer fibers. The unique nano and microstructure of the liquid crystals provide these superior properties. Additionally, their high surface to volume ratio can be useful for synthesizing novel membranes.

Previously, our group mimicked the spinning process of the silk spider by using long rod shaped M13 viruses.[4] Liquid crystalline virus suspensions were extruded through capillary tubes in a crosslinked solution of glutaraldehyde. The resulting fibers showed nematic ordered morphologies. Multifunctionalities could be employed into the virus fibers through the genetic engineering of the viruses or/and the incorporation of the inorganic nanomaterials. The inherent shape of the long viruses caused the viruses to assemble into liquid crystalline structures.

Virus-based fiber can act as a useful platform for Li ion battery fibers. A flexible battery in the form of a fiber can be embedded into textiles, which open a new possibility for designing wearable energy devices. As a first step to fabricate a complete fiber battery consisting of a cathode, anode and electrolyte, a virus-based $LiFePO_4$ fiber was synthesized via wet spinning. The engineered viruses of E4 were mixed with pre-made $LiFePO_4$ nanoparticles less than 100 nm diameter in aqueous solution. After incubation, the mixed solutions were spun into a crosslinked aldehyde solution using a syringe. Once the mixture of viruses and pre-made $LiFePO_4$ nanoparticles were extracted to the crosslinked solution, the virus based $LiFePO_4$ fiber was fabricated. Figure 6.7 shows the

virus based $LiFePO_4$ fiber wrapped around Pt conducting wire. After the fiber was wrapped around Pt wire, which is electrochemically inactive, the electrochemical property of the fiber was measured.

Chapter 6.5 References

1. C. V. Mora, M. Davison, J. M. Wild et al., *Nature* **432** (7016), 508 (2004).
2. Y. Liu, R. Edge, K. Henbest et al., *Chem Commun* (2), 174 (2005).
3. S. Deki, Y. Aoi, Y. Asaoka et al., *J Mater Chem* **7** (5), 733 (1997).
4. S. W. Lee and A. M. Belcher, *Nano Lett* **4** (3), 387 (2004).

Figure 6.1 Atomic arrangement of Fe and O on (100) and (111) Fe3O4 surface. Left image is (100) and right image is (111).

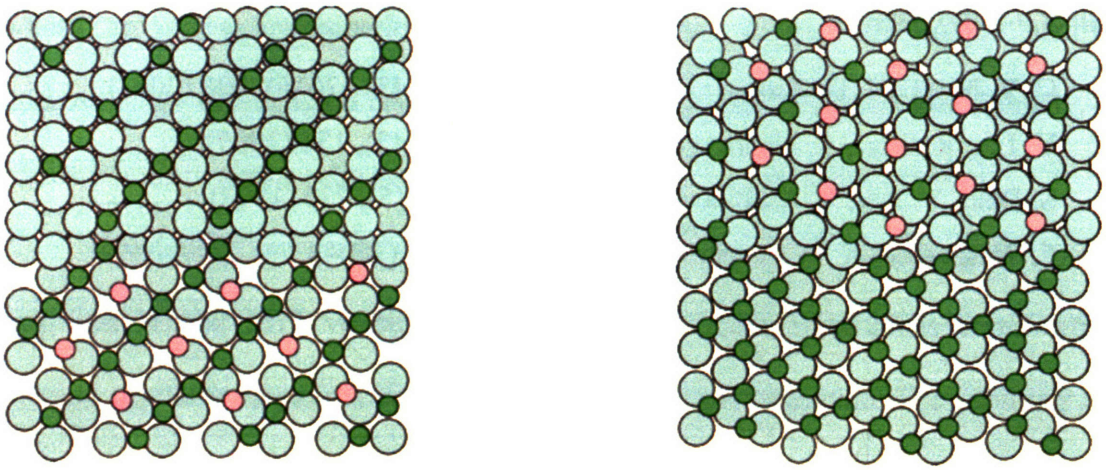

Figure 6.2 Peptide Sequences identified by phage display library without magnetic field.

(100)	S	H	P	W	N	A	Q	R	E	L	S	V
(100)	L	M	H	S	T	T	N	Q	R	L	T	V
(111)	Q	S	T	H	T	T	N	R	A	I	W	P
(111)	T	M	G	F	T	A	P	R	F	P	H	Y

Figure 6.3 Peptide sequence after third round selection against (111) Fe3O4 under magnetic field.

	H	A	T	G	T	H	G	L	S	L	S	H
	L	L	A	D	T	T	H	H	R	P	W	T
	H	A	T	G	T	H	G	L	S	L	S	H
	H	A	T	G	T	H	G	L	S	L	S	H
	Y	S	P	A	S	K	S	P	V	P	S	L
	H	A	T	G	T	H	G	L	S	L	S	H
	T	Q	T	T	V	S	S	T	Q	K	P	Y
	T	Q	T	T	V	S	S	T	Q	K	P	Y
	H	A	T	G	T	H	G	L	S	L	S	H
	H	P	I	P	P	N	S	L	F	T	S	N
	K	M	D	R	H	D	P	S	P	A	L	L

Figure 6. 4. XRD data of virus templated TiO2 nanowires.

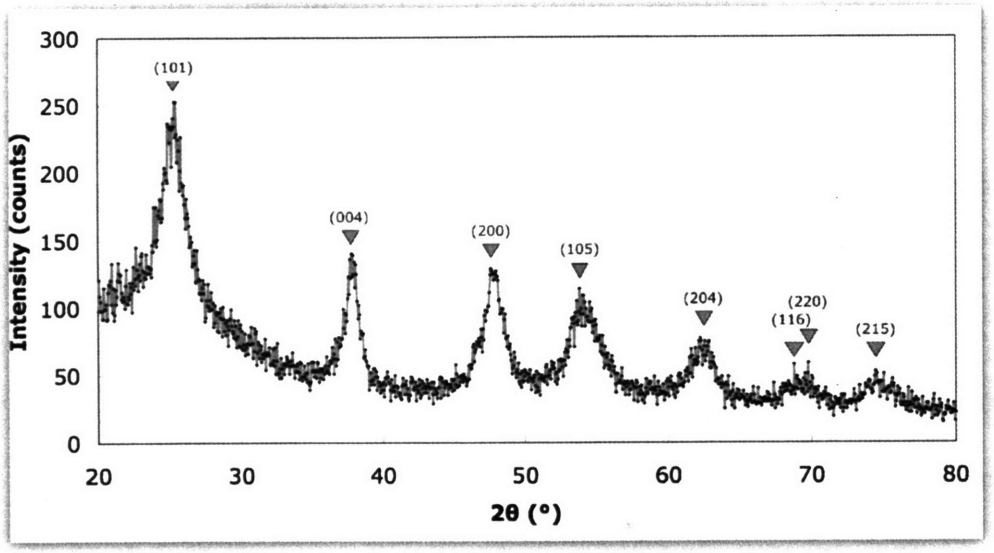

Figure 6.5. TEM images of virus based TiO_2 nanowire.

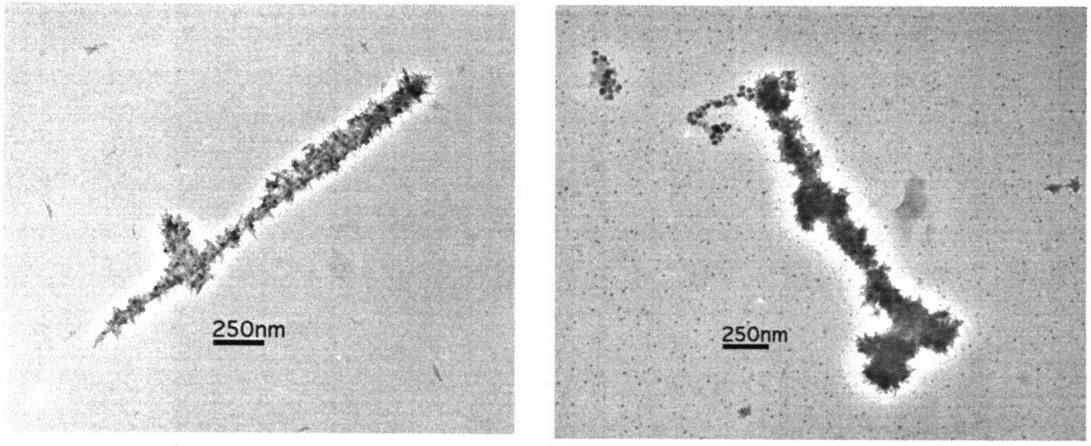

Figure 6.6. TEM images of virus based Pt nanowires.

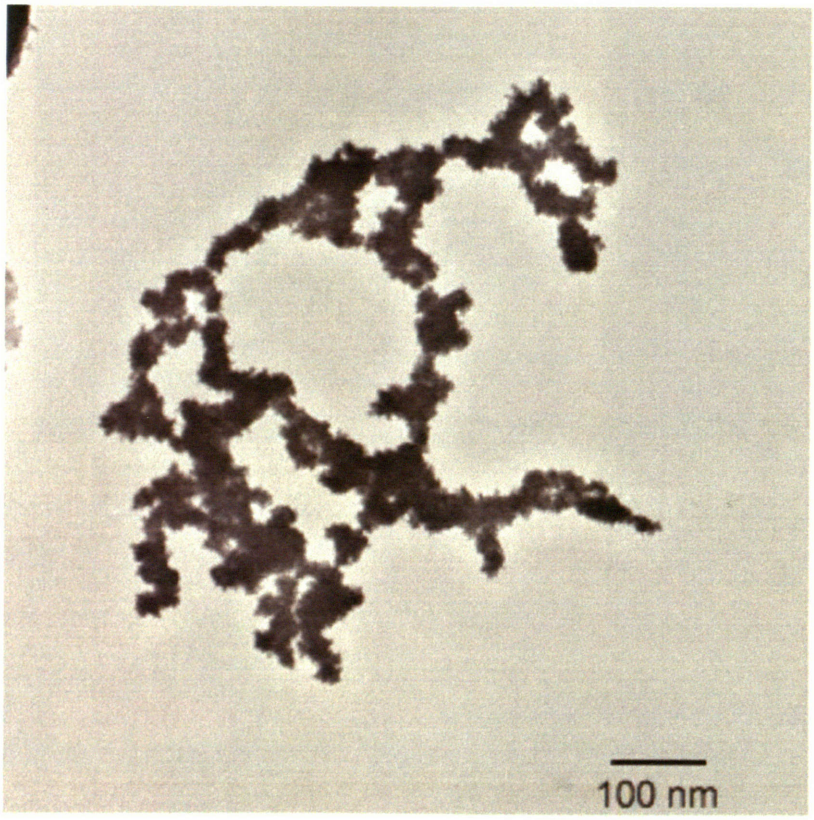

Figure 6.7 Virus based $LiFePO_4$ fiber